COMPARISON OF SINGLE, DOUBLE, AND TRIPLE LINEAR FLOW MODELS FOR SHALE GAS/OIL RESERVOIRS

A Thesis

by

VARTIT TIVAYANONDA

Submitted to the Office of Graduate Studies of
Texas A&M University
in partial fulfillment of the requirements for the degree of

MASTER OF SCIENCE

August 2012

Major Subject: Petroleum Engineering

Comparison of Single, Double, and Triple Linear Flow Models

for Shale Gas/Oil Reservoirs

COMPARISON OF SINGLE, DOUBLE, AND TRIPLE LINEAR FLOW MODELS FOR SHALE GAS/OIL RESERVOIRS

A Thesis

by

VARTIT TIVAYANONDA

Submitted to the Office of Graduate Studies of
Texas A&M University
in partial fulfillment of the requirements for the degree of

MASTER OF SCIENCE

Approved by:

Chair of Committee,	Robert A. Wattenbarger
Committee Members,	David S. Schechter
	Yuefeng Sun
Head of Department,	A. Daniel Hill

August 2012

Major Subject: Petroleum Engineering

ABSTRACT

Comparison of Single, Double, and Triple Linear Flow Models

for Shale Gas/Oil Reservoirs. (August 2012)

Vartit Tivayanonda, B.Eng., Chulalongkorn University

Chair of Advisory Committee: Dr. Robert A. Wattenbarger

There have been many attempts to use mathematical method in order to characterize shale gas/oil reservoirs with multi-transverse hydraulic fractures horizontal well. Many authors have tried to come up with a suitable and practical mathematical model. To analyze the production data of a shale reservoir correctly, an understanding and choosing the proper mathematical model is required. Therefore, three models (the homogeneous linear flow model, the transient linear dual porosity model, and the fully transient linear triple porosity model) will be studied and compared to provide correct interpretation guidelines for these models.

The analytical solutions and interpretation guidelines are developed in this work to interpret the production data of shale reservoirs effectively. Verification and derivation of asymptotic and associated equations from the Laplace space for dual porosity and triple porosity models are performed in order to generate analysis equations. Theories and practical applications of the three models (the homogeneous linear flow model, the dual porosity model, and the triple porosity model) are presented. A simplified triple porosity model with practical analytical solutions is proposed in order

to reduce its complexity. This research provides the interpretation guidelines with various analysis equations for different flow periods or different physical properties. From theoretical and field examples of interpretation, the possible errors are presented. Finally, the three models are compared in a production analysis with the assumption of infinite conductivity of hydraulic fractures.

DEDICATION

To my parents

ACKNOWLEDGEMENTS

I would like to thank my committee chair, Dr. Robert Wattenbarger, for his abundantly helpful guidance and ideas. This thesis would not have been possible without his strongly support. There are not enough words to express my gratitude for the help that he gave.

I would like to acknowledge my committee members, Dr. David S. Schechter and Dr. Yuefeng Sun, for being my advisory committee and helping improving this thesis.

I would like to thank my friends in my faculty group for their support and friendship; Ahmad Alkouh, Orkhan Samandarli, Tan Tran, Haider Abdulal, Ammar Agnia, Mohammed Kanfar, and Wahaj Khan. I would also like to thank my Thai friends and TSA for their help and friendship which makes College Station like my second home.

Thanks also go to my friends and colleagues and the department faculty and staff for making my time at Texas A&M University a great experience.

Finally, thanks to PTT Exploration and Production Public Company Limited for giving me a chance to pursue my advanced degree and sponsoring my study at Texas A&M University.

NOMENCLATURE

A_{cw}	Cross-sectional area of fluid to flow, ft^2
A_{cm}	Cross-sectional area of fluid flow from matrix to fracture, ft^2
B	Formation volume factor, rcf/scf
c_t	Total compressibility, psi^{-1}
h	Effective reservoir thickness (assume to be same as hydraulic fracture height), ft
k_F	Effective hydraulic fracture permeability, md
$k_{F,in}$	Intrinsic hydraulic fracture permeability, md
k_f	Effective natural fracture permeability, md
$k_{f,in}$	Intrinsic natural fracture permeability, md
k_m	Matrix permeability, md
L_F	Hydraulic fracture spacing (from one middle of hydraulic fracture to another middle of hydraulic fracture), ft
L_f	Natural fracture spacing (from one middle of hydraulic fracture to another middle of hydraulic fracture), ft
m_{fourth}	Slope of the fourth root of time plot
m_{square}	Slope of the square root of time plot
$m(p)$	Pseudopressure (gas), psi^2/cp $\left(m(p) = 2\int_0^p \frac{p'}{z(p')\mu(p')}\,\mathrm{d}p'\right)$
$\Delta m(p)$	Difference of initial and wellbore flowing pseudopressure, psi^2/cp

n_F	Number of hydraulic fractures
n_f	Number of natural fractures per one hydraulic fracture half-length
p_D	Dimensionless pressure
p	Pressure, psi
Δp	Difference of initial and wellbore flowing pressure, psi
q_{DL}	Dimensionless rate
SRV	Stimulated reservoir volume (Same as drainage area)
T	Absolute temperature, ^{o}R
t	Time, days
t_{DAcw}	Dimensionless time based on A_{cw} and k_F
t_{DAcm}	Dimensionless time based on A_{cm} and k_m
V_p	Pore volume, rcf
w	Fracture width, ft
x_e	Effective perforated interval (Effective well length), ft
x_f	Fracture half length, ft
y_e	Drainage area half-length (rectangular geometry, assumed to be same as hydraulic fracture half length, ft
y_{eD}	Dimensionless reservoir half-length or dimensionless hydraulic fracture half length, ft
z	Compressibility factor

Greek symbols

λ	Dimensionless interporosity parameter
ω	Dimensionless storativity ratio
ϕ	Porosity, fraction

Subscripts

end	End of the data point of the linear straight line
esr	End of straight line of the square root of time plot or end of half-slope line of log-log plot
max	Maximum
min	Minimum
F	Macro-fracture (hydraulic fracture)
f	Micro-fracture (natural fracture)
g	Gas
i	Initial condition
m	Matrix
o	Oil
t	Total system
T	Total system
wf	Bottomhole flowing

TABLE OF CONTENTS

Page

Page

Page

LIST OF FIGURES

Page

Page

Page

Page

LIST OF TABLES

Page

Page

CHAPTER I

INTRODUCTION

Shale gas/oil reservoirs have become an important source of energy in the United States with an updated production technique. Due to a very low permeability, producing shale gas/oil reservoirs requires well stimulation treatment and horizontal well technique. Recently, producing shale reservoirs through multi-transverse hydraulic fractures in horizontal wells has become a standard production strategy. However, the understanding of shale gas/oil characteristics and behaviors are still inadequate to perform reservoir management effectively.

There have been many attempts to characterize the multi-transverse hydraulic fractures horizontal shale well including numerical, analytical, and empirical methods. While the numerical method is considered the most accurate way to characterize model, it is time consuming to analyze a number of wells. The analytical method is an effective method for analyzing wells when it fits with the mathematical model. The empirical method is the fastest and easiest way to forecast production and to estimate reserves; however, this method does not explain the characteristics of the reservoir.

Based on the analytical method, many authors have tried to come up with a suitable and practical mathematical model to represent a shale well. Some (Bello and Wattenbarger 2008, 2009, 2010) utilized the dual porosity model to represent the model.

This thesis follows the style of *SPE Reservoir Evaluation & Engineering*.

Some (Ozkan et al. 2009, Brown et al. 2009, Al-Ahmadi and Wattenbarger 2011) utilized the triple porosity model.

Using the analytical methods to interpret the shale production data correctly requires the proper model. Therefore, three models (the linear flow model, the dual porosity model, and the triple porosity model will be studied and compared to provide the correct interpretation guidelines for these models.

In this study, three types of model are considered and compared to analyze the production data of a shale gas/oil reservoir. The first model is the transient linear homogeneous flow which was firstly proposed to analyze a tight gas reservoir by Wattenbarger and El-Banbi (1998). The second model is the transient linear dual porosity model given by El-Banbi (1998) and is applied to multi-transverse hydraulic fractures horizontal well by Bello (2009). The last model is the fully transient linear triple porosity model proposed by Al-Ahmadi and Wattenbarger (2011).

1.1 Objectives

The main objective of this research is to develop the analytical solutions and interpretation guidelines in order to interpret production data of shale gas/oil reservoirs effectively. Verification and derivation of asymptotic equations and associated equations from Laplace space for dual porosity and triple porosity models are required in order to generate analysis equations. With the interpretation guidelines, various analysis equations for different flow periods or different physical properties are guided to use with caution. From the examples of interpretation, the possible errors are presented.

1.2 Organization of Work

This thesis is divided into ten chapters as follows.

Chapter I is introduction and objectives of the thesis.

Chapter II is the literature review of the linear homogeneous flow model, the dual porosity model, and the triple porosity model.

Chapter III shows the application of linear homogeneous flow solution to interpret the production data of shale gas and oil reservoirs in multi-transverse hydraulic fractures horizontal well and the example of production data analysis.

Chapter IV shows the theory and associated equations of linear dual porosity model in order to interpret shale gas and oil reservoirs. Furthermore, the dual porosity model with the assumption of infinite conductivity hydraulic fractures are presented and compared with the homogeneous linear flow model.

Chapter V shows interpretation guidelines and examples of interpretation of shale gas and oil reservoirs in multi-transverse hydraulic fractures horizontal well by using transient linear dual porosity model.

Chapter VI shows the theory and associated equations of the fully transient triple porosity model in order to interpret shale gas and oil reservoirs. New 12 flow regions and model characteristic of the triple porosity model are presented.

Chapter VII describes the mathematical model and solutions of the triple porosity model with infinite conductivity of hydraulic fractures and also compares it with the modified dual porosity model.

Chapter VIII shows interpretation guidelines and examples of interpretation of shale gas and oil reservoirs in multi-transverse hydraulic fractures horizontal well when assuming infinite conductivity hydraulic fractures by using the triple porosity model.

Chapter IX shows interpretation guidelines and examples of interpretation by using both the transient dual porosity model and the fully transient triple porosity model with the assumption of infinite conductivity hydraulic fractures.

Chapter X is conclusions and recommendations.

CHAPTER II

LITERATURE REVIEW

This chapter shows the literature review of linear homogeneous flow, dual porosity model, and triple porosity model in terms of theory and application to multi-transverse hydraulic fractures in horizontal shale gas and oil well.

2.1 Linear Homogeneous Flow

Linear Flow solutions in rectangle of constant pressure case were firstly adapted into fractured tight gas reservoir wells to analyze production data by Wattenbarger and El-Banbi (1998). It is indicated that the linear flow type curve for constant pressure and constant rate cases are difference. End of linear flow or end of half-slope line is specified as $t_{Dye} = 0.5$ for constant rate case and $t_{Dye} = 0.25$ for constant pressure case. Integrating of slope of square root of time plot and end of the half-slope line in log-log plot of constant pressure case to interpret production data are introduced and utilized to analyze in-place without assuming thickness, matrix permeability and porosity.

Then, Arevalo-Villagram et al. (2001) showed the production analysis of long term linear flow in tight gas wells. It is believed that the production data of tight gas well shows transient linear flow for long time because this linear is represented by the flow from matrix to high permeability of fractures.

Ibrahim and Wattenbarger (2005) showed the effect of drawdown on transient linear flow of gas and proposed the correction factor according to the level of drawdown

in constant pressure condition. Correspondingly, the mathematical solution of tight gas well is presented by integrating the slope in square root of time plot equation and time end of transient linear flow period with the correction factor.

After that, the transient linear flow is used as a tool to analyze multi-transverse hydraulic fractures in horizontal well.

2.2 Dual Porosity Model

Analytical model of naturally fractured reservoirs which is defined by dual porosity model was firstly introduced in petroleum field by Warren and Root (1963). Warren and Root showed the analytical solution of natural fractured radial infinite-acting reservoir in Laplace space and approximation in real domain. The model is assumed as an idealized sugar cube model with pseudo-steady state flow in matrix system. The solution is applied for pressure transient testing of reservoir composing two mediums which have distinct properties, e.g. a naturally fractured or vugular reservoir. In the naturally fractured system, the primary porosity is matrix system which is high storativity and low flow capacity and the second porosity is fracture system which low storativity and high flow capacity. The liquid flow to the well is assumed occurring in fractures only and matrix feeds liquid to the fractures. Importantly, they presented two dimensionless parameters, ω and λ, which is sufficient to characterize the reservoir model. ω is represented the storativity of the fracture system. λ is related to the heterogeneity of flow capacity of two mediums. After that, Da Prat et al. (1981)

proposed type curves of dual porosity system based on the model presented Warren and Root (1963) for constant pressure case in both infinite and closed systems.

Kazemi (1969) proposed a matrix transient flow model of dual porosity model by using numerical solution. The model is represented by slab matrix and horizontal fracture model of radial closed reservoir which is composed of logarithmic grid size for matrix layers and a thin layer of fracture. The result shows that the new transient dual porosity and pseudo-steady state dual porosity models give the similar result except the transition period in the semi-log plot for both drawdown and buildup test.

De Swaan-O (1976) developed the analytical solution of radial infinite naturally fractured reservoir for both early and late time regions. The model assumes transient flow from the matrix system to fracture system. The result shows two parallel straight lines with analytical descriptions. There is no analytical description of the transition period between two straight lines.

Lai et al. (1983) proposed transient flow solution between matrix and fracture system of 3-D case by considering of three sets of orthogonal fractures. Matrix block is represented by a cube and the flow in cubes can be approximated by one-dimensional basic model or represented by one-sixth of a cube. Radial system is defined the fluid flow from the system into the well. Laplace solution of three outer boundary conditions (infinite, closed, and constant-pressure boundary) and asymptotic solutions for early and late time were presented.

Serra et al. (1983) proposed the analytical solution of dual porosity model in Laplace space and approximation in real domain. The model assumes the radial infinite

slab reservoir with equally spacing horizontal fractures same as De Swaan-O (1976) and transient flow in matrix model. Three flow regimes were introduced. Regime 1 and 3 are the classical two straight lines in semi-log plot. Regime 2 was introduced to represent the transition between two straight lines.

Chen et al. (1985) used the model of Kazemi (1969) and De Swaan-O (1976) but considered in closed reservoir. The model shows five possible flow regimes in drawdown data which is extended from three flow regimes proposed by Serra et al. (1983). From previous infinite reservoir, flow regime 1 is represented transient in fractures, flow regime 2 is represented transient in both fractures and matrix, flow regime 3 is represented transient in fractures and PSS in matrix by presence of no-flow boundary at the center line of matrix. From the existing of bound reservoir, two new flow regimes and the condition of whether regime 3 or 4 will be found are also presented. Flow regime 4 is represented transient in matrix and PSS condition in hydraulic fractures and flow regime 5 occurs when flow affects from both matrix and fracture boundaries.

Ozkan et al. (1987) presented the five possible flow regimes and their asymptotic equations of the vertical well penetrating the cylindrical closed boundary fractured reservoir and producing under constant pressure condition. The analytical solution in Laplace space for both infinite and closed boundary reservoir and associated asymptotic equations are presented based on transient radial system.

Previously, all the models are represented for radial reservoir system. Then, the dual porosity model for a linear flow was firstly presented by El-Banbi (1998). New

analytical solution of linear flow includes four different inner boundary conditions (constant rate, constant pressure, constant rate with WBS and skin, and constant pressure with skin) and three different outer boundary conditions (infinite reservoir, closed reservoir, and constant pressure outer boundary reservoir). The five different reservoir models were also proposed (homogeneous, PSS, transient slabs, transient match-sticks, and transient cubs). It is also showed that the reservoir function, $f(s)$, that is used in Laplace space is the same for both radial and linear systems. In addition, linear flow and bilinear flow which are a half-slope line and a quarter-slope line, respectively in the log-log plot were introduced.

Normally, dual porosity model was intentionally used in naturally fractured reservoir. Later, dual porosity model has been adapted to use for a fractured well and multi-transverse hydraulic fractures in horizontal well which have two different storage and flow capacity. In this case, the second porosity is characterized by hydraulic fractures.

Bello and Wattenbarger (2008), Bello (2009), Bello and Wattenbarger (2009), and Bello and Wattenbarger (2010) presented a mathematical model for analyzing the multi-transverse hydraulic fractures in horizontal shale gas well. This model is based on linear dual porosity model given by El-Banbi (1998). Five flow regions and their asymptotic equations are presented by solving analytical solution in Laplace space for both constant rate and constant pressure inner boundary cases. Nevertheless, only region 4 equation is used to analyze the long term linear line in production data because it is believed that the long term linear flow in production data is represented by transient

drainage from matrix to fractures. Also, it is showed that the transient linear homogeneous flow and the region 4 of transient dual porosity model exhibit the same response. Furthermore, a skin effect for region 4 is observed from the unanticipated early production curve that does not exhibit a linear flow behavior. As a result, the new mathematical solution included skin effect of region 4 of linear dual porosity was proposed and a procedure to analyze the field data.

Al-Ahmadi et al. (2010) presented an application of linear flow analysis to multiple hydraulic fractures in horizontal shale gas wells in constant well flowing pressure case. Two linear dual porosity models are proposed. One is a transient slab model. The other is a transient cube model. The second model assumes the natural fracture system have created after proceeding hydraulic fracture treatment. The mathematical solution applies the in-place equation incorporated linear flow region 4 equation and time end of transient linear flow period given by Ibrahim and Wattenbarger to the two models.

Samandarli et al. (2011a and 2011b) applied the regression method to history match the production data of multi-transverse hydraulic fractures in horizontal shale gas well by using the solutions given by Bello and Wattenbarger (2010).

2.3 Triple Porosity Model

The triple porosity model is the model composed of three distinct property mediums. Triple porosity model can be used to represent one fracture system and two matrix systems which have different properties or one matrix system and two fracture

systems which have different properties. The triple porosity model was firstly introduced to the petroleum field by Abdassah and Ershaghi (1986). Two geometrical configurations are used for investigation which are strata model and uniformly distributed blocks model. The transient flow solution in fracture system and two matrix systems with distinct properties are assumed in both models. Strata-type model is represented by the horizontal matrix layers separated by fractures. While uniformly distributed blocks model is based on the basic model of Lai et al. (1983).

Jalali and Ershaghi (1987) extended the Abdassah and Ershaghi (1986) model. This model, each matrix system (from two distinct properties) has own porosity, permeability, total compressibility, thickness, and flow regime which is either PSS or transient flow.

Cinco-Ley and Meng (1988) introduced the analytical solution in Laplace space and the approximation solution of the trilinear flow (exhibits 1/8 slope in a log-log plot) from the model of finite conductivity vertical fractures in dual porosity reservoirs. Two matrix flow models which are transient matrix linear flow and pseudo steady state matrix linear flow were also presented.

Al-Ghamdi and Ershaghi (1996) introduced the triple porosity model with one matrix system and dual fracture system to differentiate between microfractures and macrofractures in radial system. Two models were proposed. One is modified from Abdassah and Ershaghi (1986) model. The other is subdivided into two sub models – flow to the well comes from macrofractures only and flow to the well comes from both macro and microfractures. Liquid flow is assumed to be sequential which is matrix feeds

liquid to microfractures and microfractures feeds liquid to macrofractures and the flow between the two fracture systems and between the matrix and the microfracture systems are PSS.

Liu et al. (2003) proposed a tri-continuum medium consisting of fractures, rock matrices, and lithophysal cavities. The model defines radial flow to well occurs through the homogeneous fracture while matrices and cavities supply fluid to the fractures. The interporosity flow is assumed to be PSS condition.

Wu et al. (2007) offered analytical approach in naturally fractured vuggy reservoirs based on triple-continuum model (Liu et al. 2003) which is consisting of large fractures feed the well with radial flow, various sized vugs which are locally connected to fractures, and rock matrix which is locally connected to fractures and/or vugs. PSS flow condition is used for flow between continuums.

Ozkan et al. (2009) and Brown et al. (2009) introduced a trilinear-flow model to interpret fractured horizontal well in unconventional reservoir. The model includes linear flows in three connecting flow regions which are the outer reservoir, the inner reservoir between fractures, and the hydraulic fracture. The analytical model is presented in Laplace space and approximation asymptotic equations. The inner reservoir can be identified as homogeneous, PSS dual porosity model, or transient dual porosity model by using $f(s)$.

Leguizamon and Aguilera (2011) presented the method for optimizing hydraulic fracturing design in naturally fractured tight gas by using 3D fracture simulation. The analytical solution is recommended to acquire preliminary estimation of key parameters.

Al-Ahmadi and Wattenbarger (2011) proposed a new triple porosity model for fractured horizontal wells in naturally fractured reservoir. The model is composed of three contiguous porous mediums with the sequential flow. Matrix feeds natural fractures and natural fractures feed hydraulic fractures and only hydraulic fractures produce to the well. The new solutions are derived in Laplace space for linear reservoir with 4 sub models based on the interporosity flow assumption between mediums – fully transient model, mixed transient and PSS models, and fully PSS model. Model 1 (fully transient model) is used to analyze multi-transverse hydraulic fractures in shale gas horizontal wells by using non-linear regression.

2.4 Quadruple Porosity Model

In 2004, Dreier et al. (2004) firstly proposed a quadruple-porosity model consisting of a triple-fracture network and a single-matrix system. The model was developed in the Laplace space for a laterally infinite slab reservoir. Three types of fracture systems are composed of microfractures, macrofractures, and megafractures. While microfractures have the most dense and lowest conductivity, megafractures have the largest spacing and highest conductivity. The model assumes anisotropic in megafractures and isotropic in micro and macrofractures. The paper presented two sub models – sequential-feed model and simultaneous-feed model. Only fluid from megafractures flows to the wellbore while matrix feeds fluid to microfractures and microfractures feed liquid to macrofractures and macrofractures feed liquid to the megafractures in sequential-feed model. For simultaneous-feed model, only change from

sequential-feed model is matrix can produce to both micro and macrofractures and both micro and macrofractures can feed to megafractures. Flow is assumed to be radial in megafractures while flow is assumed to be linear in microfractures and macrofractures. Furthermore, it is assumed that flow between fractures is transient condition while flowing of fracture-matrix is PSS condition.

2.5 SRV

The Stimulated Reservoir Volume (SRV) is the drainage area of the hydraulic fractured horizontal well. In this study, SRV is defined as rectangular geometry limited to the hydraulic fractures half-length and effective wellbore drainage length. Also, it is assumed that the production of ultra-low permeability reservoirs will come from inside the SRV only. This assumption is confirmed in many petroleum literatures. It is noted that the Compound Linear Flow (CLF) or Compound Formation Linear (CFL) is the fluid flow from non-stimulated volume in direction of perpendicular to the vertical well plain.

Ozkan et al. (2009) used analytical solution of trilinear flow model and showed that the effect of outside SRV will not affect the production during the life of the well with practical matrix permeability of unconventional reservoir.

Luo et al. (2010) used streamline simulation and observed that CFL straight line slope on log-log reciprocal rate derivative plot depends on the ratio of fracture length ($2x_f$) over fracture spacing. However, the starting time of CFL is sensitive to reservoir permeability and delays when reservoir permeability decreases.

Anderson et al. (2010) found that the amount of contribution outside SRV depends on the matrix permeability and the interface area between SRV and non-stimulated reservoir. It is showed that with matrix permeability of 1e-6 md, the effect of outside SRV shows around 230 years after production and with matrix permeability of 1e-4 md, the contribution outside SRV appears around 2 years.

Samandarli et al. (2011a) used the reservoir simulation model of typical shale gas well to prove the assumption of no flow outside SRV. The result shows that CLF will not occur in 30 years for matrix permeability less than 5E-5 md.

Nobakht (2011) found that the contribution from the region outside SRV starts at t_{Dxf} = 0.01. This means that the time that outside SRV starts contribute depends on reservoir properties and length of fracture and is independent of outer reservoir boundary and fracture spacing.

CHAPTER III

LINEAR HOMOGENEOUS FLOW MODEL

3.1 Introduction

In this chapter, the application of linear homogeneous flow solution to interpret the production data of shale gas and oil reservoirs in multi-transverse hydraulic fractures horizontal well is reviewed and summarized. Also, the example of production data analysis by using linear flow is presented.

3.2 Mathematical Model

The model that uses to represent linear flow behavior of the multi-transverse hydraulic fractures horizontal well is shown in **Figure 1**. A horizontal well with multi-transverse hydraulic fractures is defined by the rectangular model of Stimulated Reservoir Volume (SRV) which is limited by uniform hydraulic fracture half-length, y_e, and effective perforated well length, x_e. Matrix blocks are assumed to be uniform and idealized as slab. In this case, the hydraulic fractures are assumed to be infinite conductivity; therefore, only linear flow from matrix to hydraulic fractures is considered.

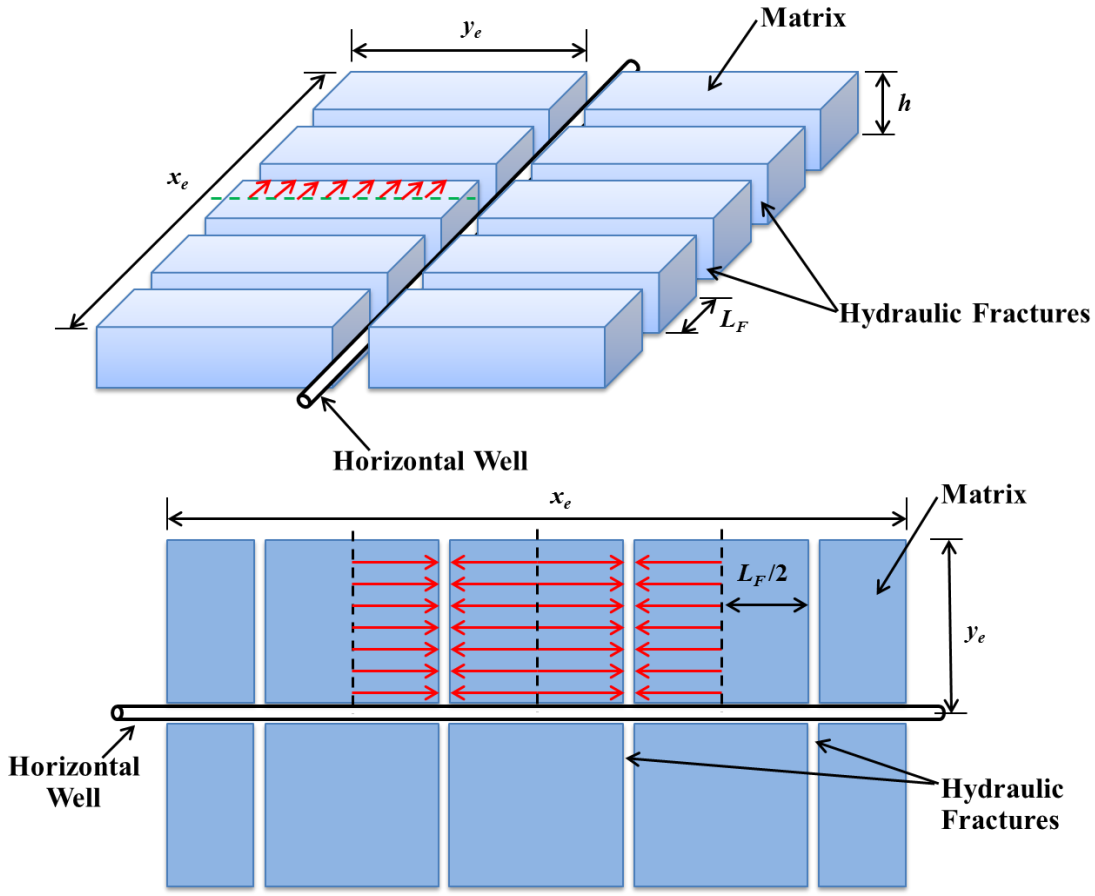

Figure 1 – Sketch of homogeneous linear flow in multi-transverse hydraulic fractures horizontal well.

3.3 Modified Mathematical Solutions of Homogeneous Linear Flow

As discussed in the literature review, linear flow solution was originally applied to tight gas fractured reservoir based on Wattenbarger and El-Banbi (1998). To apply the equations to multi-transverse hydraulic fractures horizontal well, the definition of parameters have to be modified. The derivation is shown in **Appendix A** and the summary of equations for constant pressure case is given.

$$\sqrt{k_m}\, y_e n_F = \frac{315.4T}{h\sqrt{(\phi\mu c_t)_i}} \frac{1}{m_{square}} \quad \text{..... (3. 1)}$$

$$\sqrt{k_m}\, y_e n_F = \frac{31.3B\sqrt{\mu}}{h\sqrt{(\phi c_t)_i}} \frac{1}{m_{square}} \quad \text{..... (3. 2)}$$

$$\frac{L_F}{2} = 0.159\sqrt{\frac{k_m t_{esr}}{(\phi\mu c_t)_i}} \quad \text{..... (3. 3)}$$

$$V_{p,g}(scf) = \frac{200.6T}{(\mu c_t)_i} \frac{1}{m_{square}} \sqrt{t_{esr}} \quad \text{..... (3. 4)}$$

$$V_{p,o}(scf) = \frac{19.9B}{c_{ti}} \frac{1}{m_{square}} \sqrt{t_{esr}} \quad \text{..... (3. 5)}$$

3.4 Interpretation Guidelines

The interpretation of homogeneous linear flow solution focuses only for linear flow from matrix block to hydraulic fractures. The flow in hydraulic fractures is not considered because of assuming infinite conductivity of hydraulic fractures. Therefore, the bilinear flow (considering flow in hydraulic fractures) or a quarter slope of log-log plot that shows in the production profile cannot be interpreted by homogeneous linear flow solution. Furthermore, from the industrial practice that producing at constant wellhead pressure; the constant pressure solutions are applied.

Two production scenarios and interpretation guidelines are given.

3.4.1 Only linear flow period is found

- k_m has to be known

- y_e can be found from the slope of the square root of time plot, m_{square}. The equations of gas and oil are given, respectively by

$$y_e = \frac{315.4T}{hn_F\sqrt{k_m}\sqrt{(\phi\mu c_t)_i}}\frac{1}{m_{square}} \quad \text{..... (3. 6)}$$

$$y_e = \frac{31.3B\sqrt{\mu}}{hn_F\sqrt{k_m}\sqrt{(\phi c_t)_i}}\frac{1}{m_{square}} \quad \text{..... (3. 7)}$$

- In-place can be calculated from volumetric equation.
- In case there is high uncertainty about the value of k_m, it is recommend to calculate the minimum hydraulic fracture half-length, $y_{e,min}$. $y_{e,min}$ can be calculated from the last point, t_{end} and slope of the square root of time plot.

$$y_{e,min} = \frac{100.3T}{hx_e\,(\phi\mu c_t)_i}\frac{\sqrt{t_{end}}}{m_{square}} \quad \text{..... (3. 8)}$$

$$y_{e,min} = \frac{9.95B}{hx_e\,(\phi c_t)_i}\frac{\sqrt{t_{end}}}{m_{square}} \quad \text{..... (3. 9)}$$

3.4.2 Linear and BDF periods are found

- y_e can be calculated from the end of straight line of the square root of time plot, t_{esr} and slope of the square root of time plot, m_{square}.

$$y_e = \frac{100.3T}{hx_e\,(\phi\mu c_t)_i}\frac{\sqrt{t_{esr}}}{m_{square}} \quad \text{..... (3. 10)}$$

$$y_e = \frac{9.95B}{hx_e\,(\phi c_t)_i}\frac{\sqrt{t_{esr}}}{m_{square}} \quad \text{..... (3. 11)}$$

- k_m can be calculated from t_{esr}, as given by

$$k_m = 9.89\ \frac{L_F^2(\phi\mu c_t)_i}{t_{esr}} \quad \text{..... (3. 12)}$$

- In-place can be calculated from volumetric equation.

3.5 Application to Field Example

Field production plot and data of the multi-transverse hydraulic fractures horizontal well, well#314, is shown in **Appendix B**. In this interpretation, skin effect and gas adsorption are neglected.

To analyze production data of this well, interpretation guidelines of the production scenario case 2 (Linear and BDF periods are found) are used.

From **Eq. 3.10**, y_e is 186 ft.

From **Eq. 3.12**, k_m is 1.3E-4 md.

$$OGIP = 2x_e y_e h\phi(1 - s_w)/B_{gi} \quad \text{..... (3. 13)}$$

$OGIP$ is 2.7 Bscf

CHAPTER IV

LINEAR TRANSIENT DUAL POROSITY MODEL

4.1 Introduction

In this chapter, the linear transient dual porosity model proposed by El Banbi (1998) is investigated to consider as a tool using interpret the production data of shale gas and oil reservoirs in multi-transverse hydraulic fractures horizontal well. Previously, this linear dual porosity model has already been studied and applied for shale gas well by Bello (2009). Also, five regions and the asymptotic equations have been presented. Furthermore, the dual porosity model with the assumption of infinite conductivity hydraulic fractures are presented and compared with the homogeneous linear flow model.

In this work, the theory of linear dual porosity model to interpret shale gas and oil reservoirs is reviewed and summarized. Moreover, the mathematical model of the asymptotic equations is re-derived systematically to fit the purpose of finding conditions and periods of each region. The characteristic of the dual porosity model is presented clearly with the specific conditions.

4.2 Mathematical Model

The dual porosity model that uses to represent flow behavior of the multi-transverse hydraulic fractures in horizontal well is shown in **Figure 2**. Same as linear homogeneous flow model, a horizontal well with multi-transverse hydraulic fractures is

defined by the rectangular SRV and matrix blocks are assumed to be uniform and idealized as slab. In this case, the hydraulic fractures have finite conductivity; therefore, the bilinear flow which is combining transient linear flow from matrix to hydraulic fractures and hydraulic fractures to well is considered. Two transient linear flows of hydraulic fractures and matrix are considered as well.

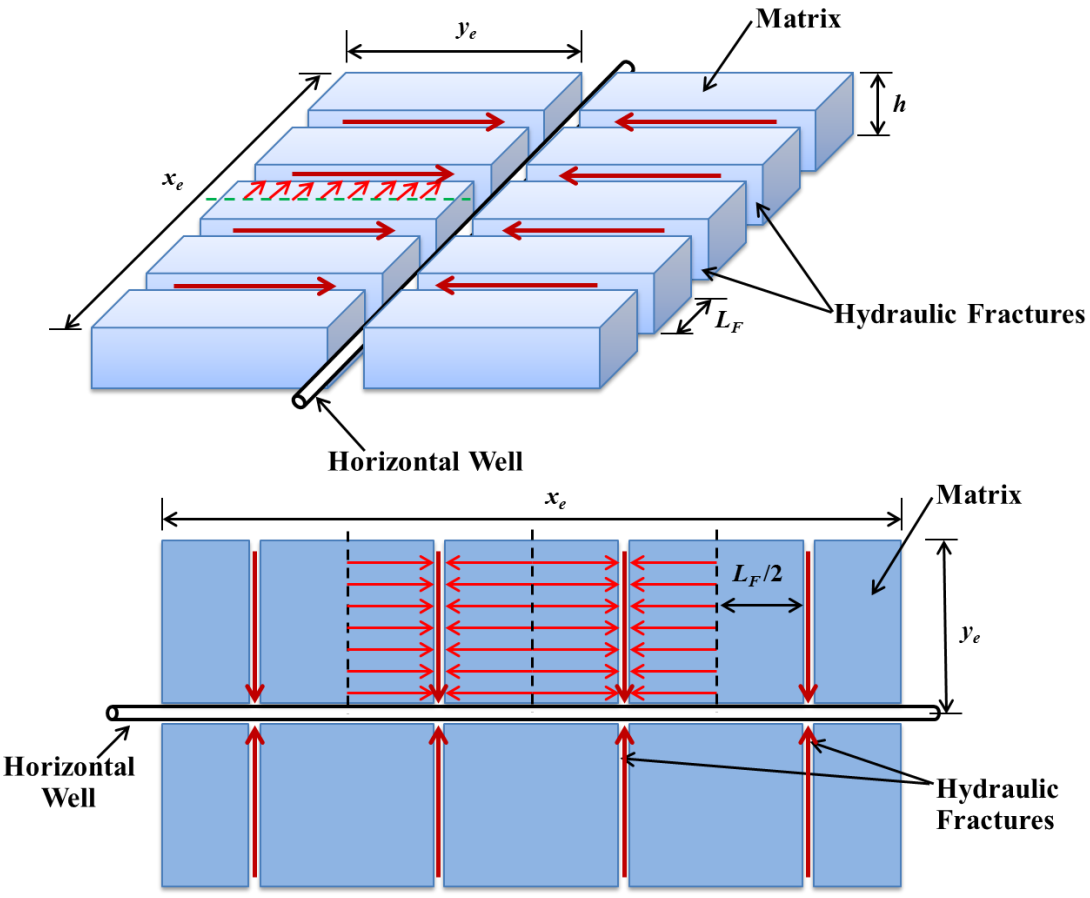

Figure 2 – Sketch of dual porosity model in multi-transverse hydraulic fractures horizontal well.

4.3 Dimensionless Variables Definition

Referring to Warren and Root (1963), dual porosity model can be identified by two dimensionless variable, λ and ω. In this study, the definition of these two variables and other dimensionless variables are modified as given.

$$\lambda_{Fm} = \frac{12 k_m A_{cw}}{L_F^2 k_F} \quad \text{..... (4. 1)}$$

$$\omega_F = \frac{(\phi V c_t)_F}{(\phi V c_t)_T} = \frac{(\phi V' c_t)_F}{(\phi V' c_t)_T} \quad \text{..... (4. 2)}$$

where

$$[\phi V' c_t]_T = (\phi V' c_t)_F + (\phi V' c_t)_m \quad \text{..... (4. 3)}$$

and

$$V_x' = \frac{V_x}{V_F + V_m} \quad \text{..... (4. 4)}$$

$$y_{eD} = \frac{y_e}{\sqrt{A_{cw}}} \quad \text{..... (4. 5)}$$

where

$$A_{cw} = 2 \times x_e \times h = 2 \times n_F \times L_F \times h \quad \text{..... (4. 6)}$$

$$q_{DL} = \frac{1422 q_g T}{k_F \sqrt{A_{cw}} \Delta m(p)} \quad \text{..... (4. 7)}$$

$$q_{DL} = \frac{141.2 q_o B \mu}{k_F \sqrt{A_{cw}} \Delta p} \quad \text{..... (4. 8)}$$

$$t_{DAcw} = \frac{0.00633\ k_F}{[\phi V' c_t]_T \mu A_{cw}} t \quad \text{..... (4. 9)}$$

In case, $c_{t,F} = c_{t,m}$,

$$t_{DAcw} = \frac{0.00633\ k_F}{\phi_T c_t \mu A_{cw}} t \quad \text{..... (4. 10)}$$

where

$$\phi_T = \frac{\phi_F V_F + \phi_m V_m}{V_F + V_m} \quad \text{..... (4. 11)}$$

4.4 Mathematical Solution and Approximation (Dimensionless)

In this study, it is based on the linear transient dual porosity model proposed by El-Banbi (1998). The mathematical derivation details of the model are shown in **Appendix C**. Bello (2009) showed five possible regions to represent the linear transient dual porosity model. The asymptotic equation of each region (region 1 – 4) has also been derived; however, the derivation is not a systematic approach. Therefore, the asymptotic equations were re-derived to fit the purpose of finding conditions and periods of each region. The completed derivations of re-derived asymptotic equation and periods of each region, and also condition of possible region are presented in **Appendix D**.

4.4.1 Asymptotic Equations

From constant pressure inner boundary and closed outer boundary, the Laplace solution is given by

$$\frac{1}{\overline{q_{DL}}} = \frac{2\pi u}{\sqrt{uf(u)}} \coth\left(\sqrt{uf(u)}\, y_{eD}\right) \quad \text{..... (4. 12)}$$

For transient slab model,

$$f(u) = \omega_F + \sqrt{\frac{\lambda_{Fm}}{3u}(1-\omega_F)} \tanh\left(\sqrt{\frac{3u}{\lambda_{Fm}}(1-\omega_F)}\right) \quad \text{..... (4. 13)}$$

The asymptotic equations are derived from the assumption of approximation terms in Laplace space. The summary of the assumptions and the asymptotic equations of the four regions in constant pressure case are shown in **Table 1**.

Table 1 - Assumptions and final asymptotic equations region 1 – 4 of the transient linear dual porosity model (constant pressure)

Region	Estimated Terms			Asymptotic Equations
	$\overline{q_{DL}}$	$f(u)$		
	$\coth\left(\sqrt{uf(u)}\, y_{eD}\right)$	ω_F	$\tanh\left(\sqrt{\frac{3u}{\lambda_{Fm}}(1-\omega_F)}\right)$	
1	1	ω_F	-	$q_{DL} = \frac{\sqrt{\omega_F}}{2\pi\sqrt{\pi}} \frac{1}{\sqrt{t_{DAcw}}}$
2	1	-	1	$q_{DL} = \frac{\lambda_{Fm}^{1/4}}{10.133} \frac{1}{t_{DAcw}^{1/4}}$
3	1	-	$\sqrt{\frac{3u}{\lambda_{Fm}}(1-\omega_F)}$	$q_{DL} = \frac{1}{2\pi\sqrt{\pi}} \frac{1}{\sqrt{t_{DAcw}}}$
4	$\frac{1}{\sqrt{uf(u)}\, y_{eD}}$	-	1	$q_{DL} = \frac{y_{eD}}{2\pi\sqrt{\pi}} \sqrt{\frac{\lambda_{Fm}}{3}} \frac{1}{\sqrt{t_{DAcw}}}$

4.4.2 Conditions and Periods of Dual Porosity Characteristic

For transient linear dual porosity model in closed boundary, only three dimensionless parameters, λ_{Fm}, ω_F, and y_{eD}, control the curve characteristic. In this study, one sensitivity set with 5 cases was run to see the curve characteristic of dual porosity. The value of λ_{Fm} and ω_F are fixed at 1E-5 and 1E-3, respectively. The sensitivity run is played with the value of y_{eD} which is $y_{eD} = 1$, $y_{eD} = 17.32$, $y_{eD} = 100$, $y_{eD} = 547.72$, and $y_{eD} = 5000$ for run 1 – 5, respectively. All of the runs (5 runs) are shown that each region has their specific conditions to happen except region 1 which can be seen in any run. From this sensitivity set, dual porosity can be defined by 5 characteristic curves as shown in **Figure 3**. The characteristic of dual transient porosity curve can be defined by 5 conditions in term of y_{eD} as follows.

1. $y_{eD} < \sqrt{\frac{3\omega_F}{\lambda_{Fm}}}$, region 1 and 4 are observed
2. $y_{eD} = \sqrt{\frac{3\omega_F}{\lambda_{Fm}}}$, region 1 and 4 are observed
3. $\sqrt{\frac{3\omega_F}{\lambda_{Fm}}} < y_{eD} < \sqrt{\frac{3}{\lambda_{Fm}}}$, region 1, 2, and 4 are observed
4. $y_{eD} = \sqrt{\frac{3}{\lambda_{Fm}}}$, region 1 and 2 are observed
5. $y_{eD} > \sqrt{\frac{3}{\lambda_{Fm}}}$, region 1, 2, and 3 are observed

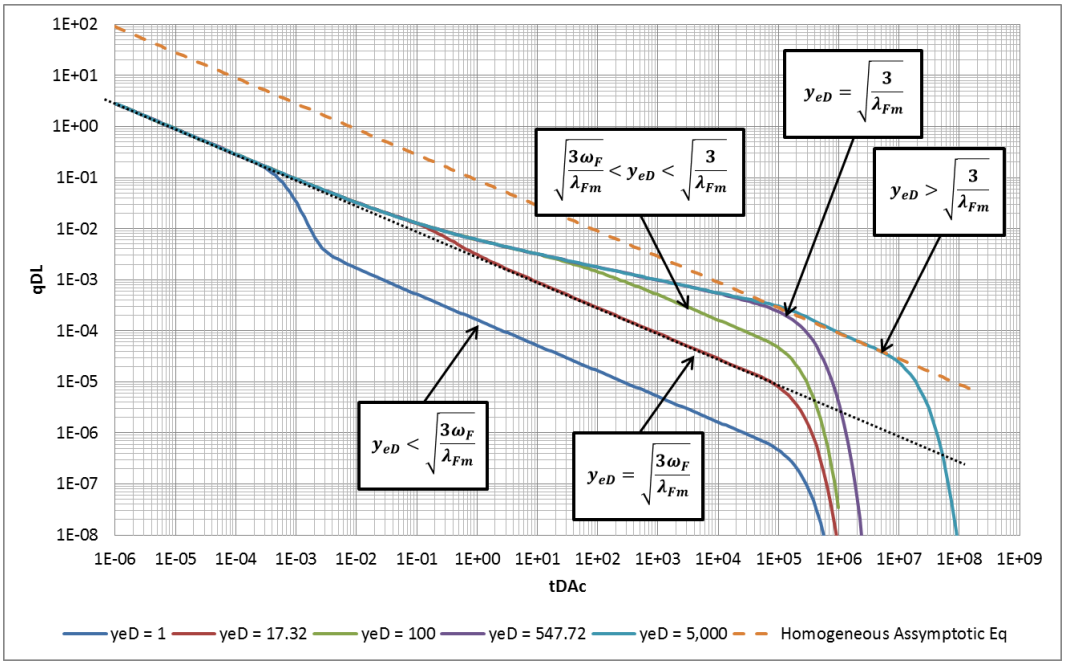

Figure 3 – Characteristic curves of transient linear dual porosity model with closed boundary in dimensionless form

From the assumptions of each asymptotic equation and check with the sensitivity run case, some of starting time and end time of each region in constant pressure case can be determined as following.

Region 1 – The end of region 1 is at $t_{DAcw} \cong \frac{y_{eD}^2\,\omega_F}{2^2}$ only when $y_{eD} < \sqrt{\frac{3\omega_F}{\lambda_{Fm}}}$.

Region 2 – The end of region 2 is at $t_{DAcw} \cong \frac{y_{eD}^4\,\lambda_{Fm}}{2^4 \times 3}$ only when $\sqrt{\frac{3\omega_F}{\lambda_{Fm}}} < y_{eD} < \sqrt{\frac{3}{\lambda_{Fm}}}$ and the end of region 2 is at $t_{DAcw} \cong \frac{3}{2^2\lambda}$ only when $y_{eD} > \sqrt{\frac{3}{\lambda_{Fm}}}$.

Region 3 – The start and the end of region 3 is at $t_{DAcw} \cong \frac{3}{\lambda_{Fm}}$ and $t_{DAcw} \cong \frac{y_{eD}^2}{2^2}$, respectively.

Region 4 – The start of region 4 is at $t_{DAcw} \cong \frac{y_{eD}^4 \lambda_{Fm}}{3}$ only when $\sqrt{\frac{3\omega_F}{\lambda_{Fm}}} < y_{eD} < \sqrt{\frac{3}{\lambda_{Fm}}}$ and the end of region 4 is at $t_{DAcw} \cong \frac{3}{2^2 \lambda_{Fm}}$.

4.5 Mathematical Solution and Approximation (Dimensional)

To make it practical, the dimensional parameter should be used for understanding the physical meaning and interpretation. The asymptotic equations of gas and oil for analysis are showed in **Table 2** and **Table 3**, respectively. The physical meaning of each region has been described by Bello (2009). However, region 3 is always described by the homogeneous reservoir. Actually, region 3 is considered as transient linear flow of total system which is dominated by hydraulic fractures flowing to the well. Therefore, all the regions are summarized as followings.

4.5.1 Region 1

This region represents the early linear flow period of the transient dual porosity model. This region is showed in the first half slope of the log-log plot. This linear flow behavior represents the transient linear flow in the hydraulic fractures producing fluid to the well. With the high conductivity hydraulic fractures, the transient period is expected to be very short and impossible to see in daily production data.

4.5.2 Region 2

This region represents the bilinear flow of the dual porosity model. This region is showed in a quarter slope of the log-log plot. This bilinear flow is formed by occurring two transient linear flows simultaneously which are transient linear flows in hydraulic fracture system (from hydraulic fractures to wellbore) and matrix system (from matrix blocks to hydraulic fractures). This occurs while the transient flow dominated period in hydraulic fractures has not ended while the transient flow dominated period in matrix still appears. This region will not happen when infinite conductivity of hydraulic fractures is considered.

4.5.3 Region 3

This region presents the late linear flow period of the dual porosity model. It shows a half slope line in the log-log plot. It represents the transient linear flow of total system which is dominated in hydraulic fractures. This occurs when the transient flow in matrix has ended while transient flow in hydraulic fractures still presents. This case will happen only when the conductivity of hydraulic fractures is very low comparing with flow capacity of matrix.

4.5.4 Region 4

This region presents the late linear flow period of the dual porosity model. It shows a half slope line in the log-log plot. It represents the transient linear flow of total system which is dominated in matrix, while the transient flow in hydraulic fractures is

already end. This case will happen when $\frac{y_e}{L_F} < \frac{1}{2}\sqrt{\frac{k_F}{k_m}}$ or conductivity of hydraulic fractures is quite high comparing with flow capacity of matrix.

4.5.5 Region 5

This region expresses the BDF or declined period of the dual porosity model that all boundaries are dominated and the influence of transient periods of both hydraulic fractures and matrix have faded. The boundary is defined by the SRV and the artifact no-flow boundary (interference effect) between hydraulic fractures.

Table 2 – Asymptotic equations of dual porosity model for gas analysis in dimensional (constant pressure)

Region	Asymptotic Equation for Gas Analysis
1 – 1st Linear	$q_g = \frac{\Delta m(p)}{1260T} A_{cw}\sqrt{k_F}\sqrt{\mu(\phi V' c_t)_F}\frac{1}{\sqrt{t}}$
2 – 1st Bilinear	$q_g = \frac{\Delta m(p)}{2183.7T} A_{cw} k_F^{1/2} k_m^{1/4}\frac{1}{\sqrt{L_F}}[\mu(\phi V' c_t)_T]^{1/4}\frac{1}{t^{1/4}}$
3 – Infinite-acting	$q_g = \frac{\Delta m(p)}{1260T} A_{cw}\sqrt{k_F}\sqrt{\mu(\phi V' c_t)_T}\frac{1}{\sqrt{t}}$
4 – 2nd Linear	$q_g = \frac{\Delta m(p)}{630T} A_{cw}\sqrt{k_m}\frac{y_e}{L_F}\sqrt{\mu(\phi V' c_t)_T}\frac{1}{\sqrt{t}}$

Table 3 – Asymptotic equations of dual porosity model for oil analysis in dimensional (constant pressure)

Region	Asymptotic Equation for Oil Analysis
1 – 1st Linear	$q_o = \frac{\Delta p}{125.1B\sqrt{\mu}} A_{cw}\sqrt{k_F}\sqrt{(\phi V' c_t)_F}\frac{1}{\sqrt{t}}$
2 – 1st Bilinear	$q_o = \frac{\Delta p}{216.8B}\frac{1}{\mu^{3/4}} A_{cw} k_F^{1/2} k_m^{1/4}\frac{1}{\sqrt{L_F}}[(\phi V' c_t)_T]^{1/4}\frac{1}{t^{1/4}}$
3 – Infinite-acting	$q_o = \frac{\Delta p}{125.1B\sqrt{\mu}} A_{cw}\sqrt{k_F}\sqrt{(\phi V' c_t)_T}\frac{1}{\sqrt{t}}$
4 – 2nd Linear	$q_o = \frac{\Delta p}{62.55B\sqrt{\mu}} A_{cw}\sqrt{k_m}\frac{y_e}{L_F}\sqrt{(\phi V' c_t)_T}\frac{1}{\sqrt{t}}$

The condition of dual porosity that is considered in this study is the criteria of whether region 3 or region 4 appears ($y_{eD} = \sqrt{\frac{3}{\lambda_{Fm}}}$) because the possible linear flow that shows in production data is believed to be either region 3 or region 4. The criteria of existing either region 3 or region 4 in dimensional is given by

$$\frac{y_e}{L_F} = \frac{1}{2}\sqrt{\frac{k_F}{k_m}} \quad \text{..... (4. 14)}$$

or

$$\frac{y_e}{L_F} = \frac{1}{4}\, F_{CD} \quad \text{..... (4. 15)}$$

where

$$F_{CD} = \frac{k_{F,in} w_F}{k_m\, y_e} \quad \text{..... (4. 16)}$$

Also, the time of ending region 3 and region 4 in dimensional are given by

$$t_{end3} \cong \frac{y_e^2 \mu (\phi V' c_t)_T}{0.00633 \times 2^2 k_F} \quad \text{..... (4. 17)}$$

$$t_{end4} \cong 9.874 \frac{L_F^2 \mu (\phi V' c_t)_T}{k_m} \quad \text{..... (4. 18)}$$

4.6 Sensitivity Analysis of Dimensional Parameters

Various dimensional parameters, $k_F, k_m, y_e, n_F,$ and $h,$ are played sensitivity analysis to see the effect of each parameters on the production curve. The sensitivity plots and analysis of these parameters are showed in **Appendix E**.

4.7 Dual Porosity Model with Infinite Conductivity Hydraulic Fractures and Homogeneous Linear Flow Model

Referring to the assumption of the dual porosity model, only two distinct medium systems are defined as hydraulic fracture and homogeneous matrix systems. In this case, the infinite conductivity of hydraulic fractures is assumed. Therefore, only matrix medium is considered. This can be implied that only transient linear flow in matrix can be presented in the production curve or only region 4 can be found in the linear period of production data.

Then, the model assumption of dual porosity model with infinite conductivity hydraulic fractures can be applied by the concept of homogeneous linear flow model in multi-transverse hydraulic fractures horizontal well. This can be confirmed by the

mathematical model comparison. The following comparison is used the gas equation for proving.

The asymptotic equation of the transient linear flow in matrix of the dual porosity model (region 4) is given as:

$$q_g = \frac{\Delta m(p)}{630T} A_{cw} \sqrt{k_m} \frac{y_e}{L_F} \sqrt{\mu(\phi V' c_t)_T} \frac{1}{\sqrt{t}} \quad \text{..... (4. 19)}$$

The asymptotic equation of the homogeneous linear flow in a fractured well is given as:

$$q_{DLxf} = \frac{2}{\pi\sqrt{\pi}} \frac{1}{\sqrt{t_{Dxf}}} \quad \text{..... (4. 20)}$$

or

$$q_g = \frac{\Delta m(p)}{315T} h x_f \sqrt{k_m} \sqrt{\mu \phi_m c_t} \frac{1}{\sqrt{t}} \quad \text{..... (4. 21)}$$

Some modifications have to be done to correct the dimension of a fractured well to a multi-transverse fractures in horizontal well as suggested in **Appendix A**. In this case, x_f of a hydraulically fractured well is converted to $y_e \times n_F$ of a multi-transverse hydraulic fractures horizontal well.

$$q_g = \frac{\Delta m(p)}{315T} h y_e n_F \sqrt{k_m} \sqrt{\mu \phi_m c_t} \frac{1}{\sqrt{t}} \times \frac{2L_F}{2L_F} \quad \text{..... (4. 22)}$$

$$q_g = \frac{\Delta m(p)}{630T} A_{cw} \sqrt{k_m} \frac{y_e}{L_F} \sqrt{\mu \phi_m c_t} \frac{1}{\sqrt{t}} \quad \text{..... (4. 23)}$$

Assume $\phi_m = \phi_T$ and $c_{tm} = c_{tT}$

Then, the asymptotic equation of the modified homogeneous flow for the multi-transverse hydraulic fractures well is same as the **Eq. 4.19**.

CHAPTER V

APPLICATION OF THE DUAL POROSITY MODEL

5.1 Introduction

In this chapter, the linear transient dual porosity model is used for production data interpretation of shale gas and oil reservoirs in multi-transverse hydraulic fractures horizontal well. The interpretation guidelines and the example of interpretation are presented.

From dual porosity model, five flow regions have been proposed as discussed earlier. Normally, the second linear flow (region 4) or transient linear effect of matrix flow is mainly used in data interpretation. However, sometimes, misinterpreting can be occurred by unawareness of existing of different flow region. The following summary theory of dual porosity model, theoretical dual porosity model cases, and field example will illustrate the procedures and cautions of interpreting the data.

5.2 Summary of Dual Porosity Model for Interpretation

For daily production data interpretation, the first linear period (linear transient period in hydraulic fractures) is not supposed to be presented. Therefore, either region 3 or region 4, which is represented for second linear period, is supposed to be showed by the linear period (a half-slope in log-log plot) in daily production data. The criteria of either region 3 or 4 will be found is given by $\frac{y_e}{L_F} = \frac{1}{4} F_{CD}$ or $\frac{y_e}{L_F} = \frac{1}{2}\sqrt{\frac{k_F}{k_m}}$.

- Region 3 will be found only when $\frac{y_e}{L_F} > \frac{1}{4} F_{CD}$ or $\frac{y_e}{L_F} > \frac{1}{2}\sqrt{\frac{k_F}{k_m}}$.
- Region 4 will be found only when $\frac{y_e}{L_F} < \frac{1}{4} F_{CD}$ or $\frac{y_e}{L_F} < \frac{1}{2}\sqrt{\frac{k_F}{k_m}}$.

The summary of dual porosity model characteristic can be illustrated in **Figure 4** and **Figure 5** which are dimensionless and dimensional forms, respectively.

The associated equations of dual porosity model for data interpretation are summarized in **Table 4**, **Table 5**, and **Table 6**.

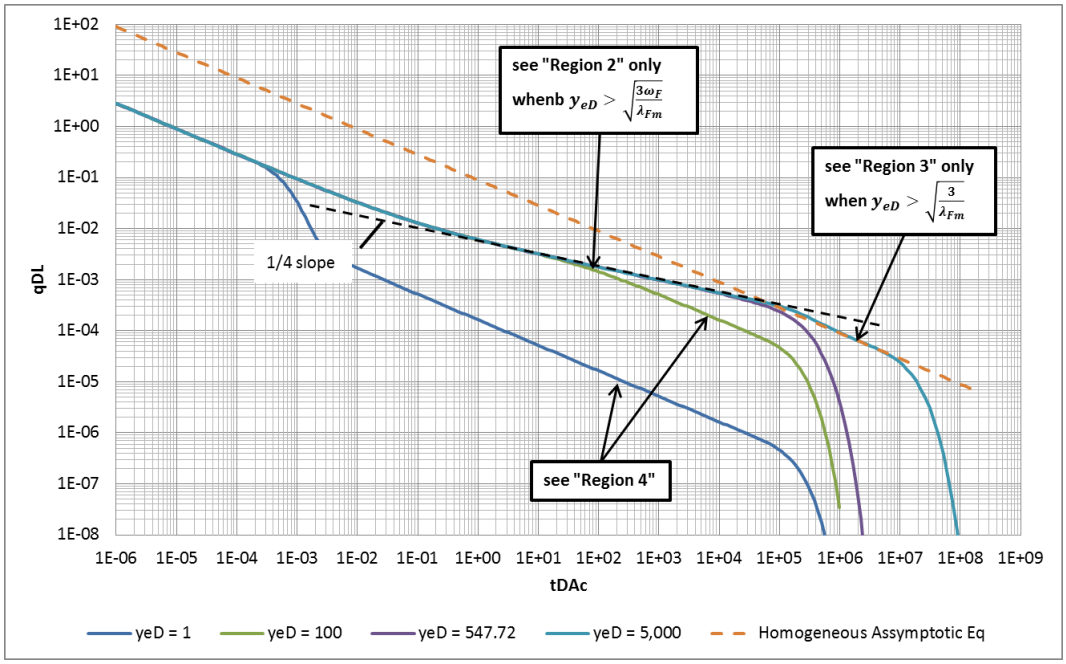

Figure 4 – Summary of dual porosity model characteristic for interpretation in dimensionless form

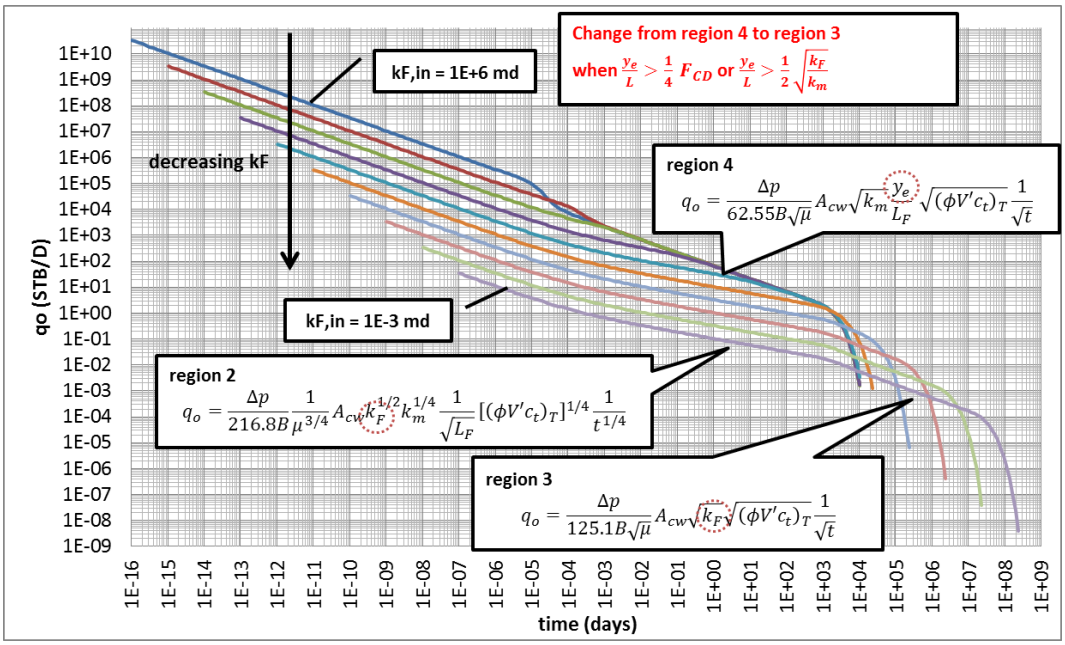

Figure 5 – Summary of dual porosity model characteristic for interpretation in dimensional form

Table 4 – Summary of associated equations for data interpretation of region 4

Region 4	Equation	Unknown
Asymptotic Equation for gas	$\frac{\Delta m(p)}{q_g} = \frac{630T}{A_{cw}\sqrt{k_m}} \frac{L_F}{y_e} \frac{1}{\sqrt{\mu(\phi V' c_t)_T}} \sqrt{t}$	$y_e, (k_m)$
Asymptotic Equation for oil	$\frac{\Delta p}{q_o} = \frac{62.55B\sqrt{\mu}}{A_{cw}\sqrt{k_m}} \frac{L_F}{y_e} \frac{1}{\sqrt{(\phi V' c_t)_T}} \sqrt{t}$	$y_e, (k_m)$
End of region 4	$t_{end\,4} \cong 9.874 \frac{L_F^2\, \mu(\phi V' c_t)_T}{k_m}$	(k_m)
Combine Slope and End of region for gas	$y_e = \frac{200.5\,T}{A_{cw}\,\mu(\phi V' c_t)_T} \frac{1}{slope4} \sqrt{t_{end\,4}}$	
Combine Slope and End of region for oil	$y_e = \frac{19.9B}{A_{cw}\,(\phi V' c_t)_T} \frac{1}{slope4} \sqrt{t_{end\,4}}$	

Table 5 – Summary of associated equations for data interpretation of region 3

Region 3	Equation	Unknown
Asymptotic Equation for gas	$\frac{\Delta m(p)}{q_g} = \frac{1260T}{A_{cw}\sqrt{k_F}} \frac{1}{\sqrt{\mu(\phi V' c_t)_T}} \sqrt{t}$	k_F
Asymptotic Equation for oil	$\frac{\Delta p}{q_o} = \frac{125.1B\sqrt{\mu}}{A_{cw}\sqrt{k_F}} \frac{1}{\sqrt{(\phi V' c_t)_T}} \sqrt{t}$	k_F
End of region 3	$t_{end\,3} \cong \frac{y_e^2 \mu(\phi V' c_t)_T}{0.00633 \times 2^2 k_F}$	k_F, y_e
Combine Slope and End of region for gas	$y_e = \frac{200.5\,T}{A_{cw}\ \mu(\phi V' c_t)_T} \frac{1}{slope3} \sqrt{t_{end\,3}}$	
Combine Slope and End of region for oil	$y_e = \frac{19.9B}{A_{cw}\ (\phi V' c_t)_T} \frac{1}{slope3} \sqrt{t_{end\,3}}$	

Table 6 – Summary of associated equations for data interpretation of region 2

Region 2	Equation	Unknown
Asymptotic Equation for gas	$\frac{\Delta m(p)}{q_g} = \frac{2183.7T}{A_{cw} k_F^{1/2} k_m^{1/4}} \frac{\sqrt{L_F}}{[\mu(\phi V' c_t)_T]^{1/4}}\ t^{1/4}$	$k_F, (k_m)$
Asymptotic Equation for oil	$\frac{\Delta p}{q_o} = \frac{216.8B\ \mu^{3/4}}{A_{cw} k_F^{1/2} k_m^{1/4}} \frac{\sqrt{L_F}}{[(\phi V' c_t)_T]^{1/4}}\ t^{1/4}$	$k_F, (k_m)$
Intersection of region 2 and region 4	$t_{int\,2,4} = 144.37\ \mu(\phi V' c_t)_T \frac{y_e^4}{L_F^2} \frac{k_m}{k_F^2}$	$k_F, y_e, (k_m)$
Intersection of region 2 and region 3	$t_{int\,2,3} = 9.023\ \mu(\phi V' c_t)_T \frac{L_F^2}{k_m}$	(k_m)

5.3 Interpretation Guidelines

The interpretation of dual porosity model focuses for possible bilinear and second linear flow. The early linear flow is supposed not to be presented in daily production data. Therefore, the possible five production scenarios are listed in **Table 7**.

Please note that in this interpretation guidelines, the total compressibility, c_t, is assumed to be same for both hydraulic fracture and matrix systems in order to provide the simplify equations for interpretation. Moreover, since the production of shale gas/oil reservoirs normally produce at constant pressure, constant pressure solutions are applied.

Table 7 – Five possible production scenarios in daily production data

Case	Bilinear	Linear	BDF
1		Yes	
2		Yes	Yes
3	Yes		
4	Yes	Yes	
5	Yes	Yes	Yes

5.3.1 Production Scenario Case 1

- There are two possible answers from interpretation but only one answer is correct. Two possible answers are calculated from region 4 and region 3 asymptotic equations.
- Normally, it is believed that $\frac{y_e}{L_F} < \frac{1}{4} F_{CD}$ or high conductivity in hydraulic fractures, region 4 asymptotic equation is used.

- It is recommend to calculate the minimum hydraulic fracture half-length, $y_{e,min}$. $y_{e,min}$ can be calculated from the last point, t_{end} and slope of the square root of time plot.

Choice 1 – Region 4

k_m has to be known

y_e can be found from slope of the square root of time plot, m_{square}

The equations of gas and oil are given, respectively by

$$y_e = \frac{630\ T\ L_F}{A_{cw}\sqrt{k_m}} \frac{1}{\sqrt{\mu \phi_T c_t}} \frac{1}{m_{square}} \quad \text{..... (5. 1)}$$

$$y_e = \frac{62.55 B \sqrt{\mu}\ L_F}{A_{cw}\sqrt{k_m}\ \sqrt{\phi_T c_t}} \frac{1}{m_{square}} \quad \text{..... (5. 2)}$$

In case the value of k_m is not certain, maximum k_m can be find from t_{end}

$$k_{m,max} = 9.874 \frac{L_F^2\ \mu \phi_T c_t}{t_{end}} \quad \text{..... (5. 3)}$$

Choice 2 – Region 3

y_e cannot be determined but minimum y_e can be calcualated

k_F can be found from slope of the square root of time plot, m_{square}

The equations of gas and oil are given, respectively by

$$\sqrt{k_F} = \frac{1260T}{A_{cw}} \frac{1}{\sqrt{\mu \phi_T c_t}} \frac{1}{m_{square}} \quad \text{..... (5. 4)}$$

$$\sqrt{k_F} = \frac{125.1B\sqrt{\mu}}{A_{cw}} \frac{1}{\sqrt{\phi_T c_t}} \frac{1}{m_{square}} \quad \text{..... (5. 5)}$$

Minimum y_e

The equations of gas and oil are given, respectively by

$$y_{e,min} = \frac{200.5\,T}{A_{cw}\,\mu\phi_T c_t} \frac{\sqrt{t_{end}}}{m_{square}} \quad \text{..... (5. 6)}$$

$$y_{e,min} = \frac{19.9B}{A_{cw}\,\phi_T c_t} \frac{\sqrt{t_{end}}}{m_{square}} \quad \text{..... (5. 7)}$$

5.3.2 Production Scenario Case 2

- It is impossible to determine whether region 3 or region 4 is found
- Unique solution of y_e and in-place whether region 3 or region 4 is assumed
- By combining asymptotic equation and end of straight line on square rood of time plot, calculated y_e will be the same for both region 3 and region 4 cases
- The value of k_m is not required

For gas

$$y_e = \frac{200.5\,T}{A_{cw}\,\mu\phi_T c_t} \frac{\sqrt{t_{esr}}}{m_{square}} \quad \text{..... (5. 8)}$$

$$OGIP\ (MMscf) = \frac{200.5 \times 10^{-6}\,T}{\mu\ c_t} \frac{\sqrt{t_{esr}}}{m_{square}} (1 - s_{wi}) \frac{1}{B_g} \quad \text{..... (5. 9)}$$

For oil

$$y_e = \frac{19.9B}{A_{cw}\,\phi_T c_t}\frac{\sqrt{t_{esr}}}{m_{square}} \quad \text{..... (5. 10)}$$

$$OOIP\ (MMSTB) = \frac{3.545 \times 10^{-6}}{c_t}\frac{\sqrt{t_{esr}}}{m_{square}}(1 - s_{wi}) \quad \text{..... (5. 11)}$$

In case assuming region 4 is found, k_m can be calculated from

$$k_m = 9.874\frac{L_F^2\,\mu\phi_T c_t}{t_{esr}} \quad \text{..... (5. 12)}$$

5.3.3 Production Scenario Case 3

- k_F can be calculated with assuming k_m
- y_e cannot be determined

The equations of gas and oil are given, respectively by

$$\sqrt{k_F} = \frac{2183.7T}{A_{cw}k_m^{1/4}}\frac{\sqrt{L_F}}{[\mu\phi_T c_t]^{1/4}}\frac{1}{m_{fourth}} \quad \text{..... (5. 13)}$$

$$\sqrt{k_F} = \frac{216.8B\,\mu^{3/4}}{A_{cw}k_m^{1/4}}\frac{\sqrt{L_F}}{[\phi_T c_t]^{1/4}}\frac{1}{m_{fourth}} \quad \text{..... (5. 14)}$$

5.3.4 Production Scenario Case 4

- Whether region 3 or 4 can be determined
- y_e can be calculated only region 4 is found

Procedures:

1. From bilinear flow period, find k_F from region 2 equation with assumingk_m. (**Eq. 5.13** or **Eq. 5.14**)
2. From linear flow period, find k_F from region 3 equation. (**Eq. 5.4** or **Eq. 5.5**)
3. Check whether k_F from region 2 is close to region 3 or not.
4. If yes, the linear flow period is represented by region 3 and y_e cannot be determined. However, minimum y_e can be calculated from **Eq. 5.6** or **Eq. 5.7**.

   If no, the linear flow period is represented by region 4 and y_e can be calculated from region 4 equation (**Eq. 5.1** or **Eq. 5.2**). The value of k_m is need. If the value of k_m is not certain, calculating maximum k_m by **Eq. 5.3** is recommended.

5.3.5 Production Scenario Case 5

- Interpret the data as production scenario case 2.
- Determine whether region 3 or 4 is found by using the same method as production scenario case 4.

5.4 Examples of Dual Porosity Interpretation

5.4.1 Well D01

The theoretical model of multi-transverse hydraulic fractures in horizontal well of shale oil reservoir was generated by using dual porosity model. The data table and generated daily production data are shown in **Table 8** and **Figure 6** below. This well

represents a very good fracturing job with effective hydraulic fracturing of 0.4 md (with fracture width 0.01 ft, intrinsic permeability is 10,000 md). The OOIP from this case is 5.48 MMSTB. The linear flow period of this well is represented by region 4.

Table 8 – Well D01 data

Thickness	h	200	ft	Hydraulic Fracture Half-Length	y_e	500	ft
Perforation Interval	x_e	5000	ft	Hydraulic Fracture Effective Permeability	k_F	0.4	md
Total Porosity	ϕ	0.05		Hydraulic Fracture Width	w_F	0.01	ft
Hydraulic Fracture Spacing	L_F	250	ft	Hydraulic Fracture Intrinsic Permeability	$k_{F,in}$	10,000	md
Number of Hydraulic Fracture	n_F	20		Hydraulic Fracture Porosity	ϕ_F	0.5	
Matrix Permeability	k_m	1.0E-05	md	Matrix Porosity	ϕ_m	0.05	
Water Saturation	S_w	0.2		Viscosity	μ	1.3	cp
Formation Volume Factor	B_o	1.3	rcf/scf	Total Compressibility	c_{ti}	2.0E-07	psi-1
Initial Pressure	p_i	3000	psia	Bottomhole Flowing Pressure	p_{wf}	500	pisa

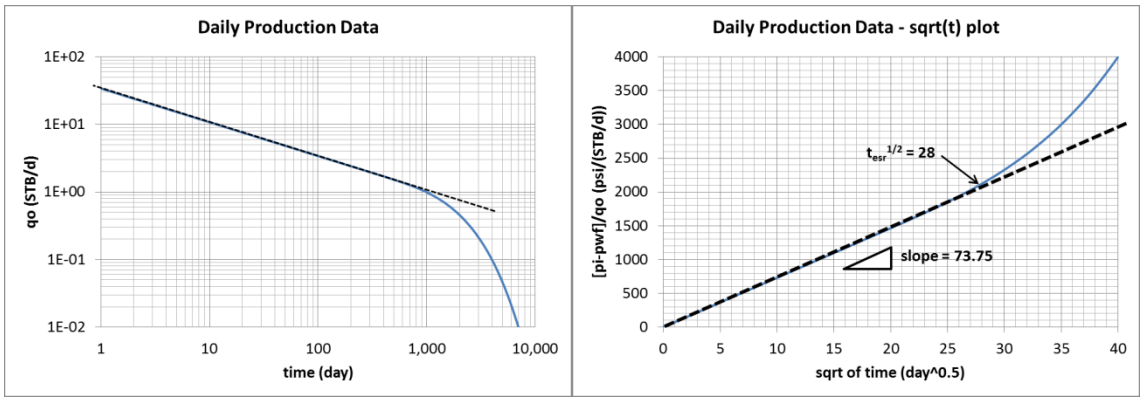

Figure 6 – Production data and square root of time plots of well D01

To simulate the real situation when interpreting data, the provided information for interpretation is same as provided data except hydraulic fracture half-length, y_e, and hydraulic fracture effective permeability, k_F.

To analyze production data of this well, interpretation guidelines of the production scenario case 2 (Linear and BDF periods are found) are used.

From **Eq. 5.10**, y_e is 497 ft.

From **Eq. 5.11**, $OOIP$ is 5.38 MMSTB

In case, it is believed that region 4 is found, k_m is 1.02E-5 md. from **Eq. 5.12**.

5.4.2 Well D02

Another theoretical well was generated with the data as showed in **Table 9** and the production data was generated only 1,000 days as showed in **Figure 7**. No deviation from the half-slope line on log-log plot. The linear flow period is represented by region 3.

Table 9 – Well D02 data

Thickness	h	200	ft	Hydraulic Fracture Half-Length	y_e	500	ft
Perforation Interval	x_e	5000	ft	Hydraulic Fracture Effective Permeability	k_F	0.0001	md
Total Porosity	ϕ	0.05		Hydraulic Fracture Width	w_F	0.01	ft
Hydraulic Fracture Spacing	L_F	100	ft	Hydraulic Fracture Intrinsic Permeability	$k_{F,in}$	1	md
Number of Hydraulic Fracture	n_F	50		Hydraulic Fracture Porosity	ϕ_F	0.5	
Matrix Permeability	k_m	1.0E-04	md	Matrix Porosity	ϕ_m	0.05	
Water Saturation	S_w	0.2		Viscosity	μ	1.3	cp
Formation Volume Factor	B_o	1.3	rcf/scf	Total Compressibility	c_{ti}	2.0E-07	psi-1
Initial Pressure	p_i	3000	psia	Bottomhole Flowing Pressure	p_{wf}	500	pisa

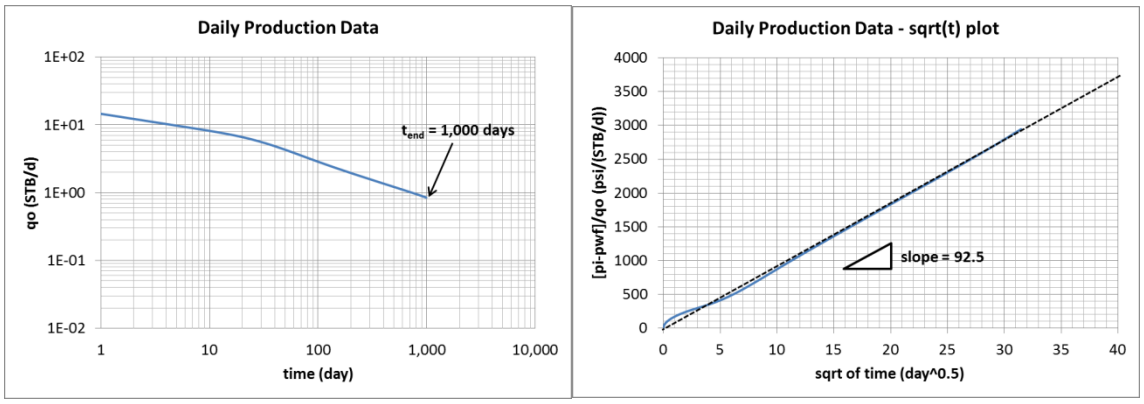

Figure 7 – Production data and square root of time plots of well D02

The values of hydraulic fracture half-length, y_e, and hydraulic fracture effective permeability, k_F, are unknown. In this case, the early 10 days of the production data is assumed to be skin effect from water flowing back from hydraulic fracturing treatment. The interpretation guidelines of the production scenario case 1 (Only linear period is found) are used to analyze production data of this well.

Choice 1 – Region 4 is selected

Assume k_m is 10^{-4} md

From **Eq. 5.2**, y_e is 50 ft.

Choice 2 – Region 3 is selected

y_e cannot be determined

From **Eq. 5.5**, k_F is 10^{-4} md

Minimum y_e

From **Eq. 5.7**, $y_{e,min}$ is 442 ft.

In summary, the last linear line is supposed to be region 3 rather than region 4 because the calculated y_e from asymptotic equation of region 4 is much more less than the minimum calculated y_e. Therefore, the exact value of y_e cannot be determined, only minimum value (442 ft) can be found.

5.4.3 Well 314

Field production plot and data of the multi-transverse hydraulic fractures horizontal well, well#314, is shown in **Appendix B**. In this interpretation, skin effect and gas adsorption are neglected. To analyze production data of this well, interpretation guidelines of the production scenario case 2 (Linear and BDF periods are found) are used.

From **Eq. 5.8**, y_e is 186 ft.

From **Eq. 5.9**, $OGIP$ is 2.7E+3 MMscf

In case, it is believed that region 4 is found, k_m is 1.3E-4 md from **Eq. 5.12**.

5.4.4 Well B-86

Field production plot and data of the multi-transverse hydraulic fractures horizontal well, well#B-86, is shown in **Appendix B**. In this interpretation, skin effect and gas adsorption are neglected. To analyze production data of this well, interpretation

guidelines of the production scenario case 4 (Bilinear and linear periods are found) are used.

1. By assuming k_m is 1.5E-4 md, k_F is 2.59E-3 md from **Eq. 5.13** or by assuming k_m is 1E-5 md, k_F is 10E-3 md.
2. From **Eq. 5.4**, k_F is 8.4E-4 md.
3. The calculated value of k_F from region 3 equation is not close to the value of k_F from region 2 equation; therefore, the late linear flow period is supposed to be region 4.
4. Maximum k_m from **Eq. 5.3** is 2.5E-4 md; then, $y_{e,min}$ from **Eq. 5.1** is 131 ft.

   In case the value of k_m is assumed to be 1E-4 md, y_e from **Eq. 5.1** is 205 ft.

   In case, the value of k_m is assumed to be 1E-5 md, y_e from **Eq. 5.1** is 649 ft.

CHAPTER VI

LINEAR TRANSIENT TRIPLE POROSITY MODEL

6.1 Introduction

In this chapter, the fully transient triple porosity model that proposed as Model 1 by Al-Ahmadi (2010) is investigated to consider as a tool using interpret the production data of shale gas and oil reservoirs in multi-transverse hydraulic fractures horizontal well. In this work, new 12 flow regions of the triple porosity model are defined. The asymptotic equations are derived in Laplace space. The investigation of model characteristic is presented.

6.2 Mathematical Model

The triple porosity model that uses to represent flow behavior of the multi-transverse hydraulic fractures in horizontal well is shown in **Figure 8**. Same as linear homogeneous flow model and dual porosity model, a horizontal well with multi-transverse hydraulic fractures is defined by the rectangular geometry or the SRV. The matrix blocks are assumed to be idealized as slab. Three mediums – the hydraulic fractures, the natural fractures, and the matrix are assumed to be uniform. The flow between mediums is assumed to be linear transient and sequential flow behaviors. Matrix feeds liquid to natural fractures and natural fractures feed liquid to hydraulic fractures and only hydraulic fractures produce the liquid to the well. Al-Ahmadi (2010) also presented 6 flow regimes (3 linear flows, 2 bilinear flows, and BDF period) to

represent his triple porosity model (Linear flows from matrix, natural fractures, and hydraulic fractures, Bilinear flow from the combination of matrix and natural fractures and natural fractures and hydraulic fractures). Actually, the transient linear triple porosity model can be represented by 12 flow regimes which are 6 linear flow regions, 4 bilinear flow regions, 1 trilinear flow region, and BDF period. This can be confirmed by deriving asymptotic equation systematically as shown in **Appendix H**. The asymptotic equation of each region can be solved in the Laplace space. The new trilinear flow behavior can be presented when all the flows in three mediums (hydraulic fractures, natural fractures, and matrix) are dominated by transient linear flow simultaneously. To see the transient period of all mediums simultaneously or the trilinear flow period, finite conductivity of hydraulic fractures and natural fractures are assumed. The bilinear flow can be showed by the conditions of two transients happen simultaneously. The two transients can be the combination of hydraulic fractures-matrix, hydraulic fractures-natural fractures, or natural fractures-matrix. The BDF period is found when all the boundaries of the three mediums reaches.

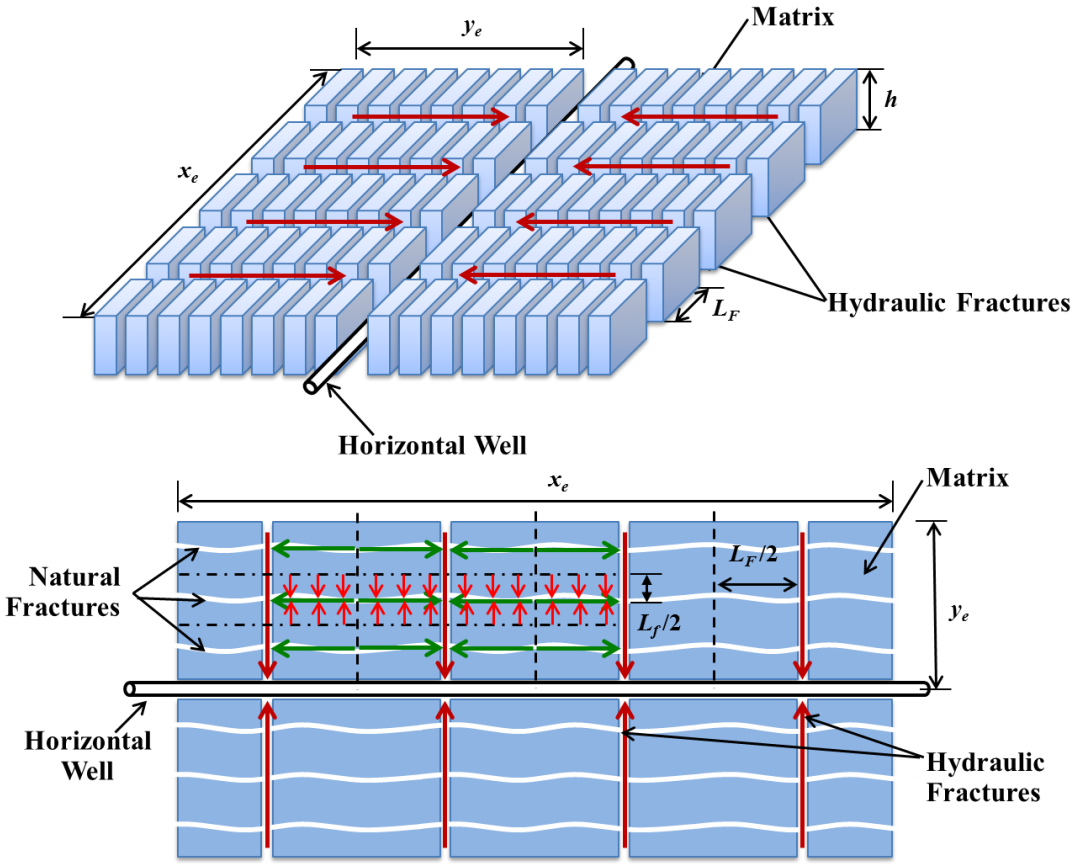

Figure 8 – Sketch of triple porosity model in multi-transverse hydraulic fractures horizontal well.

6.3 Dimensionless Variables Definition

In this study, the definition of triple porosity model variables which have not mentioned in the dual porosity model are given by

$$\lambda_{fm} = \frac{12 k_m A_{cw}}{L_f^2 k_F} \quad \text{..... (6. 1)}$$

$$\lambda_{Ff} = \frac{12 k_f A_{cw}}{L_F^2 k_F} \quad \text{..... (6. 2)}$$

$$\omega_F = \frac{(\phi V c_t)_F}{(\phi V c_t)_T} = \frac{(\phi V' c_t)_F}{(\phi V' c_t)_T} \quad \text{..... (6. 3)}$$

$$\omega_f = \frac{(\phi V c_t)_f}{(\phi V c_t)_T} = \frac{(\phi V' c_t)_f}{(\phi V' c_t)_T} \quad \text{..... (6. 4)}$$

$$\omega_m = \frac{(\phi V c_t)_m}{(\phi V c_t)_T} = \frac{(\phi V' c_t)_m}{(\phi V' c_t)_T} \quad \text{..... (6. 5)}$$

where

$$[\phi V' c_t]_T = (\phi V' c_t)_F + (\phi V' c_t)_f + (\phi V' c_t)_m \quad \text{..... (6. 6)}$$

and

$$V_x' = \frac{V_x}{V_F + V_f + V_m} \quad \text{..... (6. 7)}$$

$$\phi_T = \frac{\phi_F V_F + \phi_f V_f + \phi_m V_m}{V_F + V_f + V_m} \quad \text{..... (6. 8)}$$

6.4 Mathematical Solution and Approximation (Dimensionless)

This study is based on the fully transient triple porosity model proposed as Model 1 by Al-Ahmadi et al. (2010). The mathematical derivation details of the model are shown in **Appendix F**. The triple porosity model is validated by numerical method as showed in **Appendix G**. Previously; Samandarli (2011) showed the asymptotic equation of 12 flow regimes by using empirical method. Some of the equations are wrong due to the curve fitting. In this study, the asymptotic equation of each region is solved in Laplace space. Therefore, the exact solution is found. The completed derivations of 11 asymptotic equations (6 linear flow regions, 4 bilinear flow regions, 1 trilinear flow region) for constant pressure case are presented in **Appendix H**.

6.4.1 Asymptotic Equations

From constant pressure inner boundary and closed outer boundary, the Laplace solution is given by

$$\frac{1}{\overline{q_{DL}}} = \frac{2\pi u}{\sqrt{uf(u)}} \coth\left(\sqrt{uf(u)}\, y_{eD}\right) \quad \text{..... (6. 9)}$$

For fully transient slab model (Model 1),

$$f(u) = \omega_F + \frac{\lambda_{Ff}}{3u}\sqrt{uf_f(u)}\tanh\left(\sqrt{uf_f(u)}\right) \quad \text{..... (6. 10)}$$

$$f_f(u) = \frac{3\omega_f}{\lambda_{Ff}} + \frac{\lambda_{fm}}{\lambda_{Ff}}\frac{1}{u}\sqrt{\frac{3\omega_m u}{\lambda_{fm}}}\tanh\sqrt{\frac{3\omega_m u}{\lambda_{fm}}} \quad \text{..... (6. 11)}$$

The asymptotic equations are derived from the assumption of approximation terms in Laplace space. The summary of the assumptions and results of the eleven regions are shown in **Table 10**.

6.4.2 Conditions and Periods of Triple Porosity Characteristic

For fully transient linear triple porosity model in closed boundary, three medium systems affect the curve characteristic. The conditions to distinct one characteristic of curve are defined by 5 dimensionless parameters,λ_{Ff}, $\lambda_{fm}, \omega_F, \omega_f$, and y_{eD}, which is much more complicate than the dual porosity model which has only 3 dimensionless parameters. Moreover, from observation, the curve characteristic of triple porosity model can vary more than 20 conditions. Therefore, in this section, only last linear line and the possible bilinear line and trilinear line prior to the last linear period are considered only. The derivation of conditions and periods associated to the last linear period are showed in **Appendix H**.

From observation, the last linear line can be represented by possible 3 regions which are region L3, L5, and L6. The possible bilinear can be represented by possible 3 regions which are region B2, B3, and B4. The possible trilinear is represented by region T1. Moreover, it is found most of the time that bilinear and trilinear lines prior to the last linear period are combined or overlapped and shows the long transition period which cannot be identified the region.

Table 10 - Assumptions and final asymptotic equations region 1 – 11 of the fully transient linear triple porosity model (constant pressure)

Region	Estimated Terms					Asymptotic Equations
	$\overline{q_{DL}}$	$f(u)$		$f_f(u)$		
	$\coth\left(\sqrt{uf(u)}y_{eD}\right)$	ω_F	$\tanh\sqrt{uf_f(u)}$	$\frac{3\omega_f}{\lambda_{Ff}}$	$\tanh\sqrt{\frac{3\omega_m u}{\lambda_{fm}}}$	
L1	1	ω_F	-			$q_{DL} = \frac{\sqrt{\omega_F}}{2\pi\sqrt{\pi}}\frac{1}{\sqrt{t_{DAcw}}}$
L2	1	-	$\sqrt{uf_f(u)}$	$\frac{3\omega_f}{\lambda_{Ff}}$	-	$q_{DL} = \frac{\sqrt{\omega_f}}{2\pi\sqrt{\pi}}\frac{1}{\sqrt{t_{DAcw}}}$
L3	1	-	$\sqrt{uf_f(u)}$	-	$\sqrt{\frac{3\omega_m u}{\lambda_{fm}}}$	$q_{DL} = \frac{1}{2\pi\sqrt{\pi}}\frac{1}{\sqrt{t_{DAcw}}}$
L4	$\frac{1}{\sqrt{uf(u)}\,y_{eD}}$	-	1	$\frac{3\omega_f}{\lambda_{Ff}}$	-	$q_{DL} = \frac{\lambda_{Ff}^{1/2}\,\omega_f^{1/2}}{2\pi\sqrt{\pi}\,3^{1/2}}\,y_{eD}\frac{1}{\sqrt{t_{DAcw}}}$
L5	$\frac{1}{\sqrt{uf(u)}\,y_{eD}}$	-	1	-	$\sqrt{\frac{3\omega_m u}{\lambda_{fm}}}$	$q_{DL} = \frac{\lambda_{Ff}^{1/2}}{2\pi\sqrt{\pi}\,3^{1/2}}\,y_{eD}\frac{1}{\sqrt{t_{DAcw}}}$
L6	$\frac{1}{\sqrt{uf(u)}\,y_{eD}}$	-	$\sqrt{uf_f(u)}$	-	1	$q_{DL} = \frac{\lambda_{fm}^{1/2}}{2\pi\sqrt{\pi}\,3^{1/2}}\,y_{eD}\frac{1}{\sqrt{t_{DAcw}}}$
B1	1	-	1	$\frac{3\omega_f}{\lambda_{Ff}}$	-	$q_{DL} = \frac{\lambda_{Ff}^{1/4}\,\omega_f^{1/4}}{10.133}\frac{1}{t_{DAcw}^{1/4}}$
B2	1	-	1	-	$\sqrt{\frac{3\omega_m u}{\lambda_{fm}}}$	$q_{DL} = \frac{\lambda_{Ff}^{1/4}}{10.133}\frac{1}{t_{DAcw}^{1/4}}$
B3	1	-	$\sqrt{uf_f(u)}$	-	1	$q_{DL} = \frac{\lambda_{fm}^{1/4}}{10.133}\frac{1}{t_{DAcw}^{1/4}}$
B4	$\frac{1}{\sqrt{uf(u)}\,y_{eD}}$	-	1	-	1	$q_{DL} = \frac{\lambda_{Ff}^{1/2}\,\lambda_{fm}^{1/4}}{17.551}\,y_{eD}\frac{1}{t_{DAcw}^{1/4}}$
T1	1	-	1	-	1	$q_{DL} = \frac{\lambda_{fm}^{1/8}\,\lambda_{Ff}^{1/4}}{10.337}\frac{1}{t_{DAcw}^{1/8}}$

From the last linear line, possible region is composed of 3 regions – region L3, L5, and L6. The conditions of presenting each region are illustrated by **Figure 9**, **Figure 10**, and **Figure 11** and given by

- When $\lambda_{Ff} > \lambda_{fm}$,
    - If $y_{eD} < \sqrt{3/\lambda_{fm}}$, region L6 is found.
    - If $y_{eD} > \sqrt{3/\lambda_{fm}}$, region L3 is found.
- When $\lambda_{Ff} < \lambda_{fm}$,
    - If $y_{eD} < \sqrt{3/\lambda_{Ff}}$, region L5 is found.
    - If $y_{eD} > \sqrt{3/\lambda_{Ff}}$, region L3 is found.

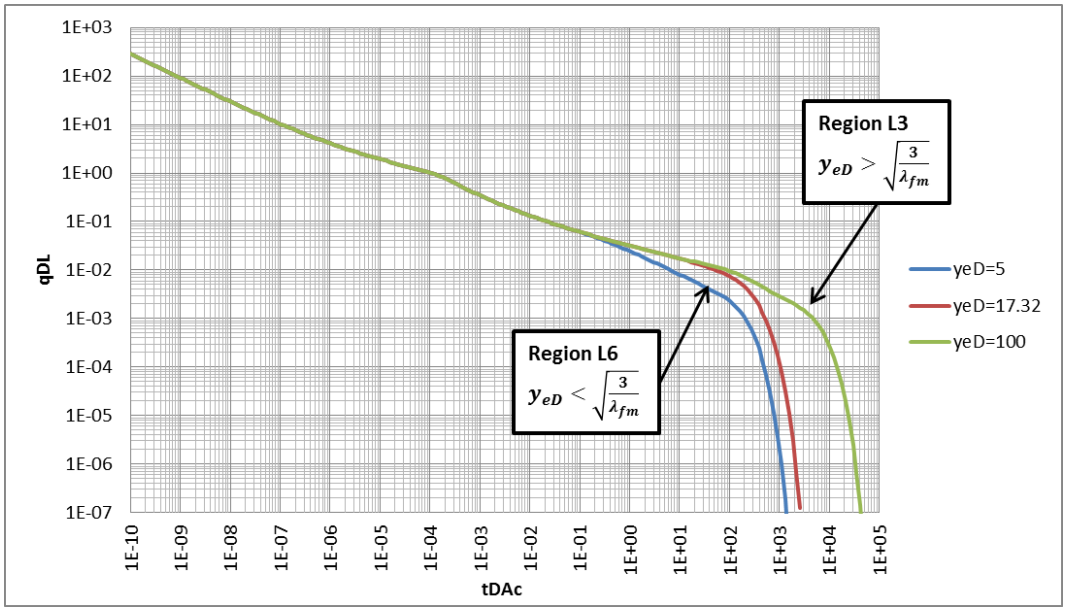

Figure 9 – Comparison plot of region L3 and L6 with $\lambda_{Ff} = 100$, $\lambda_{fm} = 0.01$, $\omega_F = 0.001$, $\omega_f = 0.01$

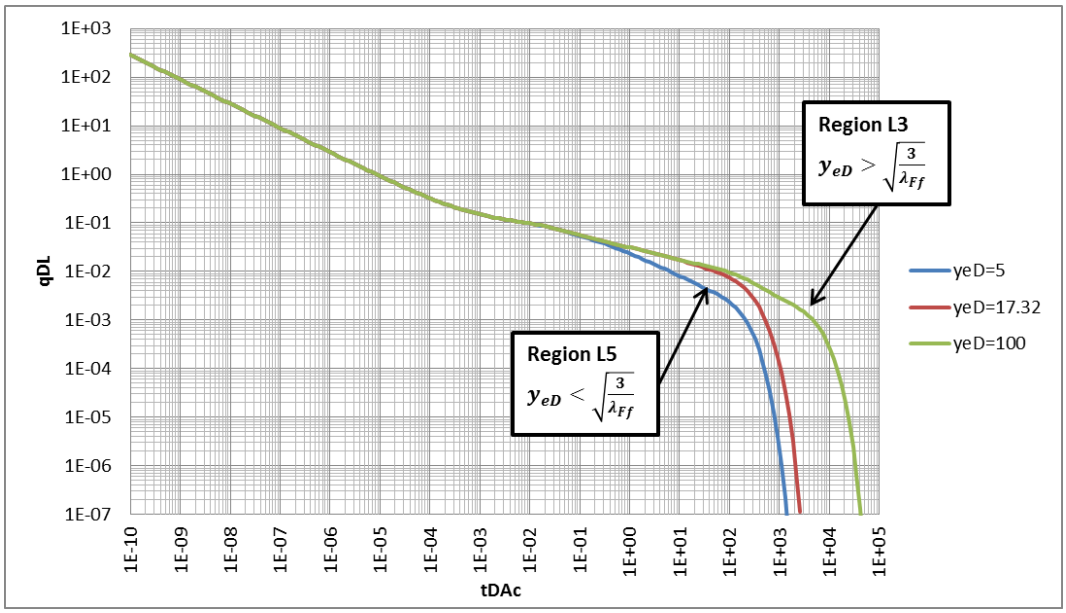

Figure 10 – Comparison plot of region L3 and L5 with $\lambda_{Ff} = 0.01$, $\lambda_{fm} = 100$, $\omega_F = 0.001$, $\omega_f = 0.01$

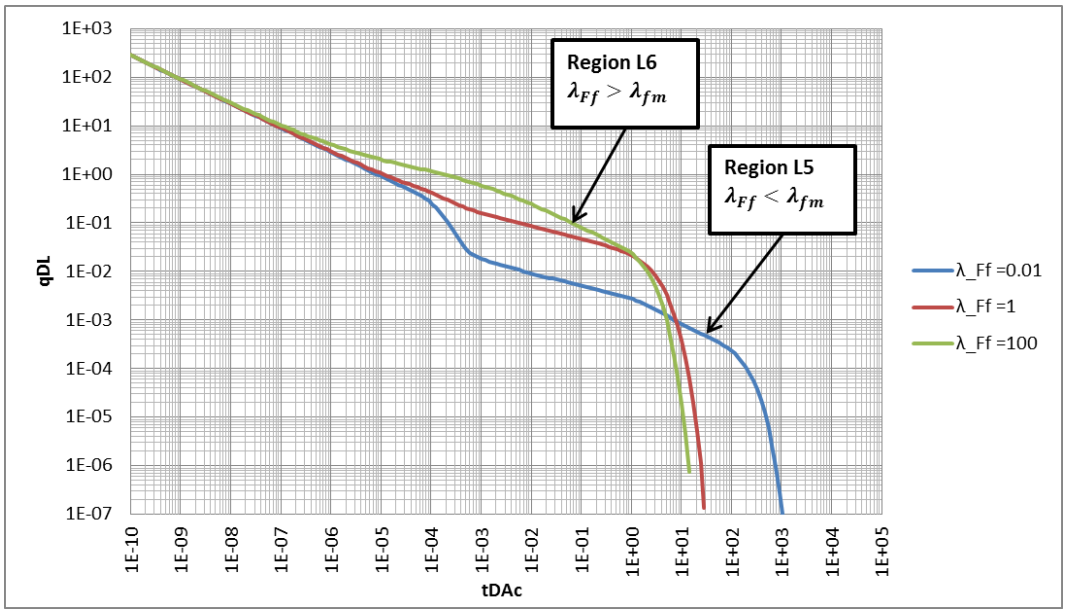

Figure 11 – Comparison plot of region L5 and L6 with $y_{eD} = 0.5$, $\lambda_{fm} = 1$, $\omega_F = 0.001$, $\omega_f = 0.01$

For the bilinear line, possible bilinear region is composed of 3 regions – region B2, B3, and B4. The conditions of presenting each region are given by

- Among region B3, B4, and BDF can be appeared before region L6.
    - Two set of plots are illustrated the possible region prior to region L6 in **Figure 12** and **Figure 13**.
    - The first set is either region B4 or BDF is presented prior to region L6. The selective condition is $\sqrt{\frac{\lambda_{Ff}\omega_f}{\lambda_{fm}}} = 1$.
    - The second set is either region B3 or BDF is presented prior to region L6. The selective condition is $y_{eD} = \sqrt{\frac{3\omega_f}{\lambda_{fm}}}$.
- Among region B2, B4, and BDF can be appeared before region L5.
    - Two set of plots are illustrated the possible region prior to region L5 in **Figure 14** and **Figure 15.**
    - The first set is either region B2 or B4 is presented prior to region L5. The selective condition is $y_{eD} = \frac{\sqrt{3}}{\lambda_{Ff}^{1/4}\,\lambda_{fm}^{1/4}}$.
    - The second set is either region B2 or BDF is presented prior to region L5. The selective condition is $y_{eD} = \sqrt{\frac{3\omega_F}{\lambda_{Ff}}}$.
- Either region B2 or B3 can be appeared before region L3.
    - The selective condition is $\lambda_{Ff} = \lambda_{fm}$ and can be illustrated by **Figure 16**.

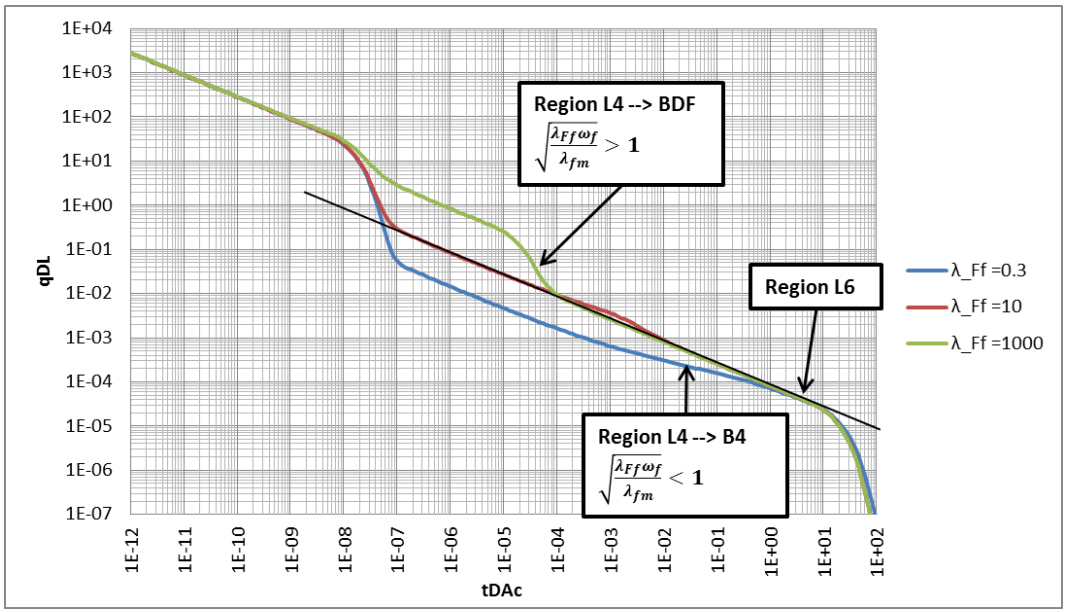

Figure 12 – Comparison plot of region B4 and BDF prior to region L6 with $y_{eD} = 0.005$, $\lambda_{fm} = 0.1$, $\omega_F = 0.001$, $\omega_f = 0.01$

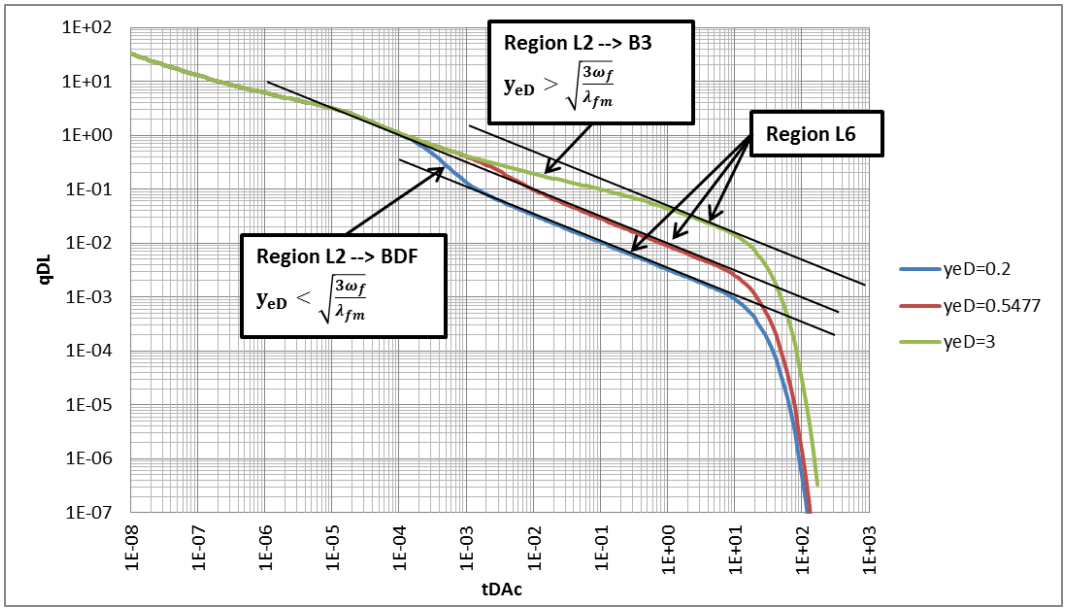

Figure 13 – Comparison plot of region B3 and BDF prior to region L6 with $\lambda_{Ff} = 1000$, $\lambda_{fm} = 0.1$, $\omega_F = 0.001$, $\omega_f = 0.01$

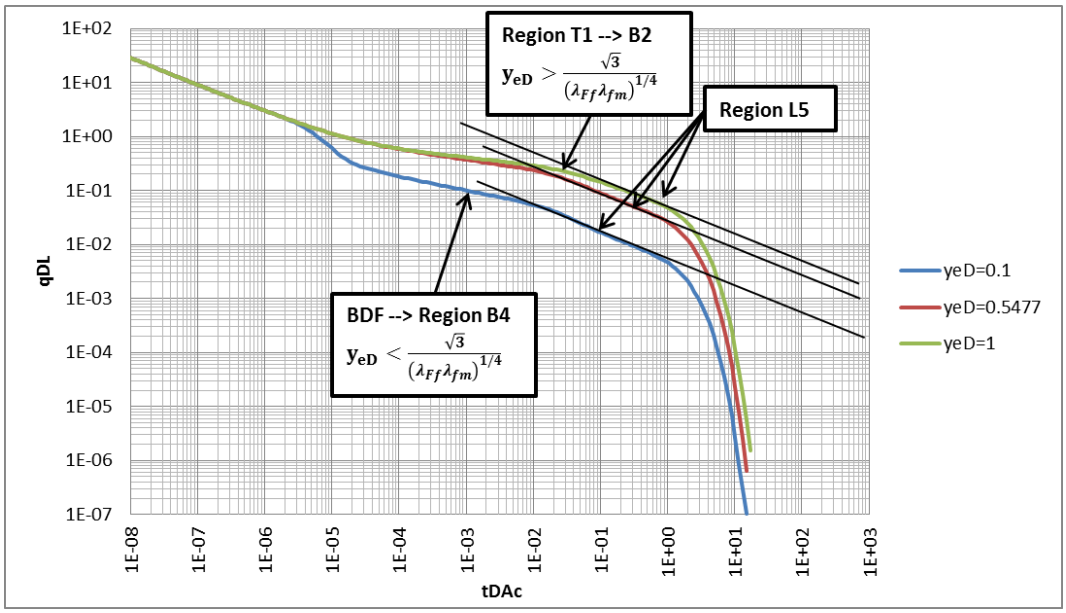

Figure 14 – Comparison plot of region B2 and B4 prior to region L5 with $\lambda_{Ff} = 1$, $\lambda_{fm} = 100$, $\omega_F = 0.001$, $\omega_f = 0.01$

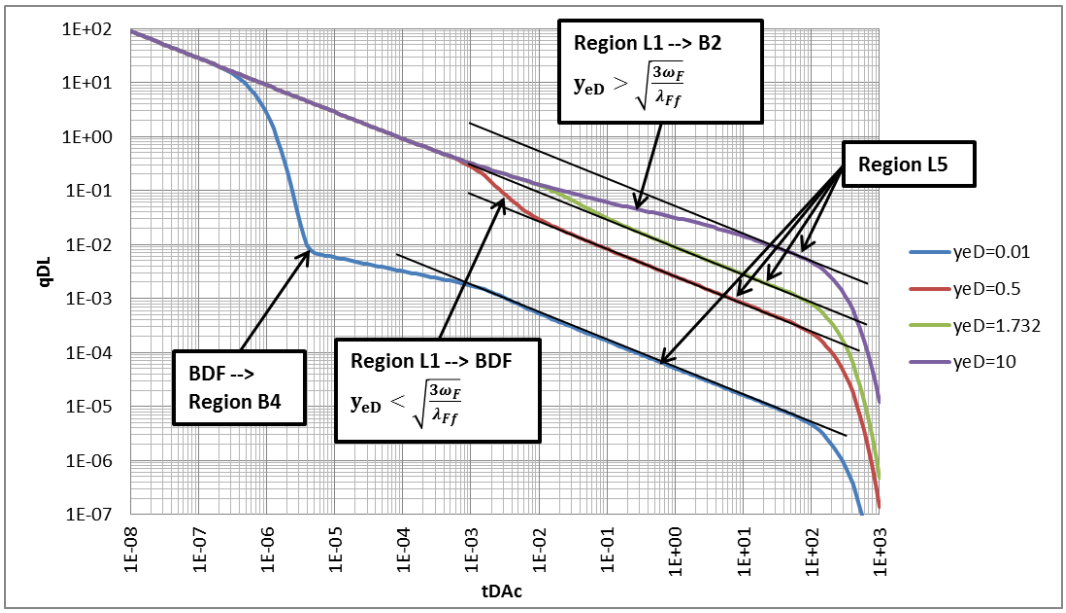

Figure 15 – Comparison plot of region B2 and BDF prior to region L5 with $\lambda_{Ff} = 0.01$, $\lambda_{fm} = 1000$, $\omega_F = 0.01$, $\omega_f = 0.0001$

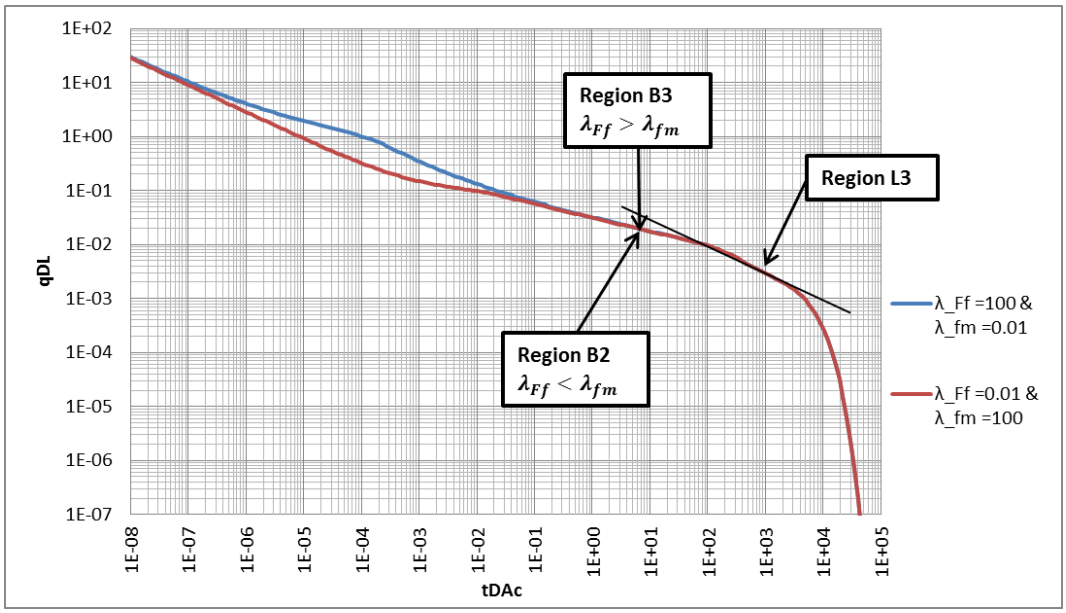

Figure 16 – Comparison plot of region B2 and B3 prior to region L3 with $y_{eD} = 100$, $\omega_F = 0.001$, $\omega_f = 0.01$

From the assumptions of the asymptotic equation and check with the sensitivity run case, end time of region L3, L5, and L6 for constant pressure case can be derived in Laplace space and convert to time domain as following.

Region L3 – The end of region is at $t_{DAcw,end\ L3} \cong \frac{y_{eD}^2}{2^2}$.

Region L5 – The end of region is at $t_{DAcw,end\ L5} \cong \frac{3}{2^2}\frac{1}{\lambda_{Ff}}$.

Region L6 – The end of region is $t_{DAcw,end\ L6} \cong \frac{3}{2^2}\frac{1}{\lambda_{fm}}$.

6.5 Mathematical Solution and Approximation (Dimensional)

The asymptotic equations of gas and oil in dimensional form are showed in **Table 11** and **Table 12**, respectively.

The conditions of the triple porosity model characteristic as discussed in the previous section are converted to the dimensional form and given by

From the last linear line,

- When $\lambda_{Ff} > \lambda_{fm}$ or $\frac{L_f}{L_F} > \sqrt{\frac{k_m}{k_f}}$,
    - If $y_{eD} < \sqrt{3/\lambda_{fm}}$ or $\frac{y_e}{L_f} < \frac{1}{2}\sqrt{\frac{k_F}{k_m}}$, region L6 is found.
    - If $y_{eD} > \sqrt{3/\lambda_{fm}}$ or $\frac{y_e}{L_f} > \frac{1}{2}\sqrt{\frac{k_F}{k_m}}$, region L3 is found.
- When $\lambda_{Ff} < \lambda_{fm}$ or $\frac{L_f}{L_F} < \sqrt{\frac{k_m}{k_f}}$,
    - If $y_{eD} < \sqrt{3/\lambda_{Ff}}$ or $\frac{y_e}{L_F} < \frac{1}{2}\sqrt{\frac{k_F}{k_f}}$, region L5 is found.
    - If $y_{eD} > \sqrt{3/\lambda_{Ff}}$ or $\frac{y_e}{L_F} > \frac{1}{2}\sqrt{\frac{k_F}{k_f}}$, region L3 is found.

For the bilinear line,

- Among region B3, B4, and BDF can be appeared before region L6.
    - Two set of conditions are used to identify the possible region prior to region L6.
    - The first set is either region B4 or BDF is presented prior to region L6. The selective condition is $\sqrt{\frac{\lambda_{Ff}\omega_f}{\lambda_{fm}}} = 1$ or $\frac{k_f}{k_m}\frac{L_f^2}{L_F^2}\frac{(\phi V c_t)_f}{(\phi V c_t)_T} = 1$.

- The second set is either region B3 or BDF is presented prior to region L6. The selective condition is $y_{eD} = \sqrt{\frac{3\omega_f}{\lambda_{fm}}}$ or $y_e = \frac{L_f}{2}\sqrt{\frac{k_F}{k_m}}\sqrt{\frac{(\phi V c_t)_f}{(\phi V c_t)_T}}$.

- Among region B2, B4, and BDF can be appeared before region L5.
  - Two set of conditions are used to identify the possible region prior to region L5**.**
  - The first set is either region B2 or B4 is presented prior to region L5. The selective condition is $y_{eD} = \frac{\sqrt{3}}{\lambda_{Ff}^{1/4}\,\lambda_{fm}^{1/4}}$ or $y_e = \frac{1}{2}\frac{L_F^{1/2}L_f^{1/2}k_F^{1/2}}{k_f^{1/4}k_m^{1/4}}$.
  - The second set is either region B2 or BDF is presented prior to region L5. The selective condition is $y_{eD} = \sqrt{\frac{3\omega_F}{\lambda_{Ff}}}$ or $y_e = \frac{L_F}{2}\sqrt{\frac{k_F}{k_f}}\sqrt{\frac{(\phi V c_t)_F}{(\phi V c_t)_T}}$.

- Either region B2 or B3 can be appeared before region L3.
  - The selective condition is $\lambda_{Ff} = \lambda_{fm}$ or $\frac{L_f}{L_F} = \sqrt{\frac{k_m}{k_f}}$.

Also, the time of ending region L3, region L5, and region L6 in dimensional form are given by

$$t_{end\ L3} \cong \frac{[\phi V' c_t]_T \mu\, y_e^2}{2^2 \times 0.00633 \times k_F} \quad \text{..... (6. 12)}$$

$$t_{end\ L5} \cong 9.874\ [\phi V' c_t]_T \mu \frac{L_F^2}{k_f} \quad \text{..... (6. 13)}$$

$$t_{end\ L6} \cong 9.874\ [\phi V' c_t]_T \mu \frac{L_f^2}{k_m} \quad \text{..... (6. 14)}$$

Table 11 – Asymptotic equations of triple porosity model for gas analysis in dimensional (constant pressure)

Region	Gas Equation
L1	$q_g = \frac{\Delta m(p)}{1260\,T}\sqrt{k_F}\,A_{cw}\sqrt{\mu(\phi V' c_t)_F}\,\frac{1}{\sqrt{t}}$
L2	$q_g = \frac{\Delta m(p)}{1260\,T}\sqrt{k_F}\,A_{cw}\sqrt{\mu(\phi V' c_t)_f}\,\frac{1}{\sqrt{t}}$
L3	$q_g = \frac{\Delta m(p)}{1260\,T}\sqrt{k_F}\,A_{cw}\sqrt{\mu(\phi V' c_t)_T}\,\frac{1}{\sqrt{t}}$
L4	$q_g = \frac{\Delta m(p)}{630\,T}\,A_{cw}\,\frac{k_f^{1/2}}{L_F}\sqrt{\mu(\phi V' c_t)_f}\,y_e\,\frac{1}{\sqrt{t}}$
L5	$q_g = \frac{\Delta m(p)}{630\,T}\,A_{cw}\,\frac{k_f^{1/2}}{L_F}\sqrt{\mu(\phi V' c_t)_T}\,y_e\,\frac{1}{\sqrt{t}}$
L6	$q_g = \frac{\Delta m(p)}{630\,T}\,A_{cw}\,\frac{k_m^{1/2}}{L_f}\sqrt{\mu(\phi V' c_t)_T}\,y_e\,\frac{1}{\sqrt{t}}$
B1	$q_g = \frac{\Delta m(p)}{2183.7\,T}\sqrt{k_F}\,A_{cw}\,k_f^{1/4}\frac{1}{\sqrt{L_F}}\,\mu^{1/4}(\phi V' c_t)_f^{1/4}\,\frac{1}{t^{1/4}}$
B2	$q_g = \frac{\Delta m(p)}{2183.7\,T}\sqrt{k_F}\,A_{cw}\,k_f^{1/4}\frac{1}{\sqrt{L_F}}\,\mu^{1/4}(\phi V' c_t)_T^{1/4}\,\frac{1}{t^{1/4}}$
B3	$q_g = \frac{\Delta m(p)}{2183.7\,T}\sqrt{k_F}\,A_{cw}\,k_m^{1/4}\frac{1}{\sqrt{L_f}}\,\mu^{1/4}(\phi V' c_t)_T^{1/4}\,\frac{1}{t^{1/4}}$
B4	$q_g = \frac{\Delta m(p)}{1091.86\,T}\,A_{cw}\,\frac{k_f^{1/2}k_m^{1/4}}{L_F\,L_f^{1/2}}\,\mu^{1/4}(\phi V' c_t)_T^{1/4}\,y_e\,\frac{1}{t^{1/4}}$
T1	$q_g = \frac{\Delta m(p)}{3074.5\,T}\sqrt{k_F}\,A_{cw}\,\frac{k_f^{1/4}k_m^{1/8}}{L_F^{1/2}L_f^{1/4}}\,\mu^{1/8}(\phi V' c_t)_T^{1/8}\,\frac{1}{t^{1/8}}$

Table 12 – Asymptotic equations of triple porosity model for oil analysis in dimensional (constant pressure)

Region	Oil Equation
L1	$q_o = \frac{\Delta p}{125.1\, B\mu}\sqrt{k_F}\, A_{cw}\sqrt{\mu(\phi V' c_t)_F}\,\frac{1}{\sqrt{t}}$
L2	$q_o = \frac{\Delta p}{125.1\, B\mu}\sqrt{k_F}\, A_{cw}\sqrt{\mu(\phi V' c_t)_f}\,\frac{1}{\sqrt{t}}$
L3	$q_o = \frac{\Delta p}{125.1\, B\mu}\sqrt{k_F}\, A_{cw}\sqrt{\mu(\phi V' c_t)_T}\,\frac{1}{\sqrt{t}}$
L4	$q_o = \frac{\Delta p}{62.55\, B\mu}\, A_{cw}\, \frac{k_f^{1/2}}{L_F}\sqrt{\mu(\phi V' c_t)_f}\, y_e\, \frac{1}{\sqrt{t}}$
L5	$q_o = \frac{\Delta p}{62.55\, B\mu}\, A_{cw}\, \frac{k_f^{1/2}}{L_F}\sqrt{\mu(\phi V' c_t)_T}\, y_e\, \frac{1}{\sqrt{t}}$
L6	$q_o = \frac{\Delta p}{62.55\, B\mu}\, A_{cw}\, \frac{k_m^{1/2}}{L_f}\sqrt{\mu(\phi V' c_t)_T}\, y_e\, \frac{1}{\sqrt{t}}$
B1	$q_o = \frac{\Delta p}{216.8\, B\mu}\sqrt{k_F}\, A_{cw}\, k_f^{1/4}\frac{1}{\sqrt{L_F}}\,\mu^{1/4}(\phi V' c_t)_f^{1/4}\,\frac{1}{t^{1/4}}$
B2	$q_o = \frac{\Delta p}{216.8\, B\mu}\sqrt{k_F}\, A_{cw}\, k_f^{1/4}\frac{1}{\sqrt{L_F}}\,\mu^{1/4}(\phi V' c_t)_T^{1/4}\,\frac{1}{t^{1/4}}$
B3	$q_o = \frac{\Delta p}{216.8\, B\mu}\sqrt{k_F}\, A_{cw}\, k_m^{1/4}\frac{1}{\sqrt{L_f}}\,\mu^{1/4}(\phi V' c_t)_T^{1/4}\,\frac{1}{t^{1/4}}$
B4	$q_o = \frac{\Delta p}{108.4\, B\mu}\, A_{cw}\, \frac{k_f^{1/2}k_m^{1/4}}{L_F\, L_f^{1/2}}\,\mu^{1/4}(\phi V' c_t)_T^{1/4}\, y_e\,\frac{1}{t^{1/4}}$
T1	$q_o = \frac{\Delta p}{305.3\, B\mu}\sqrt{k_F}\, A_{cw}\, \frac{k_f^{1/4}k_m^{1/8}}{L_F^{1/2}L_f^{1/4}}\,\mu^{1/8}(\phi V' c_t)_T^{1/8}\,\frac{1}{t^{1/8}}$

CHAPTER VII

THE TRIPLE POROSITY MODEL WITH INFINITE CONDUCTIVITY OF HYDRAULIC FRACTURES

7.1 Introduction

In this chapter, the fully transient triple porosity model described in **Chapter VI** is assumed infinite conductivity of hydraulic fractures. Mathematical model and solutions of the triple porosity model with infinite conductivity of hydraulic fractures are presented. Also, the triple porosity model with infinite conductivity of hydraulic fractures model is compared with the modified dual porosity model.

From the triple porosity model, 12 flow regimes (6 linear, 4 bilinear, 1 trilinear, and BDF) have been presented. Three possible regions can represent the last linear flow. Other three possible regions can represent the bilinear region prior to the last linear period. Moreover, trilinear flow can appear prior to the last linear period or between the bilinear. With this complexity of triple porosity model, it is too complicate to interpret production data of shale gas/oil reservoir with the triple porosity model. Therefore, infinite conductivity of hydraulic fractures is assumed to simplify the model. With considering infinite conductivity of hydraulic fractures, only two mediums responses which are natural fracture and matrix systems are expected to be found in production analysis. This can be interpreted as modified dual porosity which is represented two mediums (natural fracture and matrix).

7.2 Mathematical Model

The triple porosity model that uses to represent flow behavior of the multi-transverse (infinite conductivity) hydraulic fractures in horizontal well is shown in **Figure 17**. The model is modified from the original fully transient linear triple porosity model provided in **Chapter VI** by neglecting the hydraulic fracture transient flow effect. With infinite conductivity of hydraulic fractures, the transient period of hydraulic fractures will appear very early time compared to the rest mediums flowing period. This means that only two medium systems are considered in this case – natural fracture and matrix systems.

The new model can be identified the last linear period with only two possible linear regions and the bilinear line prior to the last linear period with only one bilinear region. For the last linear flow, one possible regime is represented the transient linear flow of the total system dominated by matrix flow. The other is dominated by natural fracture flow. For the bilinear, this bilinear regime represents two transient flows of natural fractures and matrix happening simultaneously.

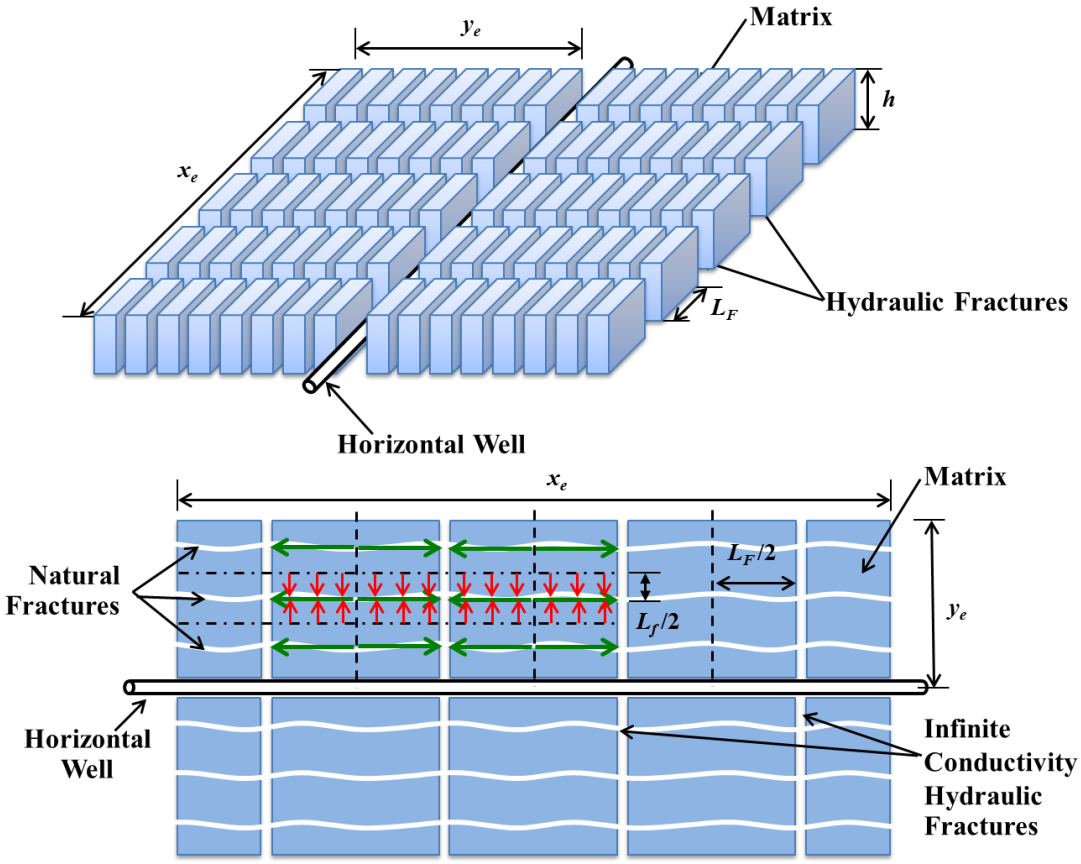

Figure 17 – Sketch of the triple porosity model of the infinite conductivity hydraulic fractures in horizontal well.

7.3 Physical Model Explanation

By assuming infinite conductivity hydraulic fractures, only five regions are considered in the mathematical model. Two regions from the last linear line are region L5 and L6. One region from the middle linear line is region L4. One region from the first linear line is region L1. The other from the bilinear line is region B4. Nevertheless, in practical, only last linear and the bilinear prior to it are considered. Two examples of the

triple porosity model which have very high permeability in hydraulic fractures are showed in **Figure 18** and **Figure 19**. The physical meaning of each region is given.

7.3.1 Region L1

This region represents the first transient linear of the fully transient triple porosity model. This region is showed by the first half slope of the log-log plot. This linear flow behavior represents the transient linear flow in the hydraulic fractures producing fluid to the well. With the high conductivity hydraulic fractures, the transient period is expected to be very short or impossible to see in daily production data.

7.3.2 Region L4

This region represents the middle transient linear of the fully transient triple porosity model. This region is showed in the second half slope of the log-log plot only when the conductivity of hydraulic fractures is very high (infinite conductivity) or the effect of transient linear flow of hydraulic fractures faded away. This linear flow behavior represents the transient linear flow in the natural fractures feeding fluid to hydraulic fractures. Normally, the conductivity of hydraulic fractures is not high enough to completely fade away before this transient dominates; therefore, it is almost impossible to see this region in the production data.

7.3.3 Region B4

This region represents the bilinear flow of the fully transient triple porosity model when infinite conductivity of hydraulic fractures is assumed. This region is showed in a quarter slope of the log-log plot prior to the last linear period. This bilinear flow is formed by occurring two transient linear flows simultaneously which are transient linear flow in natural fracture system (from natural fractures to hydraulic fractures) and matrix system (from matrix blocks to natural fractures). This occurs while the transient flow dominated period in natural fractures has not ended and the transient flow dominated period in matrix has started to appear.

7.3.4 Region L5

This region presents the late transient linear of the fully transient triple porosity model. It shows the last half slope line in the log-log plot. It represents the transient linear flow of total system which is dominated by natural fractures. This occurs when the transient flow in matrix has ended while transient flow in natural fractures still presents. This case will happen when the conductivity of natural fractures is very low comparing with flow capacity of matrix or the natural fracture spacing (boundary of the matrix flow) is small while the hydraulic fracture spacing (boundary of the natural fracture flow) is large.

7.3.5 Region L6

This region presents the late transient linear of the fully transient triple porosity model. It shows the last half slope line in the log-log plot. It represents the transient linear flow of total system which is dominated by matrix. This occurs when the transient flow in natural fractures has ended while transient flow in matrix still presents. This case will happen when the conductivity of natural fractures is high comparing with flow capacity of matrix or the natural fracture spacing (boundary of the matrix flow) is large while the hydraulic fracture spacing (boundary of the natural fracture flow) is small.

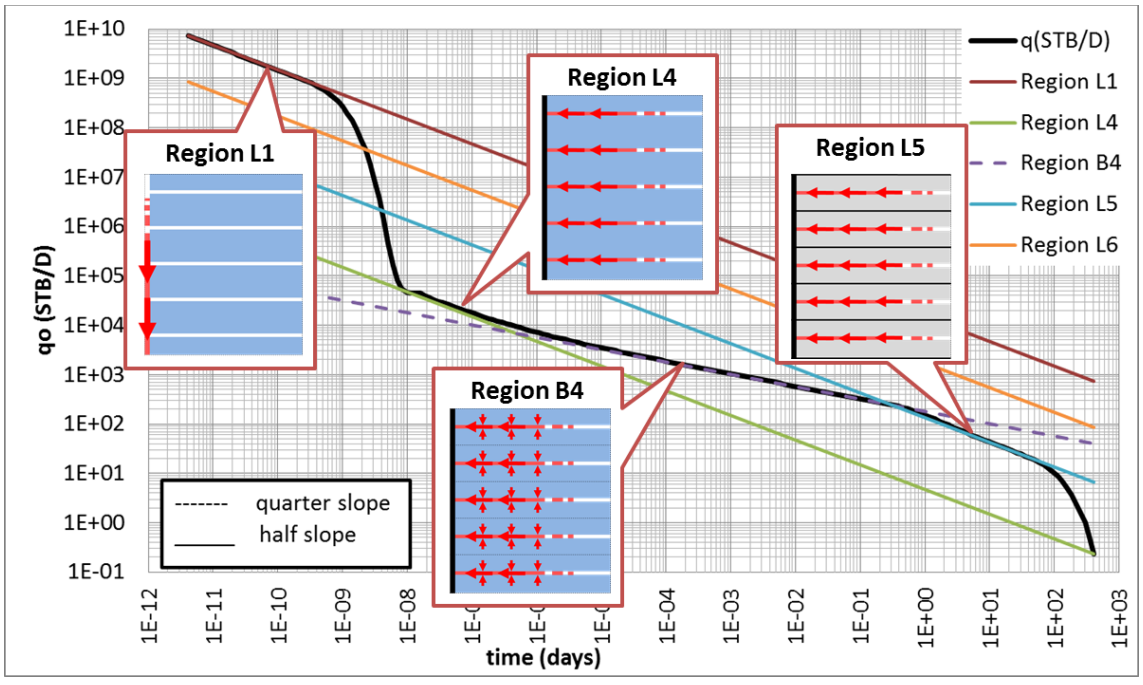

Figure 18 – Example of triple porosity model with infinite conductivity hydraulic fractures with region L6 as the last linear line

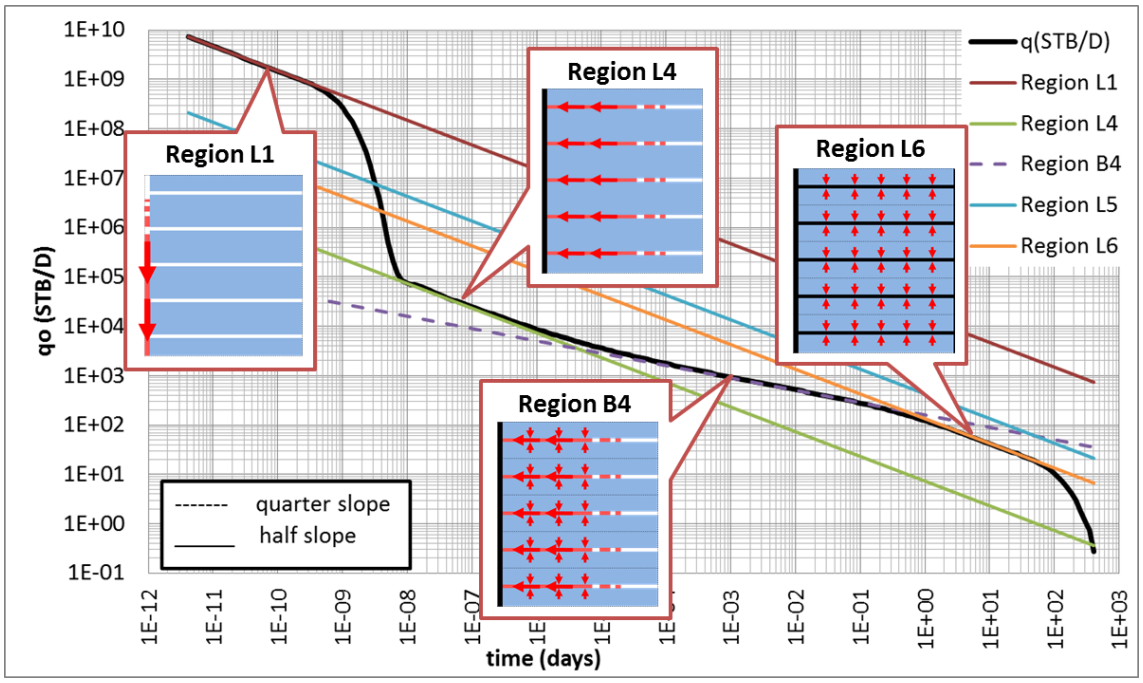

Figure 19 – Example of triple porosity model with infinite conductivity hydraulic fractures with region L5 as the last linear line

7.4 Modified Dual Porosity Model

As discussed earlier, the effect of hydraulic fracture flow period can be neglected by assuming infinite conductivity of hydraulic fractures and only two mediums are left to consider which are natural fractures system and matrix system. Consequently, triple porosity model with infinite conductivity of hydraulic fractures can be reduced its form to dual porosity model by considering hydraulic fractures in original dual porosity model as natural fractures of triple porosity model.

From the original dual porosity system of hydraulic fracture and matrix to the modified dual porosity system of natural fractures and matrix, the following changes (**Table 13**) are required.

Table 13 – Conversion table of parameters from original dual porosity model to modified dual porosity model

	Original Parameters	**Modified Parameters**
Thickness	h	$= h$
Perforation Interval	x_e	$= 2*y_e*n_F$
Hydraulic Fracture Half-Length	y_e	$= L_F/2$
Hydraulic Fracture Effective Permeability	k_F	$= k_f$
Hydraulic Fracture Spacing	L_F	$= L_f$
Number of Hydraulic Fracture	n_F	$= 2*n_f*n_F$
Matrix Permeability	k_m	$= k_m$
Hydraulic Fracture Width	w_F	$= w_f$
Hydraulic Fracture Intrinsic Permeability	$k_{F,in}$	$= k_{f,in}$
Hydraulic Fracture Porosity	ϕ_F	$= \phi_f$
Matrix Porosity	ϕ_m	$= \phi_m$

To simulate the modified dual porosity model by using numerical simulator to represent the triple porosity with infinite conductivity of hydraulic fractures, the modification of parameter variables have to be changed as suggested earlier. The model is simulated only one-fourth of a natural fracture. The parameters inside the model are generated same as original dual porosity except using natural fracture dimension instead of hydraulic fracture dimension as illustrated in **Figure 20**. The output production rate of the simulator has to be multiplied by $8 \times n_f \times n_F$ to represent the well production.

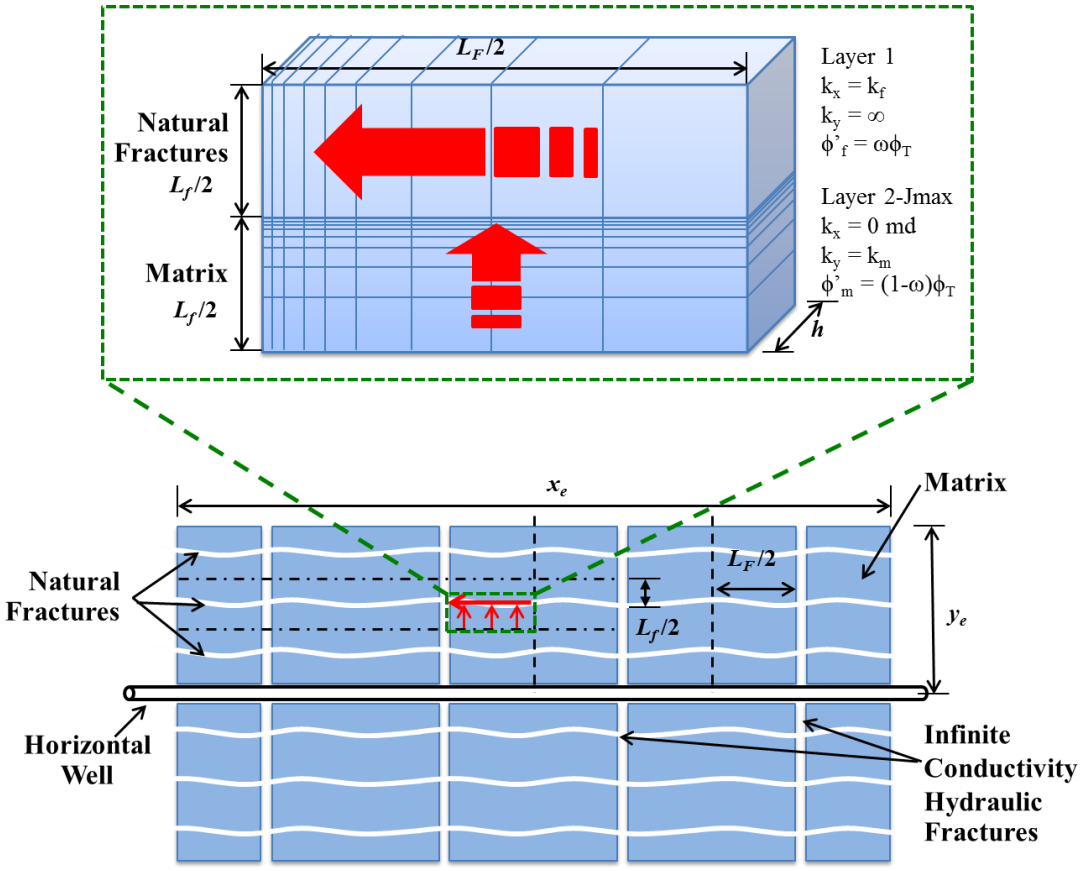

Figure 20 – Illustration of modified dual porosity model for numerical method

7.4.1 Theoretical Examples Comparison

The following examples illustrate this triple porosity model (high conductivity of hydraulic fracture) and compare between the triple porosity model and the modified dual porosity model.

Example A

Theoretical data of triple porosity model is generated with the data as shown in **Table 14**. The hydraulic fracture permeability is set to 2E+5 md to represent infinite conductivity fractures. Then, modified dual porosity model (natural fracture and matrix systems) is generated with the modified data as showed in **Table 15**.

Table 14 – Data of triple porosity model of example A

h	200 ft	y_e	500 ft
x_e	5000 ft	w_F	0.01 ft
k_F	10 md	$k_{F,in}$	2.00E+05 md
L_F	200 ft	ϕ_F	0.3
n_F	25	w_f	0.001 ft
k_f	0.1 md	$k_{f,in}$	2000 md
L_f	20 ft	ϕ_f	0.3
n_f	25	ϕ_m	0.05
k_m	1.00E-05 md	μ	1.3 cp
ϕ	0.05	c_{ti}	2.00E-07 psi-1
S_w	0.2	p_i	3000 psia
B_o	1.3 rcf/scf	p_{wf}	500 pisa

Table 15 – Data of modified dual porosity model of example A

h	200 ft	y_e	100 ft
x_e	25000 ft	w_F	0.001 ft
k_F	0.1 md	$k_{F,in}$	2000 md
L_F	20 ft	ϕ_F	0.3
n_F	1250	ϕ_m	0.05
k_m	1.00E-05 md	μ	1.3 cp
ϕ	0.05	c_{ti}	2.00E-07 psi-1
S_w	0.2	p_i	3000 psia
B_o	1.3 bbl/STB	p_{wf}	500 pisa

From the triple porosity model, region L1 follows by region B4, and L6 are found respectively. While, region 1 follows by region 2 and 4 are found in dual porosity

model, respectively. Plotting of the triple porosity model with the modified dual porosity model is showed in **Figure 21**. It is shown that last bilinear and linear periods of triple porosity model are overlaid with bilinear and second linear periods of dual porosity model (B4 is overlaid with 2 and L6 is overlaid with 4). This case can be explained that hydraulic fractures response disappears before the responses of natural fractures and matrix appear simultaneously (bilinear period – region B4 of triple porosity and region 2 of dual porosity). Then, the matrix flow of both models appears as linear flow when the effect of natural fractures fades away. Since the permeability of natural fractures is quite high in this case (2,000 md), only transient in matrix is expected to be found in the daily production data.

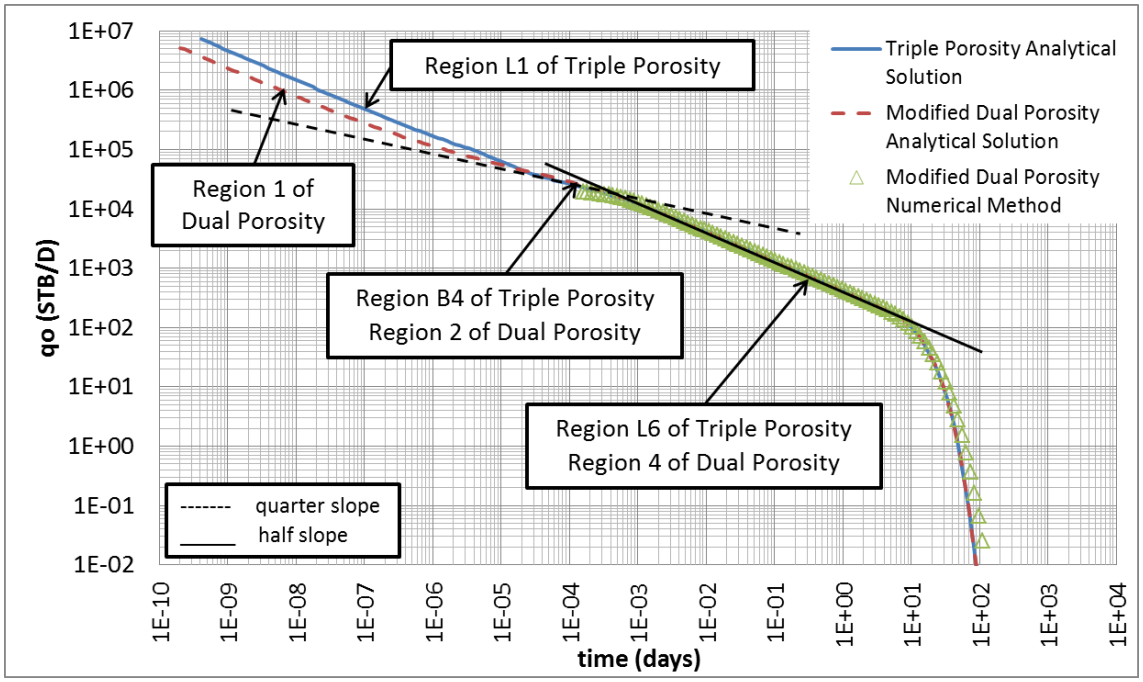

Figure 21 – Comparison plot of triple porosity model and modified dual porosity model of example A

Example B

Theoretical data of triple porosity model is generated with the data as shown in table above. All data are same as Example A except natural fracture permeability. The intrinsic natural fracture permeability is reduced from 2,000 md to 1 md. Then, modified dual porosity model (natural fracture and matrix systems) is generated with the modified data of hydraulic fracture permeability.

From the triple porosity model, region L1 follows by the BDF, region B4, and L5 are found respectively. While, region 1 follows by region 2 and 3 are found in dual porosity model, respectively. Plotting the triple porosity model with the modified dual porosity model, it is shown that last bilinear and linear periods of triple porosity model are overlaid with bilinear and second linear periods of dual porosity model (B4 is overlaid with 2 and L5 is overlaid with 3) as shown in **Figure 22**. In this case, the responses of natural fractures and matrix of triple porosity model (bilinear flow – region B4 of triple porosity and region 2 of dual porosity) dominate after transient period of hydraulic fractures ends. Then, the transient period of matrix flow ends and the transient period of natural fracture flow still dominates which is represented by region L5 and region 3 of triple porosity and dual porosity, respectively.

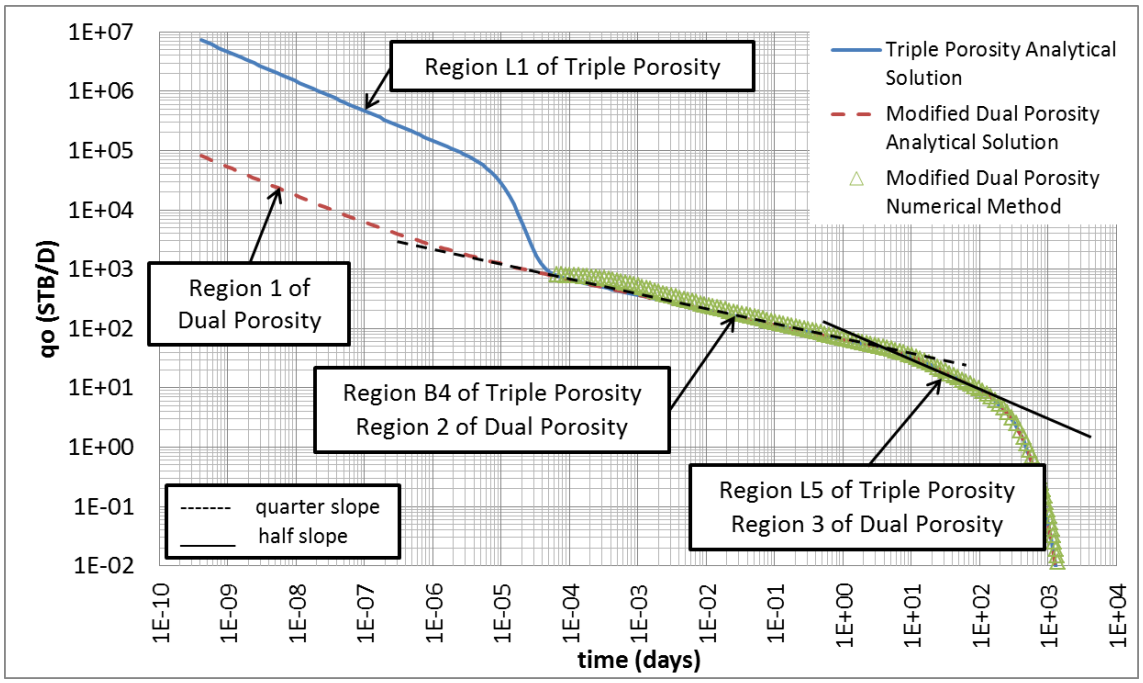

Figure 22 – Comparison plot of triple porosity model and modified dual porosity model of example B

Example C

Theoretical data of triple porosity model and modified dual porosity model are generated with the data as shown in **Table 16** and **Table 17**, respectively. This example case is generated to demonstrate the complicated case of specifying region before last linear flow.

From the triple porosity model, region L1 follows by the transition period before the region L6 is dominated. While, region 1 follows by region 3 is found in dual porosity model, respectively. Plotting the triple porosity model with the modified dual porosity model, it is shown that only last linear period of triple porosity model are overlaid with the second linear period of dual porosity model (L6 is overlaid with 4) as shown in

Figure 23. The period before last linear flow of triple porosity model does not fit with dual porosity model because the effect of hydraulic fractures in triple porosity has still appeared when natural fracture response is showed. Nevertheless, when the effects of hydraulic and natural fractures fade out, the transient period of matrix linear flow of two models (region L6 and 4 of triple and dual porosity models, respectively) will be identical. Since the permeability of natural fractures is quite high in this case (5,000 md), only transient in matrix is expected to be found in the daily production data.

Table 16 – Data of triple porosity model of example C

h	200 ft	y_e	500 ft
x_e	5000 ft	w_F	0.01 ft
k_F	10 md	$k_{F,in}$	1.00E+05 md
L_F	100 ft	ϕ_F	0.3
n_F	50	w_f	0.001 ft
k_f	1 md	$k_{f,in}$	5000 md
L_f	5 ft	ϕ_f	0.3
n_f	100	ϕ_m	0.05
k_m	1.00E-07 md	μ	1.3 cp
ϕ	0.05	c_{ti}	2.00E-07 psi-1
S_w	0.2	p_i	3000 psia
B_o	1.3 bbl/STB	p_{wf}	500 pisa

Table 17 – Data of modified dual porosity model of example C

h	200 ft	y_e	50 ft
x_e	50000 ft	w_F	0.001 ft
k_F	1 md	$k_{F,in}$	5000 md
L_F	5 ft	ϕ_F	0.3
n_F	10000	ϕ_m	0.05
k_m	1.00E-07 md	μ	1.3 cp
ϕ	0.05	c_{ti}	2.00E-07 psi-1
S_w	0.2	p_i	3000 psia
B_o	1.3 bbl/STB	p_{wf}	500 pisa

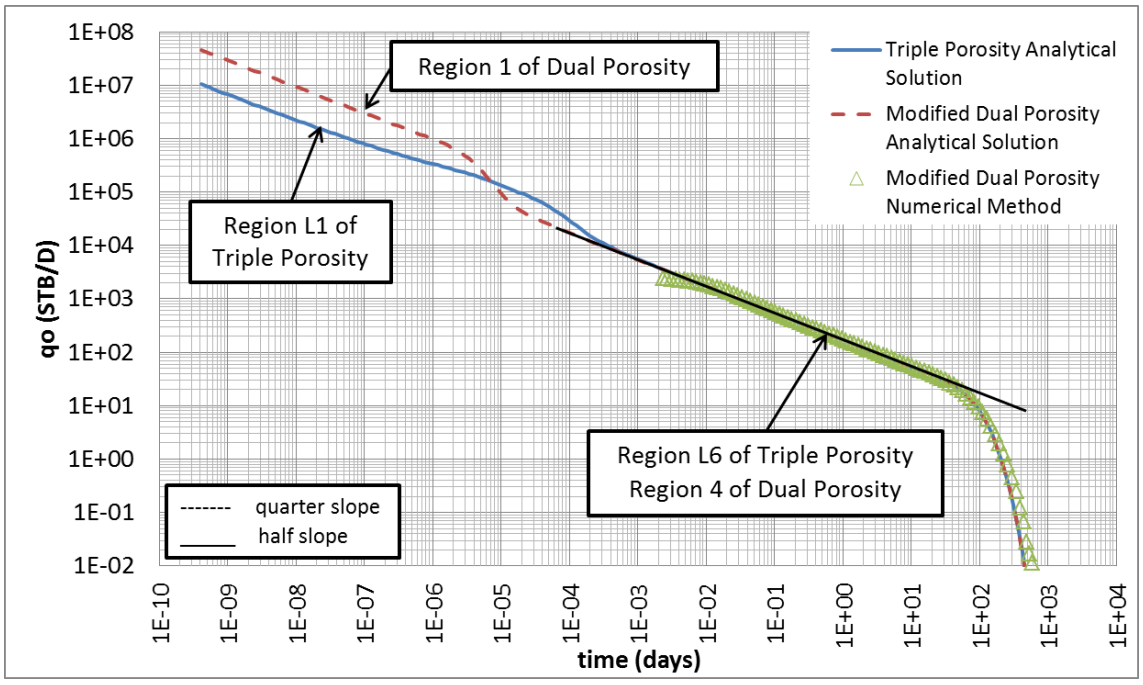

Figure 23 – Comparison plot of triple porosity model and modified dual porosity model of example C

7.4.2 Mathematic Solution Comparison

From the given examples, it can be implied that one region of modified dual porosity model can be represented by one region of triple porosity model when infinite conductivity of hydraulic fractures is applied.

Region 4 and Region L6

From region 4 of dual porosity model asymptotic equation,

$$q_g = \frac{\Delta m(p)}{630T}(2x_e h)\sqrt{k_m}\frac{y_e}{L_F}\sqrt{\mu(\phi V' c_t)_T}\frac{1}{\sqrt{t}} \quad \text{..... (7. 1)}$$

Modify parameters of dual porosity to triple porosity as following

$$q_g = \frac{\Delta m(p)}{630T}(2 \times 2y_e n_F \times h)\sqrt{k_m}\frac{L_F/2}{L_f}\sqrt{\mu(\phi V' c_t)_T}\frac{1}{\sqrt{t}} \quad \text{..... (7. 2)}$$

where

$$2L_F n_F h = A_{cw} \quad \text{..... (7. 3)}$$

Therefore,

$$q_g = \frac{\Delta m(p)}{630\,T}\,A_{cw}\sqrt{k_m}\,\frac{y_e}{L_f}\,\sqrt{\mu(\phi V' c_t)_T}\,\frac{1}{\sqrt{t}} \quad \text{..... (7. 4)}$$

which is region L6 of triple porosity model

Region 3 and Region L5

From region 3 of dual porosity model asymptotic equation,

$$q_g = \frac{\Delta m(p)}{1260T}(2x_e h)\sqrt{k_F}\sqrt{\mu(\phi V' c_t)_T}\frac{1}{\sqrt{t}} \quad \text{..... (7. 5)}$$

Modify parameters of dual porosity to triple porosity as following

$$q_g = \frac{\Delta m(p)}{1260T}(2 \times 2y_e n_F \times h)\sqrt{k_f}\sqrt{\mu(\phi V' c_t)_T}\frac{1}{\sqrt{t}} \quad \text{..... (7. 6)}$$

$$q_g = \frac{\Delta m(p)}{1260T}(2 \times L_F n_F \times h) \times 2y_e/L_F \times \sqrt{k_f}\sqrt{\mu(\phi V' c_t)_T}\frac{1}{\sqrt{t}} \quad \text{..... (7. 7)}$$

Therefore,

$$q_g = \frac{\Delta m(p)}{630\,T}\,A_{cw}\sqrt{k_f}\,\frac{y_e}{L_F}\,\sqrt{\mu(\phi V' c_t)_T}\,\frac{1}{\sqrt{t}} \quad \text{..... (7. 8)}$$

which is region L5 of triple porosity model

Region 2 and Region B4

From region 2 of dual porosity model asymptotic equation,

$$q_g = \frac{\Delta m(p)}{2183.7T}(2x_e h)k_F^{1/2}k_m^{1/4}\frac{1}{\sqrt{L_F}}[\mu(\phi V' c_t)_T]^{1/4}\frac{1}{t^{1/4}} \quad \text{..... (7. 9)}$$

Modify parameters of dual porosity to triple porosity as following

$$q_g = \frac{\Delta m(p)}{2183.7T}(2 \times 2y_e n_F \times h)k_f^{1/2}k_m^{1/4}\frac{1}{\sqrt{L_f}}[\mu(\phi V' c_t)_T]^{1/4}\frac{1}{t^{1/4}} \quad \text{.... (7. 10)}$$

$$q_g = \frac{\Delta m(p)}{2183.7T}(2 \times L_F n_F \times h)\frac{2y_e}{L_F}k_f^{1/2}k_m^{1/4}\frac{1}{\sqrt{L_f}}[\mu(\phi V' c_t)_T]^{1/4}\frac{1}{t^{1/4}} \quad \text{.. (7. 11)}$$

Therefore,

$$q_g = \frac{\Delta m(p)}{1091.86\,T}\,A_{cw}\,y_e\frac{k_f^{1/2}k_m^{1/4}}{L_F\,L_f^{1/2}}\,\mu^{1/4}(\phi V' c_t)_T^{1/4}\,\frac{1}{t^{1/4}} \quad \text{..... (7. 12)}$$

which is region B4 of triple porosity model

Region 1 and Region L4

From region 1 of dual porosity model asymptotic equation,

$$q_g = \frac{\Delta m(p)}{1260T}(2x_e h)\sqrt{k_F}\sqrt{\mu(\phi V' c_t)_F}\frac{1}{\sqrt{t}} \quad \text{..... (7. 13)}$$

Modify parameters of dual porosity to triple porosity as following

$$q_g = \frac{\Delta m(p)}{1260T}(2 \times 2y_e n_F \times h)\sqrt{k_f}\sqrt{\mu(\phi V' c_t)_f}\frac{1}{\sqrt{t}} \quad \text{..... (7. 14)}$$

$$q_g = \frac{\Delta m(p)}{1260T}(2 \times L_F n_F \times h) \times 2y_e/L_F \times \sqrt{k_f}\sqrt{\mu(\phi V' c_t)_f}\frac{1}{\sqrt{t}} \quad \text{..... (7. 15)}$$

Therefore,

$$q_g = \frac{\Delta m(p)}{630\,T}\, A_{cw}\sqrt{k_f}\, \frac{y_e}{L_F} \sqrt{\mu(\phi V' c_t)_f}\, \frac{1}{\sqrt{t}} \quad \text{..... (7. 16)}$$

which is region L4 of triple porosity model

CHAPTER VIII

APPLICATION OF THE TRIPLE POROSITY MODEL

8.1 Introduction

In this chapter, the fully transient triple porosity model with the assumption of infinite conductivity hydraulic fractures is used for production data interpretation of shale gas and oil reservoirs in multi-transverse hydraulic fractures horizontal well. The interpretation guidelines and the example of interpretation are presented.

From triple porosity model, 12 flow regimes (6 linear, 4 bilinear, 1 trilinear, and BDF) have been proposed as discussed earlier. Also, to reduce the complexity and confusion of the model, infinite conductivity of hydraulic fractures has been proposed. With considering infinite conductivity of hydraulic fractures, only two mediums responses which are natural fracture and matrix systems are expected to be found in production analysis. This can be interpreted as modified dual porosity as discussed earlier.

In this interpretation, 3 flow regimes (2 linear and 1 bilinear) remain to be considered for production data analysis. The summary of triple porosity model with infinite conductivity of hydraulic fractures, theoretical triple porosity model cases, and field example will illustrate the procedures and cautions of interpreting the data with triple porosity model.

8.2 Summary of Triple Porosity Model for Interpretation

For daily production data interpretation, either region L5 or region L6, which is represented for the last linear period, is supposed to be showed by the linear period (a half-slope in log-log plot). The criteria of either region L5 or L6 will be found is given by $\frac{L_f}{L_F} = \sqrt{\frac{k_m}{k_f}}$.

- Region L5 will be found only when $\frac{L_f}{L_F} < \sqrt{\frac{k_m}{k_f}}$.
- Region L6 will be found only when $\frac{L_f}{L_F} > \sqrt{\frac{k_m}{k_f}}$.

The summary of triple porosity model with infinite conductivity hydraulic fractures characteristic can be illustrated in **Figure 24** and **Figure 25** which are dimensionless and dimensional forms, respectively.

The associated equations of triple porosity model for data interpretation are summarized in **Table 18**, **Table 19**, and **Table 20**.

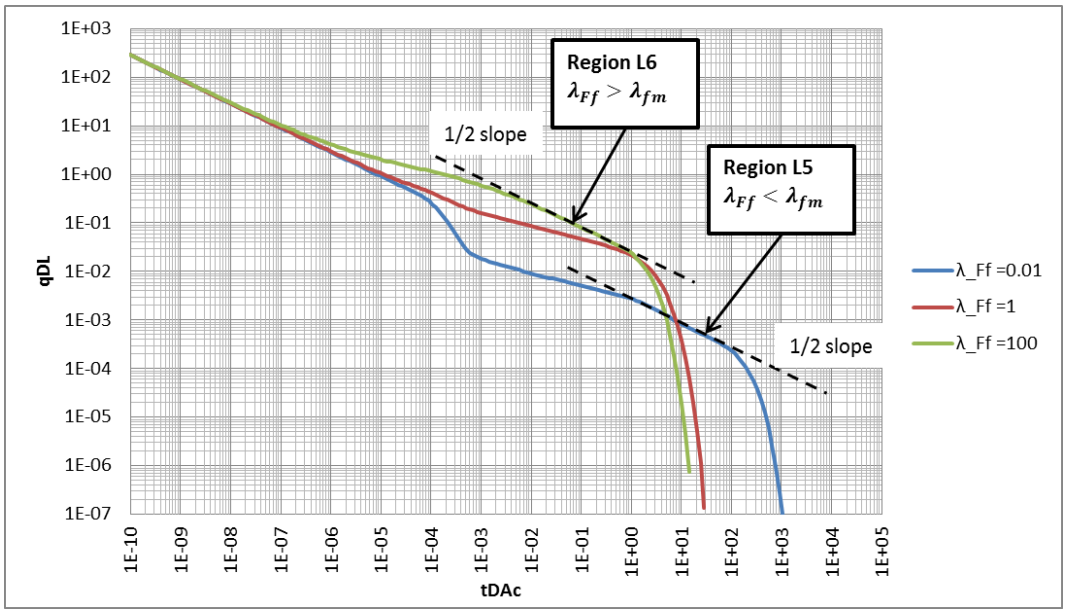

Figure 24 – Summary of triple porosity model characteristic for interpretation in dimensionless form

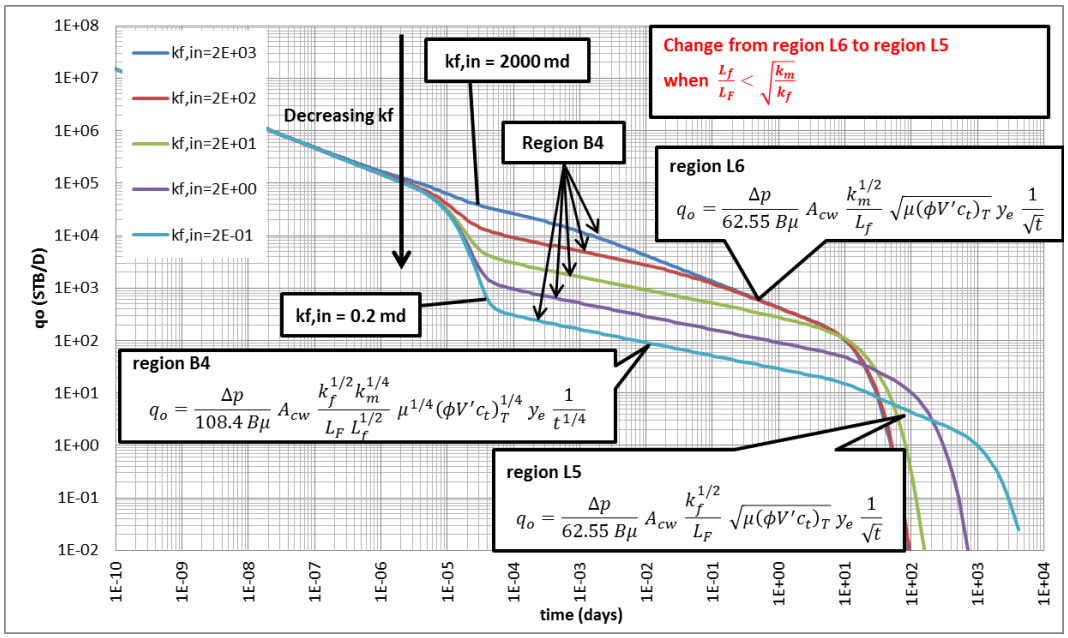

Figure 25 – Summary of triple porosity model characteristic for interpretation in dimensional form

Table 18 – Summary of associated equations for data interpretation of region L6

Region L6	Equation	Unknown
Asymptotic Equation for gas	$\frac{\Delta m(p)}{q_g} = \frac{630\,T}{A_{cw}} \frac{L_f}{k_m^{1/2}} \frac{1}{y_e} \frac{1}{\sqrt{\mu(\phi V' c_t)_T}} \sqrt{t}$	$y_e, L_f, (k_m)$
Asymptotic Equation for oil	$\frac{\Delta p}{q_o} = \frac{62.55\,B\mu}{A_{cw}} \frac{L_f}{k_m^{1/2}} \frac{1}{y_e} \frac{1}{\sqrt{\mu(\phi V' c_t)_T}} \sqrt{t}$	$y_e, L_f, (k_m)$
End of region L6	$t_{end\ L6} \cong 9.874\,[\phi V' c_t]_T \mu \frac{L_f^2}{k_m}$	$L_f, (k_m)$
Combine Slope and End of region for gas	$y_e = \frac{200.5\,T}{A_{cw}\,[\phi V' c_t]_T} \frac{1}{slope} \sqrt{t_{end\ L6}}$	
Combine Slope and End of region for oil	$y_e = \frac{19.9\,B}{A_{cw}\,[\phi V' c_t]_T} \frac{1}{slope} \sqrt{t_{end\ L6}}$	

Table 19 – Summary of associated equations for data interpretation of region L5

Region L5	Equation	Unknown
Asymptotic Equation for gas	$\frac{\Delta m(p)}{q_g} = \frac{630\,T}{A_{cw}} \frac{L_F}{k_f^{1/2}} \frac{1}{y_e} \frac{1}{\sqrt{\mu(\phi V' c_t)_T}} \sqrt{t}$	k_f, y_e
Asymptotic Equation for oil	$\frac{\Delta p}{q_o} = \frac{62.55\,B\mu}{A_{cw}} \frac{L_F}{k_f^{1/2}} \frac{1}{y_e} \frac{1}{\sqrt{\mu(\phi V' c_t)_T}} \sqrt{t}$	k_f, y_e
End of region L5	$t_{end\ L5} \cong 9.874\,[\phi V' c_t]_T \mu \frac{L_F^2}{k_f}$	k_f
Combine Slope and End of region for gas	$y_e = \frac{200.5\,T}{A_{cw}\,[\phi V' c_t]_T} \frac{1}{slope} \sqrt{t_{end\ L5}}$	
Combine Slope and End of region for oil	$y_e = \frac{19.9\,B}{A_{cw}\,[\phi V' c_t]_T} \frac{1}{slope} \sqrt{t_{end\ L5}}$	

Table 20 – Summary of associated equations for data interpretation of region B4

Region B4	Equation	Unknown
Asymptotic Equation for gas	$\frac{\Delta m(p)}{q_g} = \frac{1091.86\,T}{A_{cw}} \frac{L_F\,L_f^{1/2}}{k_f^{1/2}k_m^{1/4}\,\mu^{1/4}(\phi V' c_t)_T^{1/4}} \frac{1}{y_e}\,t^{1/4}$	$k_f, L_f, y_e, (k_m)$
Asymptotic Equation for oil	$\frac{\Delta p}{q_o} = \frac{108.4\,B\mu}{A_{cw}} \frac{L_F\,L_f^{1/2}}{k_f^{1/2}k_m^{1/4}\,\mu^{1/4}(\phi V' c_t)_T^{1/4}} \frac{1}{y_e}\,t^{1/4}$	$k_f, L_f, y_e, (k_m)$
Intersection of region B4 and region L6	$t_{int\ B4,L6} = 9.023\,\mu[\phi V' c_t]_T \frac{L_F^4}{L_f^2} \frac{k_m}{k_f^2}$	$L_f, k_f, (k_m)$
Intersection of region B4 and region L5	$t_{int\ B4,L5} = 9.023\,\mu[\phi V' c_t]_T \frac{L_f^2}{k_m}$	$L_f, (k_m)$

8.3 Interpretation Guidelines

The interpretation of triple porosity model focuses for possible bilinear and the last linear flow. Same as dual porosity model, the possible five production scenarios are listed in **Table 7**. Also, please note that in this interpretation guidelines, the total compressibility, c_t, is assumed to be same for all medium systems in order to provide the simplify equations for interpretation. Moreover, constant pressure solutions are applied due to the normal production practice of shale gas/oil reservoir that producing at constant wellhead pressure.

8.3.1 Production Scenario Case 1

- There are two possible answers from interpretation but only one answer is correct. Two possible answers are calculated from region L5 and region L6 asymptotic equations.

- Normally, if high conductivity in natural fractures and low permeability of matrix is expected, region L6 asymptotic equation is recommended to use. On the other hand, if low conductivity of natural fractures and high permeability of matrix, region L5 asymptotic equation is recommended.
- There is a high uncertainty in calculation due to some natural fracture properties have to be assumed.
- It is recommend to calculate the minimum hydraulic fracture half-length, $y_{e,min}$. $y_{e,min}$ can be calculated from the last point, t_{end} and slope of the square root of time plot.

Choice 1 – Region L6

L_f and k_m have to be known

y_e can be found from slope of the square root of time plot, m_{square}

The equations of gas and oil are given, respectively by

$$y_e = \frac{630\ T\ L_f}{A_{cw}\sqrt{k_m}} \frac{1}{\sqrt{\mu \phi_T c_t}} \frac{1}{m_{square}} \quad \text{..... (8. 1)}$$

$$y_e = \frac{62.55 B \sqrt{\mu}\ L_f}{A_{cw}\sqrt{k_m}\ \sqrt{\phi_T c_t}} \frac{1}{m_{square}} \quad \text{..... (8. 2)}$$

In case the value of k_m and L_f are not certain, minimum $L_f/\sqrt{k_m}$ can be find from t_{end}

$$\left(\frac{L_f}{\sqrt{k_m}}\right)_{min} = 0.318 \sqrt{\frac{t_{end}}{\mu \phi_T c_t}} \quad \text{..... (8. 3)}$$

Choice 2 – Region L5

k_f has to be assumed

y_e can be found from slope of the square root of time plot, m_{square}

The equations of gas and oil are given, respectively by

$$y_e = \frac{630\ T\ L_F}{A_{cw}\sqrt{k_f}} \frac{1}{\sqrt{\mu\phi_T c_t}} \frac{1}{m_{square}} \quad \text{..... (8. 4)}$$

$$y_e = \frac{62.55B\sqrt{\mu}\ L_F}{A_{cw}\sqrt{k_f}\ \sqrt{\phi_T c_t}} \frac{1}{m_{square}} \quad \text{..... (8. 5)}$$

Maximum k_f can be calculated from t_{end}

$$k_{f,max} = 9.874 \frac{L_F^2\ \mu\phi_T c_t}{t_{end}} \quad \text{..... (8. 6)}$$

Minimum y_e

The equations of gas and oil are given, respectively by

$$y_{e,min} = \frac{200.5\ T}{A_{cw}\ \mu\phi_T c_t} \frac{\sqrt{t_{end}}}{m_{square}} \quad \text{..... (8. 7)}$$

$$y_{e,min} = \frac{19.9B}{A_{cw}\ \phi_T c_t} \frac{\sqrt{t_{end}}}{m_{square}} \quad \text{..... (8. 8)}$$

8.3.2 Production Scenario Case 2

- It is impossible to determine whether region L5 or region L6 is found
- Unique solution of y_e and in-place whether region L5 or region L6 is assumed

- By combining asymptotic equation and end of straight line on square rood of time plot, calculated y_e will be the same for both region L5 and region L6 cases
- The value of $k_F, k_f,\ k_m, L_f$ is not required

For gas

$$y_e = \frac{200.5\ T}{A_{cw}\ \mu\phi_T c_t}\frac{\sqrt{t_{esr}}}{m_{square}} \quad \text{..... (8. 9)}$$

$$OGIP\ (MMscf) = \frac{200.5 \times 10^{-6}\ T}{\mu\ c_t}\frac{\sqrt{t_{esr}}}{m_{square}}(1 - s_{wi})\frac{1}{B_g} \quad \text{..... (8. 10)}$$

For oil

$$y_e = \frac{19.9B}{A_{cw}\ \phi_T c_t}\frac{\sqrt{t_{esr}}}{m_{square}} \quad \text{..... (8. 11)}$$

$$OOIP\ (MMSTB) = \frac{3.545 \times 10^{-6}}{c_t}\frac{\sqrt{t_{esr}}}{m_{square}}(1 - s_{wi}) \quad \text{..... (8. 12)}$$

In case assuming region L5 is found, k_f can be calculated from

$$k_f = 9.874\frac{L_F^2\ \mu\phi_T c_t}{t_{esr}} \quad \text{..... (8. 13)}$$

8.3.3 Production Scenario Case 3

- k_f, L_f, and k_m have to be assumed
- y_e can be determined from slope of the fourth root of time plot, m_{fourth}
- There is a high uncertainty in calculation due to some natural fracture properties have to be assumed

The equations of gas and oil are given, respectively by

$$y_e = \frac{1091.86\,T}{A_{cw}} \frac{L_F\,L_f^{1/2}}{k_f^{1/2}k_m^{1/4}\,[\mu\phi_T c_t]^{1/4}} \frac{1}{m_{fourth}} \quad \text{..... (8. 14)}$$

$$y_e = \frac{108.4\,B\mu}{A_{cw}} \frac{L_F\,L_f^{1/2}}{k_f^{1/2}k_m^{1/4}\,[\mu\phi_T c_t]^{1/4}} \frac{1}{m_{fourth}} \quad \text{..... (8. 15)}$$

8.3.4 Production Scenario Case 4

- Whether region L5 or L6 can be determined only when k_m and L_f are assumed and reliable.

Procedures:

1. From bilinear flow period, find $\sqrt{k_f}\,y_e$ from region B4 equation with assumingk_m and L_f. (**Eq. 8.14** or **Eq. 8.15**)
2. From linear flow period, find $\sqrt{k_f}\,y_e$ from region L5 equation. (**Eq. 8.4** or **Eq. 8.5**)
3. Check whether $\sqrt{k_f}\,y_e$ from region B4 is close to region L5 or not.
4. If yes, the linear flow period is represented by region L5 and y_e can be determined from $\sqrt{k_f}\,y_e$ term by assuming k_f. Furthermore, maximum k_f can be calculated from **Eq. 8.6**.

   If no, the linear flow period is represented by region L6 and y_e can be calculated from region L6 equation by assuming k_m and L_f (**Eq. 8.1** or **Eq. 8.2**). The minimum value of $L_f/\sqrt{k_m}$ is calculated by **Eq. 8.3** and used for cross-checking the value.

8.3.5 Production Scenario Case 5

- Interpret the data as production scenario case 2.
- Determine whether region L5 or L6 is found by using the same method as production scenario case 4.

8.4 Examples of Triple Porosity Interpretation

8.4.1 Well T01

The theoretical model of multi-transverse hydraulic fractures in horizontal well of shale oil reservoir was generated by using triple porosity model. High conductivity hydraulic fractures is assumed. High permeability in natural fractures and low permeability in matrix are also assumed in this case. The data table and generated daily production data are shown in **Table 21** and **Figure 26**. The OOIP of this well is 5.48 MMSTB. The linear flow period of this well is represented by region L6.

Table 21 – Well T01 data

Thickness	h	200 ft	Hydraulic Fracture Half-Length	y_e	500 ft
Perforation Interval	x_e	5000 ft	Hydraulic Fracture Effective Permeability	k_F	100 md
Hydraulic Fracture Spacing	L_F	200 ft	Hydraulic Fracture Width	w_F	0.01 ft
Number of Hydraulic Fracture	n_F	25	Hydraulic Fracture Intrinsic Permeability	$k_{F,in}$	2.00E+06 md
Natural Fracture Spacing	L_f	20 ft	Hydraulic Fracture Porosity	ϕ_F	0.3
Number of Natural Fracture	n_f	25	Natural Fracture Effective Permeability	k_f	0.1 md
Matrix Permeability	k_m	1.00E-07 md	Natural Fracture Width	w_f	0.001 ft
Total Porosity	ϕ	0.05	Natural Fracture Intrinsic Permeability	$k_{f,in}$	2000 md
Water Saturation	S_w	0.2	Natural Fracture Porosity	ϕ_f	0.3
Formation Volume Factor	B_o	1.3 rcf/scf	Matrix Porosity	ϕ_m	0.05
Viscosity	μ	1.3 cp	Total Compressibility	c_{ti}	2.00E-07 psi-1
Initial Pressure	p_i	3000 psia	Bottomhole Flowing Pressure	p_{wf}	500 pisa

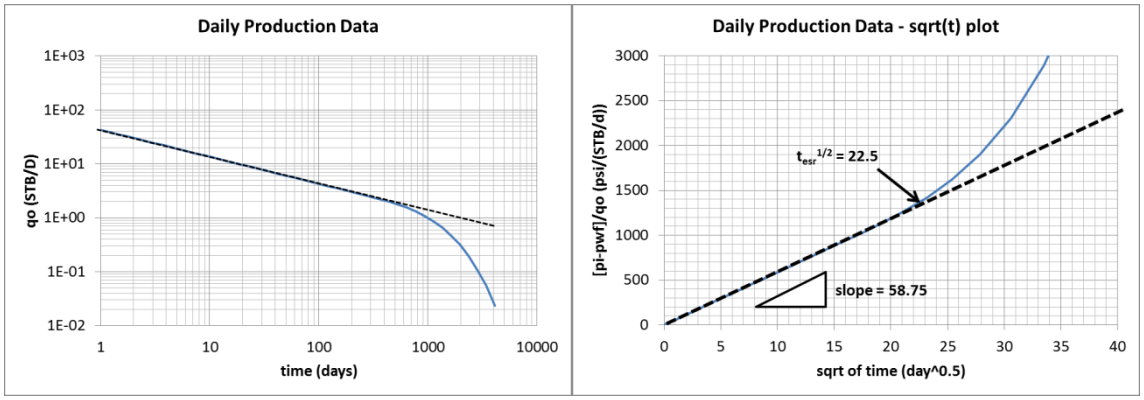

Figure 26 – Production data and square root of time plots of well T01

To simulate the real situation when interpreting data, the provided information for interpretation is same as provided data except hydraulic fractures and natural fractures information e.g. y_e, k_F, k_f, L_f.

To analyze production data of this well, interpretation guidelines of the production scenario case 2 (Linear and BDF periods are found) are used.

From **Eq. 8.11**, y_e is 495 ft.

From **Eq. 8.12**, $OOIP$ is 5.43 MMSTB

In case, region L5 is expected, k_f is 1E-5 md. from **Eq. 8.13**.

8.4.2 Well T02

Another theoretical shale oil well was generated by triple porosity model. This well is assumed permeability in natural fractures is low. The data table and generated daily production data are shown in **Table 22** and **Figure 27**. The OOIP from this well is 5.48 MMSTB. The linear flow period is represented by region L5.

Table 22 – Well T02 data

Thickness	h	200 ft	Hydraulic Fracture Half-Length	y_e	500 ft
Perforation Interval	x_e	5000 ft	Hydraulic Fracture Effective Permeability	k_F	100 md
Hydraulic Fracture Spacing	L_F	200 ft	Hydraulic Fracture Width	w_F	0.01 ft
Number of Hydraulic Fracture	n_F	25	Hydraulic Fracture Intrinsic Permeability	$k_{F,in}$	2.00E+06 md
Natural Fracture Spacing	L_f	10 ft	Hydraulic Fracture Porosity	ϕ_F	0.3
Number of Natural Fracture	n_f	50	Natural Fracture Effective Permeability	k_f	0.00001 md
Matrix Permeability	k_m	1.00E-05 md	Natural Fracture Width	w_f	0.001 ft
Total Porosity	ϕ	0.05	Natural Fracture Intrinsic Permeability	$k_{f,in}$	0.1 md
Water Saturation	S_w	0.2	Natural Fracture Porosity	ϕ_f	0.3
Formation Volume Factor	B_o	1.3 rcf/scf	Matrix Porosity	ϕ_m	0.05
Viscosity	μ	1.3 cp	Total Compressibility	c_{ti}	2.00E-07 psi-1
Initial Pressure	p_i	3000 psia	Bottomhole Flowing Pressure	p_{wf}	500 pisa

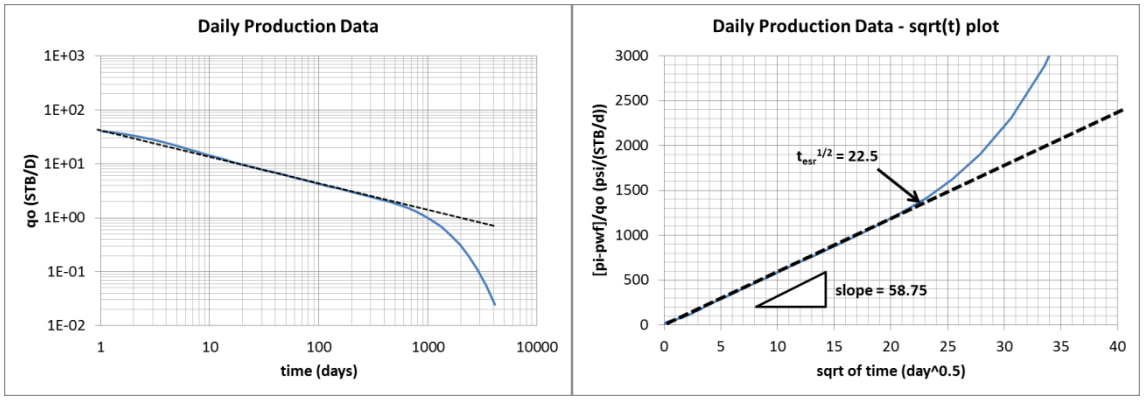

Figure 27 – Production data and square root of time plots of well T02

To simulate the real situation when interpreting data, the provided information for interpretation is same as provided data except hydraulic fractures and natural fractures information e.g. y_e, k_F, k_f, L_f.

From the interpretation guide line, this case matches the production scenario case 2 which is linear and BDF period. Moreover, this case has the same parameters as case well T01; therefore, the calculated parameters will be the same as case well T01 which are $y_e = 495$ ft and $OOIP = 5.43$ MMSTB.

8.4.3 Well T03

Another theoretical well was generated with the same data as Well T02 as showed in **Table 22** and the production data was generated only 1,000 days as showed in **Figure 28**. No deviation from the half-slope line on log-log plot.

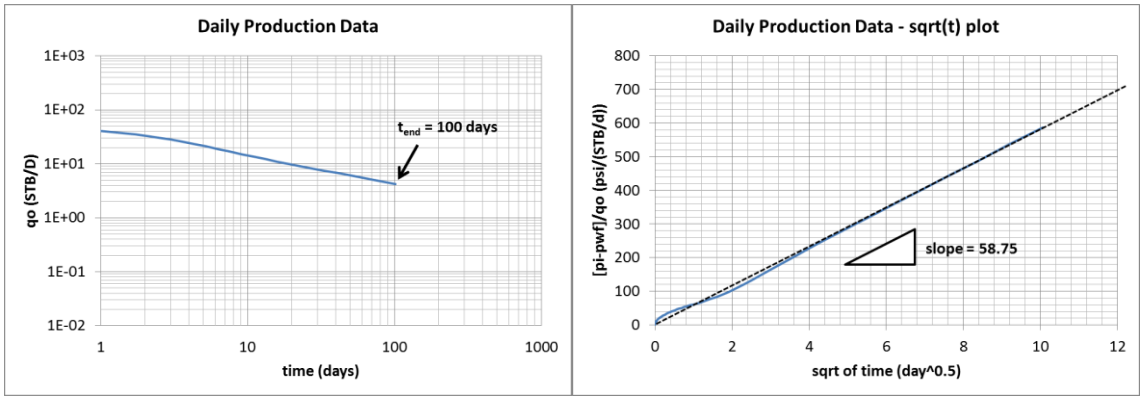

Figure 28 – Production data and square root of time plots of well T03

The provided information for interpretation is same as provided data except hydraulic fractures and natural fractures information e.g. y_e, k_F, k_f. Assume L_f and k_m are known from core data analysis.

In this case, the production data shows only linear flow or production curve have not shown BDF yet. From the interpretation guide line, this case matches the production scenario case 1 which is only linear period is found. Whether region L5 or region L6 is found for the linear flow cannot be determined. Therefore, two asymptotic equations are used to see the properties.

Choice 1 – Region L6 is selected

L_f and k_m are known from core data analysis

From **Eq. 8.2**, y_e is 25 ft.

Choice 2 – Region L5 is selected

k_f has to be assumed with the maximum limit which is calculated by **Eq. 8.6**, $k_{f,max}$ is 5.1E-5 md. Thus, k_f of 1E-5 md is assumed ($k_{f,in}$ 0.1 md with w_f 0.001 ft).

From **Eq. 8.5**, y_e is 499 ft.

If k_f is assumed as 1E-6 md ($k_{f,in}$ 0.01 md with w_f 0.001 ft), y_e is 1,578 ft.

Minimum y_e

From **Eq. 8.8**, $y_{e,min}$ is 220 ft.

In summary, the last linear is supposed to be region L5 rather than region L6 because the calculated y_e from asymptotic equation of region L6 is much more less than the minimum calculated y_e. Therefore, the value of y_e may be any value higher than 220 ft.

8.4.4 Well 314

Field production plot and data of the multi-transverse hydraulic fractures horizontal well, well#314, is shown in **Appendix B**. In this interpretation, skin effect and gas adsorption are neglected. To analyze production data of this well, interpretation guidelines of the production scenario case 2 (Linear and BDF periods are found) are used.

From **Eq. 8.9**, y_e is 186 ft.

From **Eq. 8.10**, $OGIP$ is 2.7E+3 MMscf

In case, region L5 is expected, k_f is 1.3E-4 md. from **Eq. 8.13**.

8.4.5 Well B-86

Field production plot and data of the multi-transverse hydraulic fractures horizontal well, well#B-86, is shown in **Appendix B**. In this interpretation, skin effect and gas adsorption are neglected. To analyze production data of this well, interpretation guidelines of the production scenario case 4 (Bilinear and linear periods are found) are used.

1. By assuming k_m is 1.5E-4 md and L_f is 25 ft, $\sqrt{k_f}y_e$ is 1.5 from **Eq. 8.14** or by assuming k_m is 5E-5 md, $\sqrt{k_f}y_e$ is 2.

2. From **Eq. 8.4**, $\sqrt{k_f}y_e$ is 2.05.
3. The calculated value of $\sqrt{k_f}y_e$ from region L5 equation is close to the value of $\sqrt{k_f}y_e$ from region B4 equation; therefore, the late linear flow period is supposed to be region L5.
4. Maximum k_f from **Eq. 8.6** is 2.5E-4 md. If using maximum k_f, minimum y_e from $\sqrt{k_f}y_e$ in step 2 is 131 ft. In case, k_f is assumed to be 1E-5 md, y_e is 649 ft from $\sqrt{k_f}y_e = 2.05$ in step 2.

In summary, region L5 is expected to represent the linear period, and the minimum value of y_e is 131 ft.

CHAPTER IX

APPLICATION OF DUAL POROSITY MODEL AND TRIPLE POROSITY MODEL

In this chapter, the transient dual porosity model and the fully transient triple porosity model with the assumption of infinite conductivity hydraulic fractures are used for production data interpretation of shale gas and oil reservoirs in multi-transverse hydraulic fractures horizontal well. The interpretation guidelines and the example of interpretation are presented.

To reduce the complication of interpretation, all of the following interpretations will focus on assumption of infinite conductivity of hydraulic fractures for interpreting daily production data of shale gas/oil reservoir. With the assumption of homogeneous reservoir and infinite conductivity hydraulic fractures of dual porosity model, only one medium (matrix system) is left for considering. Therefore, only one region of linear flow is considered for dual porosity model which is region 4. Regarding the assumption of infinite conductivity hydraulic fractures of triple porosity model, two mediums (natural fractures and matrix systems) are left for considering. Consequently, two regions of linear flow are considered for triple porosity model which are region L5 and L6. Moreover, region B4 of triple porosity model are considered as bilinear flow region.

9.1 Interpretation Guidelines

To emphasize the solutions of the dual porosity model and the triple porosity model, all the associated and guidelines are re-summarized from **Chapter V** and **Chapter VIII** as follows. The interpretation guidelines follow the possible five production scenarios showed in **Table 7**. Also, please note that in the interpretation guidelines, the total compressibility, c_t, is assumed to be same for all medium systems in order to provide the simplify equations for interpretation.

Referring to the assumption of infinite conductivity of hydraulic fractures, production scenario case 3, 4, and 5, which have bilinear flow period in the production profile, can be represented by the triple porosity model only because the dual porosity model cannot present bilinear flow in this assumption.

9.1.1 Production Scenario Case 1

- There are three possible answers from interpretation but only one answer is correct. One possible answer is calculated from the region 4 of dual porosity model asymptotic equation. The other two possible answers are calculated from the region L5 and L6 of triple porosity model asymptotic equations.
- If homogeneous reservoir is assumed, region 4 of dual porosity model is applied. If reopen natural fractures is expected, triple porosity model is applied. Normally, if high conductivity in natural fractures and low permeability of matrix is expected, region L6 asymptotic equation is recommended to use. On

the other hand, if low conductivity of natural fractures and high permeability of matrix, region L5 asymptotic equation is recommended.

- There is a high uncertainty in calculation due to some natural fracture properties have to be assumed for triple porosity model calculation.
- It is recommend to calculate the minimum hydraulic fracture half-length, $y_{e,min}$. $y_{e,min}$ can be calculated from the last point, t_{end} and slope of the square root of time plot. The equations for dual porosity and triple porosity models are the same.

Choice 1 – Region 4 of Dual Porosity Model

k_m has to be known

y_e can be found from slope of the square root of time plot, m_{square}

The equations of gas and oil are given, respectively by

$$y_e = \frac{630\ T\ L_F}{A_{cw}\sqrt{k_m}} \frac{1}{\sqrt{\mu\phi_T c_t}} \frac{1}{m_{square}} \quad \text{..... (5. 1)}$$

$$y_e = \frac{62.55B\sqrt{\mu}\ L_F}{A_{cw}\sqrt{k_m}\ \sqrt{\phi_T c_t}} \frac{1}{m_{square}} \quad \text{..... (5. 2)}$$

In case the value of k_m is not certain, maximum k_m can be find from t_{end}

$$k_{m,max} = 9.874 \frac{L_F^2\ \mu\phi_T c_t}{t_{end}} \quad \text{..... (5. 3)}$$

Choice 2 – Region L6 of Triple Porosity Model

L_f and k_m have to be known

y_e can be found from slope of the square root of time plot, m_{square}

The equations of gas and oil are given, respectively by

$$y_e = \frac{630\ T\ L_f}{A_{cw}\sqrt{k_m}} \frac{1}{\sqrt{\mu \phi_T c_t}} \frac{1}{m_{square}} \quad \text{..... (8. 1)}$$

$$y_e = \frac{62.55B\sqrt{\mu}\ L_f}{A_{cw}\sqrt{k_m}\ \sqrt{\phi_T c_t}} \frac{1}{m_{square}} \quad \text{..... (8. 2)}$$

In case the value of k_m and L_f are not certain, minimum $L_f/\sqrt{k_m}$ can be find from t_{end}

$$\left(\frac{L_f}{\sqrt{k_m}}\right)_{min} = 0.318 \sqrt{\frac{t_{end}}{\mu \phi_T c_t}} \quad \text{..... (8. 3)}$$

Choice 3 – Region L5 of Triple Porosity Model

k_f has to be assumed

y_e can be found from slope of the square root of time plot, m_{square}

The equations of gas and oil are given, respectively by

$$y_e = \frac{630\ T\ L_F}{A_{cw}\sqrt{k_f}} \frac{1}{\sqrt{\mu \phi_T c_t}} \frac{1}{m_{square}} \quad \text{..... (8. 4)}$$

$$y_e = \frac{62.55B\sqrt{\mu}\ L_F}{A_{cw}\sqrt{k_f}\ \sqrt{\phi_T c_t}} \frac{1}{m_{square}} \quad \text{..... (8. 5)}$$

Maximum k_f can be calculated from t_{end}

$$k_{f,max} = 9.874 \frac{L_F^2 \, \mu \phi_T c_t}{t_{end}} \quad \text{..... (8. 6)}$$

Minimum y_e

The equations of gas and oil are given, respectively by

$$y_{e,min} = \frac{200.5 \, T}{A_{cw} \, \mu \phi_T c_t} \frac{\sqrt{t_{end}}}{m_{square}} \quad \text{..... (9. 1)}$$

$$y_{e,min} = \frac{19.9 B}{A_{cw} \, \phi_T c_t} \frac{\sqrt{t_{end}}}{m_{square}} \quad \text{..... (9. 2)}$$

9.1.2 Production Scenario Case 2

- It is impossible to determine which region is found (region 4, region L5, or region L6)
- Unique solution of y_e and in-place whether dual porosity model or triple porosity model is assumed
- By combining asymptotic equation and end of straight line on square rood of time plot, calculated y_e will be the same for any case (region 4, region L5, or region L6)
- The value of $k_F, k_f, \, k_m, L_f$ is not required

For gas

$$y_e = \frac{200.5 \, T}{A_{cw} \, \mu \phi_T c_t} \frac{\sqrt{t_{esr}}}{m_{square}} \quad \text{..... (9. 3)}$$

$$OGIP\ (MMscf) = \frac{200.5 \times 10^{-6}\ T}{\mu\ c_t} \frac{\sqrt{t_{esr}}}{m_{square}} (1 - s_{wi}) \frac{1}{B_g} \quad \text{..... (9. 4)}$$

For oil

$$y_e = \frac{19.9B}{A_{cw}\ \phi_T c_t} \frac{\sqrt{t_{esr}}}{m_{square}} \quad \text{..... (9. 5)}$$

$$OOIP\ (MMSTB) = \frac{3.545 \times 10^{-6}}{c_t} \frac{\sqrt{t_{esr}}}{m_{square}} (1 - s_{wi}) \quad \text{..... (9. 6)}$$

In case assuming region 4 of dual porosity model is found, k_m can be calculated from

$$k_m = 9.874 \frac{L_F^2\ \mu \phi_T c_t}{t_{esr}} \quad \text{..... (5. 12)}$$

In case assuming region L5 of triple porosity model is found, k_f can be calculated from

$$k_f = 9.874 \frac{L_F^2\ \mu \phi_T c_t}{t_{esr}} \quad \text{..... (8. 13)}$$

9.1.3 Production Scenario Case 3

- k_f, L_f, and k_m have to be assumed
- y_e can be determined from slope of the fourth root of time plot, m_{fourth}
- There is a high uncertainty in calculation due to some natural fracture properties have to be assumed

The equations of gas and oil are given, respectively by

$$y_e = \frac{1091.86\ T}{A_{cw}} \frac{L_F\ L_f^{1/2}}{k_f^{1/2} k_m^{1/4}\ [\mu \phi_T c_t]^{1/4}} \frac{1}{m_{fourth}} \quad \text{..... (8. 14)}$$

$$y_e = \frac{108.4\ B\mu}{A_{cw}} \frac{L_F\ L_f^{1/2}}{k_f^{1/2} k_m^{1/4}\ [\mu \phi_T c_t]^{1/4}} \frac{1}{m_{fourth}} \quad \text{..... (8. 15)}$$

9.1.4 Production Scenario Case 4

- Whether region L5 or L6 can be determined only when k_m and L_f are assumed and reliable.

Procedures:

1. From bilinear flow period, find $\sqrt{k_f}\, y_e$ from region B4 equation with assumingk_m and L_f. (**Eq. 8.14** or **Eq. 8.15**)
2. From linear flow period, find $\sqrt{k_f}\, y_e$ from region L5 equation. (**Eq. 8.4** or **Eq. 8.5**)
3. Check whether $\sqrt{k_f}\, y_e$ from region B4 is close to region L5 or not.
4. If yes, the linear flow period is represented by region L5 and y_e can be determined from $\sqrt{k_f}\, y_e$ term by assuming k_f. Furthermore, maximum k_f can be calculated from **Eq. 8.6**.

   If no, the linear flow period is represented by region L6 and y_e can be calculated from region L6 equation by assuming k_m and L_f (**Eq. 8.1** or **Eq. 8.2**). The minimum value of $L_f/\sqrt{k_m}$ is calculated by **Eq. 8.3** and used for cross-checking the value.

9.1.5 Production Scenario Case 5

- Interpret the data as production scenario case 2.
- Determine whether region L5 or L6 is found by using the same method as production scenario case 4.

9.2 Examples of Interpretation

9.2.1 Well T02

The theoretical model of multi-transverse hydraulic fractures in horizontal well, the same well of well T02 of triple porosity model as generated in **Chapter VII**, is used in this interpretation.

To simulate the real situation when interpreting data, the provided information for interpretation is same as provided data except hydraulic fractures and natural fractures information e.g. y_e, k_F, k_f, L_f.

From the interpretation guide line, this case matches the production scenario case 2 which is linear and BDF period. Both dual porosity and triple porosity interpretation guidelines are shown the same equation for this production scenario case. Consequently, there is a unique solution for the production scenario case 2 (linear and BDF).

From **Eq. 9.5**, y_e is 495 ft.

From **Eq. 9.6**, $OOIP$ is 5.43 MMSTB

In case, region 4 of dual porosity model is expected, k_m is 1E-5 md. from **Eq. 5.12**.

In case, region L5 of triple porosity model is expected, k_f is 1E-5 md. from **Eq. 8.13**.

9.2.2 Well T04

Another theoretical shale oil well was generated by triple porosity model. This well is assumed permeability in natural fractures is low. The data table and the generated daily production data of 100 days are shown in **Table 23** and **Figure 29**. The OOIP from this well is 4.39 MMSTB. The linear flow period is represented by region L5.

Table 23 – Well T04 data

Thickness	h	200 ft	Hydraulic Fracture Half-Length	y_e	400 ft
Perforation Interval	x_e	5000 ft	Hydraulic Fracture Effective Permeability	k_F	100 md
Hydraulic Fracture Spacing	L_F	200 ft	Hydraulic Fracture Width	w_F	0.01 ft
Number of Hydraulic Fracture	n_F	25	Hydraulic Fracture Intrinsic Permeability	$k_{F,in}$	2.00E+06 md
Natural Fracture Spacing	L_f	10 ft	Hydraulic Fracture Porosity	ϕ_F	0.3
Number of Natural Fracture	n_f	40	Natural Fracture Effective Permeability	k_f	0.00001 md
Matrix Permeability	k_m	1.00E-04 md	Natural Fracture Width	w_f	0.001 ft
Total Porosity	ϕ	0.05	Natural Fracture Intrinsic Permeability	$k_{f,in}$	0.1 md
Water Saturation	S_w	0.2	Natural Fracture Porosity	ϕ_f	0.3
Formation Volume Factor	B_o	1.3 rcf/scf	Matrix Porosity	ϕ_m	0.05
Viscosity	μ	1.3 cp	Total Compressibility	c_{ti}	2.00E-07 psi-1
Initial Pressure	p_i	3000 psia	Bottomhole Flowing Pressure	p_{wf}	500 pisa

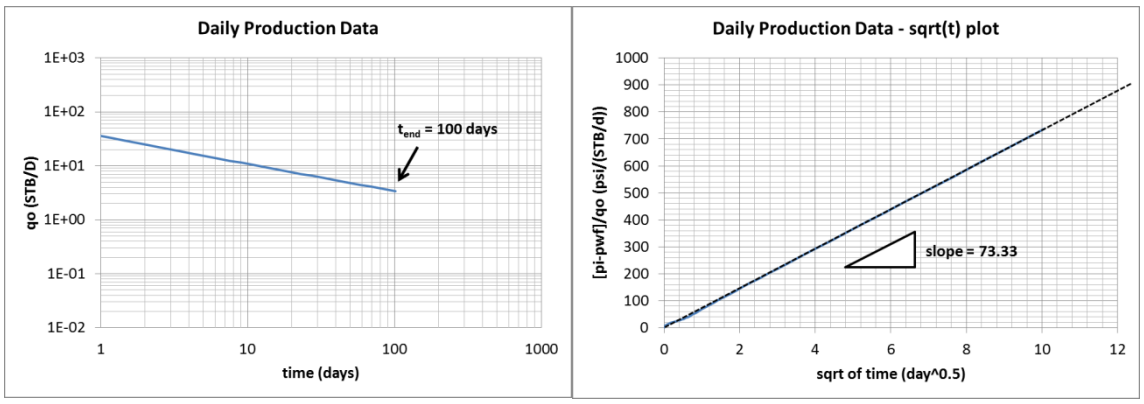

Figure 29 – Production data and square root of time plots of well T04

The provided information for interpretation is same as provided data except hydraulic fractures and natural fractures information e.g. y_e, k_F, k_f. Assume L_f and k_m are known from core data analysis.

In this case, the production data shows only linear flow or production curve have not shown BDF yet. From the interpretation guide line, this case matches the production scenario case 1 which is only linear period is found. What region (region 4, region L5, or region L6) is found for the linear flow cannot be determined. Therefore, three asymptotic equations are used to see the properties.

Choice 1 – Region 4 of Dual Porosity Model

k_m is known from core data analysis (10^{-4} md)

From **Eq. 5.2**, y_e is 126 ft.

Choice 2 – Region L6 of Triple Porosity Model

L_f and k_m are known from core data analysis

From **Eq. 8.1**, y_e is 6.3 ft.

Choice 3 – Region L5 of Triple Porosity Model

k_f has to be assumed with the maximum limit which is calculated by **Eq. 8.6**, $k_{f,max}$ is 5.1E-5 md. Thus, k_f of 1E-5 md is assumed ($k_{f,in}$ 0.1 md with w_f 0.001 ft).

From **Eq. 8.5**, y_e is 400 ft.

If k_f of 1E-6 md is assumed ($k_{f,in}$ 0.01 md with w_f 0.001 ft), y_e is 1264 ft.

Minimum y_e

From **Eq. 9.2**, $y_{e,min}$ is 176 ft.

In summary, the last linear is supposed to be region L5 rather than region L6 because the calculated y_e from asymptotic equation of region L6 is much more less than the minimum calculated y_e. Moreover, the calculated y_e from the region 4 of dual porosity model is less than the minimum value of y_e; therefore, dual porosity model is not supposed to represent this case example. As a result, the value of y_e should be calculated from region L5 equation. However, there is high uncertainty of the value of k_f. The value of y_e can be any value which is higher than 176 ft.

9.2.3 Well 314

Again, well#314 (data in **Appendix B**) is used to show the interpretation of field production data. It is noted that skin effect and gas adsorption are neglected in this case. To analyze production data of this well, interpretation guidelines of the production scenario case 2 (Linear and BDF periods are found) are used.

From **Eq. 9.3**, y_e is 186 ft.

From **Eq. 9.4**, $OGIP$ is 2.7 Bscf

In case, region 4 of dual porosity model is expected, k_m is 1.3E-4 md. from **Eq. 5.12**.

In case, region L5 of triple porosity model is expected, k_f is 1.3E-4 md. from **Eq. 8.13**.

9.2.4 Well B-145

Field production plot and data of the multi-transverse hydraulic fractures horizontal well, well#B-145, is shown in **Appendix B**. In this interpretation, skin effect and gas adsorption are neglected. To analyze production data of this well, interpretation guidelines of the production scenario case 1 (only linear period is found) are used.

Choice 1 – Region 4 of Dual Porosity Model

k_m is known from core data analysis (1.5x10^{-4} md)

From **Eq. 5.1**, y_e is 72 ft.

From **Eq. 5.3**, $k_{m,max}$ is 4.7E-5 md

Choice 2 – Region L6 of Triple Porosity Model

Assume L_f = 10 ft and from core analysis, k_m = 1.5x10^{-4} md

$\left(\frac{L_f}{\sqrt{k_m}}\right)$ is 8.2E+2 ft/md$^{0.5}$.

From **Eq. 8.1**, y_e is 9 ft.

In case this region is found, from **Eq. 8.3**, $\left(\frac{L_f}{\sqrt{k_m}}\right)_{min}$ is 1.2E+4 ft/md$^{0.5}$.

Choice 3 – Region L5 of Triple Porosity Model

k_f has to be assumed with the maximum limit which is calculated by **Eq. 8.6**, $k_{f,max}$ is 4.7E-5 md.

In case, k_f of 1E-5 md is assumed ($k_{f,in}$ 0.1 md with w_f 0.001 ft and L_f 10 ft)

From **Eq. 8.4**, y_e is 277 ft.

In case, k_f of 1E-6 md is assumed ($k_{f,in}$ 0.01 md with w_f 0.001 ft and L_f 10 ft)

From **Eq. 8.4**, y_e is 876 ft.

Minimum y_e

From **Eq. 9.1**, $y_{e,min}$ is 128 ft.

In summary, the linear flow period is supposed to be region L5. From choice 1 or region 4 of dual porosity model, calculated y_e is lower than minimum y_e and calculated k_m is higher than maximum k_m; therefore, it is believed that the linear period is not represented by the region 4. From choice 2 or region L6 of triple porosity model, calculated y_e is too low and calculated $\left(\frac{L_f}{\sqrt{k_m}}\right)$ is lower than minimum$\left(\frac{L_f}{\sqrt{k_m}}\right)$; therefore, it is believed that the linear period is not represented by the region L6. As a result, the value of y_e should be calculated from region L5 equation. However, there is high uncertainty of the value of k_f. The value of y_e can be any value which is higher than 128 ft.

9.3 Discussion and Conclusion

- In case linear and BDF periods are found, unique solution of y_e can be calculated for both dual and triple porosity models.
- In case only linear period is found,

- Three possible regions and equations are used for interpretation.
- Using dual porosity model to interpret reservoir with natural fractures can cause a significant error of value of y_e.
- An uncertainty of k_f value causes a big range of calculated $y_e$value from region L5 asymptotic equation.
- Minimum calculated y_e can be found by using the last point of data.

CHAPTER X

CONCLUSIONS AND RECOMMENDATIONS

10.1 Conclusions

The main conclusions can be summarized as follows.

- The linear homogeneous flow model can be used to analyze the transient linear flow in matrix of the dual porosity model with the condition of infinite conductivity hydraulic fractures.
- The dual porosity model can be used to analyze a fractured horizontal well with the assumption of homogeneous matrix system.
- Five regions and their asymptotic equations can be presented in the dual porosity model.
- In daily production data, long last linear flow is expected to be region 3 or region 4, while possible bilinear flow is region 2. With high conductivity hydraulic fractures, only region 4 is expected to present in production data.
- Region 4 is represented by the same equation as linear homogeneous flow model.
- The triple porosity model can be used to analyze a fractured horizontal well with the naturally fractured reservoir.
- Twelve regions and their asymptotic equations can be represented in the triple porosity model.

- In daily production data, with the assumption of infinite conductivity hydraulic fractures, long last linear flow is expected to be region L5 or region L6, while possible bilinear flow is region B4.
- To interpret production data with the assumption of infinite conductivity hydraulic fractures, if only long linear flow with no decline period is found, different three answers can be calculated. If long linear flow with decline period is found, only one unique solution can be calculated.

10.2 Recommendations

The followings are recommended for future work.

- Developing asymptotic equations and associated equations for constant rate case of triple porosity model.
- Including gas adsorption in the analysis
- More investigation on gas correction factor
- Due to high uncertainty in the natural fracture properties, general values of natural fracture properties of the field should be investigated to increase confidence in calculation.

REFERENCES

Abdassah, D. and Ershaghi, I. 1986. Triple-Porosity Systems for Representing Naturally Fractured Reservoirs. *SPE Formation Evaluation* **1** (2): 113-127. doi: 10.2118/13409-pa

Al-Ahmadi, H.A., Almarzooq, A.M., and Wattenbarger, R.A. 2010. Application of Linear Flow Analysis to Shale Gas Wells - Field Cases. Paper SPE-130370-MS presented at the SPE Unconventional Gas Conference, Pittsburgh, Pennsylvania, 23-25 February. doi: 10.2118/130370-ms

Al-Ahmadi, H.A. 2010. A Triple-Porosity Model for Fractured Horizontal Wells. M.S. Thesis. Texas A&M University, College Station, Texas.

Al-Ahmadi, H.A. and Wattenbarger, R.A. 2011. Triple-Porosity Models: One Further Step Towards Capturing Fractured Reservoirs Heterogeneity. Paper SPE-149054-MS presented at the SPE/DGS Saudi Arabia Section Technical Symposium and Exhibition, Al-Khobar, Saudi Arabia, 15-18 May. doi: 10.2118/149054-ms

Al-Ghamdi, A. and Ershaghi, I. 1996. Pressure Transient Analysis of Dually Fractured Reservoirs. *SPE Journal* **1** (1): 93-100. doi: 10.2118/26959-pa

Anderson, D.M., Nobakht, M., Moghadam, S. et al. 2010. Analysis of Production Data from Fractured Shale Gas Wells. Paper SPE-131787-MS presented at the SPE Unconventional Gas Conference, Pittsburgh, Pennsylvania, 23-25 February. doi: 10.2118/131787-ms

Arevalo-Villagran, J.A., Wattenbarger, R.A., Samaniego-Verduzco, F. et al. 2001. Production Analysis of Long-Term Linear Flow in Tight Gas Reservoirs: Case Histories. Paper SPE-71516-MS presented at the SPE Annual Technical Conference and Exhibition, New Orleans, Louisiana, 30 September-3 October. doi: 10.2118/71516-ms

Bello, R.O. 2009. Rate Transient Analysis in Shale Gas Reservoirs with Transient Linear Behavior. Ph.D. Dissertation. Texas A&M University, College Station, Texas.

Bello, R.O. and Wattenbarger, R.A. 2008. Rate Transient Analysis in Naturally Fractured Shale Gas Reservoirs. Paper SPE-114591-MS presented at the CIPC/SPE Gas Technology Symposium 2008 Joint Conference, Calgary, Alberta, Canada, 16-19 June. doi: 10.2118/114591-ms

Bello, R.O. and Wattenbarger, R.A. 2009. Modelling and Analysis of Shale Gas Production with a Skin Effect. Paper PETSOC-2009-082 presented at the Canadian International Petroleum Conference, Calgary, Alberta, 16-18 June. doi: 10.2118/2009-082

Bello, R.O. and Wattenbarger, R.A. 2010. Multi-Stage Hydraulically Fractured Horizontal Shale Gas Well Rate Transient Analysis. Paper SPE-126754-MS presented at the North Africa Technical Conference and Exhibition, Cairo, Egypt, 14-17 February. doi: 10.2118/126754-ms

Brown, M.L., Ozkan, E., Raghavan, R.S. et al. 2009. Practical Solutions for Pressure Transient Responses of Fractured Horizontal Wells in Unconventional Reservoirs. Paper SPE-125043-MS presented at the SPE Annual Technical Conference and Exhibition, New Orleans, Louisiana, 4-7 October. doi: 10.2118/125043-ms

Chen, C.-C., Serra, K., Reynolds, A.C. et al. 1985. Pressure Transient Analysis Methods for Bounded Naturally Fractured Reservoirs. *SPE Journal* **25** (3): 451-464. doi: 10.2118/11243-pa

Cinco-Ley, H. and Meng, H.-Z. 1988. Pressure Transient Analysis of Wells with Finite Conductivity Vertical Fractures in Double Porosity Reservoirs. Paper SPE-18172-MS presented at the SPE Annual Technical Conference and Exhibition, Houston, Texas, 2-5 October. doi: 10.2118/18172-ms

Da Prat, G., Cinco-Ley, H., and Ramey Jr., H. 1981. Decline Curve Analysis Using Type Curves for Two-Porosity Systems. *SPE Journal* **21** (3): 354-362. doi: 10.2118/9292-pa

De Swaan O., A. 1976. Analytic Solutions for Determining Naturally Fractured Reservoir Properties by Well Testing. *SPE Journal* **16** (3): 117-122. doi: 10.2118/5346-pa

Dreier, J., Ozkan, E., and Kazemi, H. 2004. New Analytical Pressure-Transient Models to Detect and Characterize Reservoirs with Multiple Fracture Systems. Paper SPE-92039-MS presented at the SPE International Petroleum Conference in Mexico, Puebla Pue., Mexico, 7-9 November. doi: 10.2118/92039-ms

El-Banbi, A.H. 1998. Analysis of Tight Gas Well Performance. Ph.D. Dissertation. Texas A&M University, College Station, Texas.

Everdingen, A.F.V. and Hurst, W. 1949. The Application of the Laplace Transformation to Flow Problems in Reservoirs. *Journal of Petroleum Technology* **1** (12): 305-324. doi: 10.2118/949305-g

Ibrahim, M. and Wattenbarger, R.A. 2005. Analysis of Rate Dependence in Transient Linear Flow in Tight Gas Wells. Paper PETSOC-2005-057 presented at the Canadian International Petroleum Conference, Calgary, Alberta, 7-9 June. doi: 10.2118/2005-057

Jalali, Y. and Ershaghi, I. 1987. Pressure Transient Analysis of Heterogeneous Naturally Fractured Reservoirs. Paper SPE-16341-MS presented at the SPE California Regional Meeting, Ventura, California, 8-10 April. doi: 10.2118/16341-ms

Kazemi, H. 1969. Pressure Transient Analysis of Naturally Fractured Reservoirs with Uniform Fracture Distribution. *SPE Journal* **9** (4): 451-462. doi: 10.2118/2156-a

Lai, C.H., Bodvarsson, G.S., Tsang, C.F. et al. 1983. A New Model for Well Test Data Analysis for Naturally Fractured Reservoirs. Paper SPE-11688-MS presented at the SPE California Regional Meeting, Ventura, California, 23-25 March. doi: 10.2118/11688-ms

Leguizamon, J. and Aguilera, R. 2011. Hydraulic Fracturing of Naturally Fractured Tight Gas Formations. Paper SPE-142727-MS presented at the SPE Middle East Unconventional Gas Conference and Exhibition, Muscat, Oman, 31 January-2 February. doi: 10.2118/142727-ms

Liu, J.C., Bodvarsson, G.S. and Wu, Y.S. 2003. Analysis of Flow Behavior in Fractured Lithophysal Reservoirs. *Journal of Contaminant Hydrology* **62-63**: 189-211. doi: 10.1016/S0169-7722(02)00169-9

Luo, S., Neal, L., Arulampalam, P. et al. 2010. Flow Regime Analysis of Multi-Stage Hydraulically-Fractured Horizontal Wells with Reciprocal Rate Derivative Function: Bakken Case Study. Paper SPE-137514-MS presented at the Canadian Unconventional Resources and International Petroleum Conference, Calgary, Alberta, Canada, 19-21 October. doi: 10.2118/137514-ms

Nobakht, M., Clarkson, C.R., and Kaviani, D. 2011. New Type Curves for Analyzing Horizontal Well with Multiple Fractures in Shale Gas Reservoirs. Paper SPE-149397-MS presented at the Canadian Unconventional Resources Conference, Alberta, Canada, 15-17 November. doi: 10.2118/149397-ms

Ozkan, E., Brown, M.L., Raghavan, R.S. et al. 2009. Comparison of Fractured Horizontal-Well Performance in Conventional and Unconventional Reservoirs. Paper SPE-121290-MS presented at the SPE Western Regional Meeting, San Jose, California, 24-26 March. doi: 10.2118/121290-ms

Ozkan, E., Ohaeri, U., and Raghavan, R. 1987. Unsteady Flow to a Well Produced at a Constant Pressure in a Fractured Reservoir. *SPE Formation Evaluation* **2** (2): 186-200. doi: 10.2118/9902-pa

Samandarli, O. 2011. A New Method for History Matching and Forecasting Shale Gas/Oil Reservoir Production Performance with Dual and Triple Porosity Models. M.S. Thesis. Texas A&M University, College Station, Texas.

Samandarli, O., Al-Ahmadi, H.A., and Wattenbarger, R.A. 2011a. A New Method for History Matching and Forecasting Shale Gas Reservoir Production Performance with a Dual Porosity Model. Paper SPE-144335-MS presented at the North American Unconventional Gas Conference and Exhibition, The Woodlands, Texas, 14-16 June. doi: 10.2118/144335-ms

Samandarli, O., Al-Ahmadi, H.A., and Wattenbarger, R.A. 2011b. A Semi-Analytic Method for History Matching Fractured Shale Gas Reservoirs. Paper SPE-144583-MS presented at the SPE Western North American Region Meeting, Anchorage, Alaska, 7-11 May. doi: 10.2118/144583-ms

Serra, K., Reynolds, A.C., and Raghavan, R. 1983. New Pressure Transient Analysis Methods for Naturally Fractured Reservoirs(Includes Associated Papers 12940 and 13014). *SPE Journal of Petroleum Technology* **35** (12): 2271-2283. doi: 10.2118/10780-pa

Warren, J.E. and Root, P.J. 1963. The Behavior of Naturally Fractured Reservoirs. *SPE Journal* (9): 245-255. doi: 10.2118/426-pa

Wattenbarger, R.A., El-Banbi, A.H., Villegas, M.E. et al. 1998. Production Analysis of Linear Flow into Fractured Tight Gas Wells. Paper SPE-39931-MS presented at the SPE Rocky Mountain Regional/Low-Permeability Reservoirs Symposium, Denver, Colorado, 5-8 April. doi: 10.2118/39931-ms

Wu, Y.-S., Ehlig-Economides, C.A., Qin, G. et al. 2007. A Triple-Continuum Pressure-Transient Model for a Naturally Fractured Vuggy Reservoir. Paper SPE-110044-MS presented at the SPE Annual Technical Conference and Exhibition, Anaheim, California, 11-14 November. doi: 10.2118/110044-ms

APPENDIX A

DERIVATION OF MODIFIED LINEAR HOMOGENEOUS FLOW IN MULIT-TRANSVERSE HYDRAULIC FRACTURES HORIZONTAL WELL

Based on Wattenbarger and El-Banbi (1998), the mathematical model of hydraulic fracture well is represented by **Figure 30**.

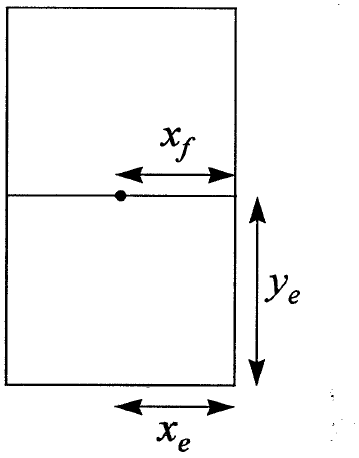

Figure 30 – A hydraulically fractured well in a rectangular reservoir (Wattenbarger and El-Banbi 1998)

The definition of all dimensionless parameters is in terms of fracture half-length, x_f, and given by

$$t_{Dxf} = \frac{0.00633\, k_m}{\phi_m c_t \mu\, x_f^2} t \qquad \text{..... (A- 1)}$$

$$t_{Dye} = \frac{0.00633\, k_m}{\phi_m c_t \mu\, y_e^2} t = \left(\frac{x_f}{y_e}\right)^2 t_{Dxf} \qquad \text{..... (A- 2)}$$

$$q_D = \frac{1422 q_g T}{k_m h \Delta m(p)} = \frac{1422 q_g T}{k_m h [m(p_i) - m(p_{wf})]} \quad \text{..... (A- 3)}$$

$$q_D = \frac{141.2 q_o B \mu}{k_m h \Delta p} = \frac{141.2 q_o B \mu}{k_m h (p_i - p_{wf})} \quad \text{..... (A- 4)}$$

The solution for constant p_{wf} production from a closed linear reservoir is given by

$$\frac{1}{q_D} = \frac{\frac{\pi}{4}\left(\frac{y_e}{x_f}\right)}{\sum_{n_{odd}}^{\infty} \exp\left[-\frac{n^2\pi^2}{4}\left(\frac{x_f}{y_e}\right)^2 t_{Dxf}\right]} \quad \text{..... (A- 5)}$$

The short term approximation solution of homogeneous linear flow during the linear flow period of constant pressure condition in terms of x_f is given.

$$q_{DLxf} = \frac{2}{\pi\sqrt{\pi}} \frac{1}{\sqrt{t_{Dxf}}} \quad \text{..... (A- 6)}$$

Converting to dimensional parameters, the slope of square root of time plot of gas and oil are given by equation A-7 and A-8, respectively.

$$m_{square} = \frac{315.4T}{h\sqrt{(\phi\mu c_t)_i}} \frac{1}{\sqrt{k_m} x_f} \quad \text{..... (A- 7)}$$

$$m_{square} = \frac{31.3B\sqrt{\mu}}{h\sqrt{(\phi c_t)_i}} \frac{1}{\sqrt{k_m} x_f} \quad \text{..... (A- 8)}$$

The end of half-slope line of the log-log plot or the end of straight line of the square root of time plot is found when t_{Dye} is 0.25 for constant p_{wf} case or when flow responds by the outer boundary.

$$y_e = 0.159\sqrt{\frac{k_m t_{esr}}{(\phi\mu c_t)_i}} \quad \text{..... (A- 9)}$$

Pore volume, V_p, can also be calculated by combining **Eq. A-7**, **Eq. A-8**, and **Eq. A-9**. The V_p for gas and oil

$$V_{p,g} = \frac{200.6T}{(\mu c_t)_i}\frac{1}{m_{square}}\sqrt{t_{esr}} \quad \text{..... (A- 10)}$$

$$V_{p,o} = \frac{19.9B}{c_{ti}}\frac{1}{m_{square}}\sqrt{t_{esr}} \quad \text{..... (A- 11)}$$

To apply this model to multi-transverse hydraulic fractures horizontal well, the definition of dimension parameters have to be modified as follows.

- y_e of A hydraulically fractured well → $L_F/2$ of A multi-transverse hydraulic fractures horizontal well
- x_f of A hydraulically fractured well → $y_e \times n_F$ of A multi-transverse hydraulic fractures horizontal well

Therefore, the modified equations of linear flow for interpreting the multi-transverse hydraulic fractures horizontal well are

$$\sqrt{k_m}\, y_e n_F = \frac{315.4T}{h\sqrt{(\phi\mu c_t)_i}}\frac{1}{m_{square}} \quad \text{..... (A- 12)}$$

$$\sqrt{k_m}\, y_e n_F = \frac{31.3B\sqrt{\mu}}{h\sqrt{(\phi c_t)_i}}\frac{1}{m_{square}} \quad \text{..... (A- 13)}$$

$$\frac{L_F}{2} = 0.159\sqrt{\frac{k_m t_{esr}}{(\phi\mu c_t)_i}} \quad \text{..... (A- 14)}$$

$$V_{p,g} = \frac{200.6T}{(\mu c_t)_i} \frac{1}{m_{square}} \sqrt{t_{esr}} \quad \text{..... (A- 15)}$$

$$V_{p,o} = \frac{19.9B}{c_{ti}} \frac{1}{m_{square}} \sqrt{t_{esr}} \quad \text{..... (A- 16)}$$

APPENDIX B

EXAMPLE FIELD DATA

Well 314

Field production plot and data of the multi-transverse hydraulic fractures horizontal well, well#314, is shown in **Figure 31** and **Table 24**, respectively. The well has been produced with a constant bottom-hole pressure. The production plot shows a half-slope on the log-log plot of rate versus time representing linear flow. Moreover, deviation from the half-slope trend line at late time is observed. The early period that does not follow the half-slope trend line may be from the effect of fractured treatment water which causes the skin effect in the early part.

From plotting $\Delta m(p)/q$ versus $\sqrt{t}$, slope is 1.75E+4 as shown in **Figure 32**. To evaluate gas production data, correction factor is calculated from drawdown given by Ibrahim and Wattenbarger (2005).

$$D_D = \frac{m(p_i) - m(p_{wf})}{m(p_i)} \quad \text{..... (B- 1)}$$

$$f_{CP} = 1 - 0.0852D_D - 0.0857D_D^2 \quad \text{..... (B- 2)}$$

The calculated f_{CP} is 0.838. Then, corrected slope is 20,883. The end of half-slope on log-log plot or the end of straight line on square root of time plot, t_{esr}, is around 225 days.

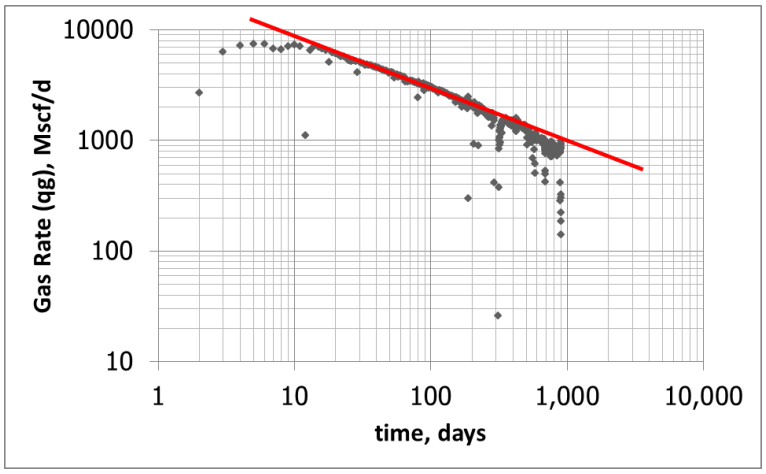

Figure 31 – Log-log plot of production gas rate versus time of well 314

Table 24 – Well 314 data

Thickness	h	300	ft
Perforation Interval	x_e	2968	ft
Hydraulic Fracture Spacing	L_F	106	ft
Number of Hydraulic Fracture	n_F	28	
Porosity	ϕ	0.06	
Water Saturation	S_{wi}	0.3	
Formation Volume Factor	B_{gi}	0.00509	rcf/scf
Viscosity	μ_i	0.0201	cp
Total Compressibility	c_{ti}	2.20E-04	psi^{-1}
Pseudo Initial Pressure	$m(p_i)$	5.97E+08	psi^2/cp
Pseudo Bottomhole Flowing Pressure	$m(p_{wf})$	2.03E+07	psi^2/cp
Temperature	T	610	^oR

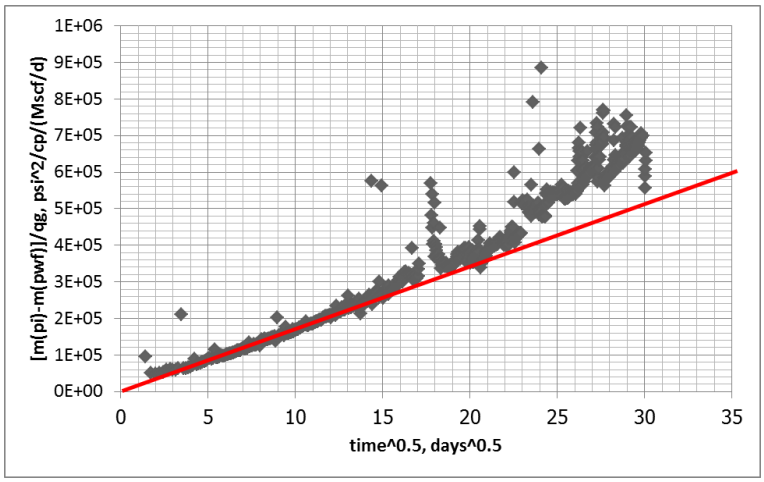

Figure 32 – Square root of time plot of well 314

Well B-86

Field production plot and data of the multi-transverse hydraulic fractures horizontal well, well#B-86, is shown in **Figure 33** and **Table 25**, respectively. The well has been produced with a constant bottom-hole pressure. The production plot shows a quarter-slope and a half-slope on the log-log plot of rate versus time representing bilinear and linear flows, respectively. There is no deviation from the half-slope trend line at late time. The early period that does not follow the quarter-slope trend line may be from the effect of fractured treatment water which causes the skin effect in the early part.

From plotting $\Delta m(p)/q$ versus $\sqrt{t}$, slope is 17,200. From plotting $\Delta m(p)/q$ versus $t^{0.25}$, slope is 45,000 as shown in **Figure 34**. To evaluate gas production data, correction factor of gas properties given by **Eq. B-1** and **Eq. B-2** is applied to the slopes.

The calculated f_{CP} is 0.838. Then, corrected slope is 20,525 and 53,700 for square root of time and fourth root of time plots, respectively. The end of production data, t_{end}, is around 300 days.

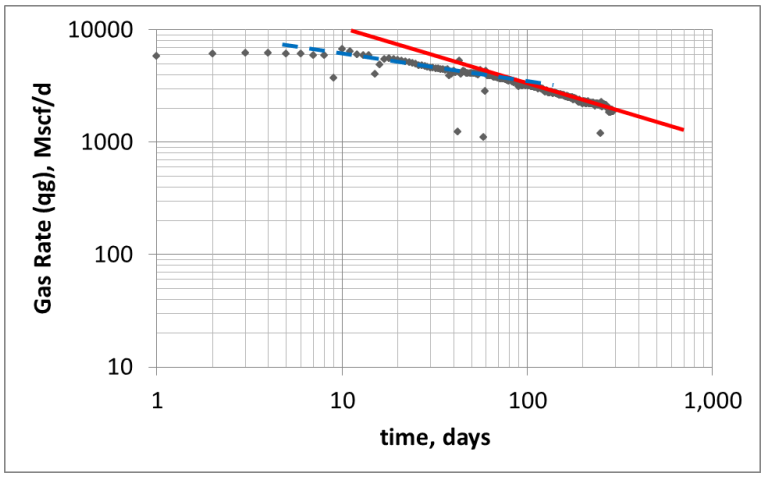

Figure 33 – Log-log plot of production gas rate versus time of well B-86

Table 25 – Well B-86 data

Thickness	h	300	ft
Perforation Interval	x_e	3550	ft
Hydraulic Fracture Spacing	L_F	142	ft
Number of Hydraulic Fracture	n_F	25	
Porosity	ϕ	0.085	
Water Saturation	S_{wi}	0.3	
Formation Volume Factor	B_{gi}	0.0051	rcf/scf
Viscosity	μ_i	0.0195	cp
Total Compressibility	c_{ti}	2.23E-04	psi^{-1}
Pseudo Initial Pressure	$m(p_i)$	5.96E+08	psi^2/cp
Pseudo Bottomhole Flowing Pressure	$m(p_{wf})$	2.01E+07	psi^2/cp
Temperature	T	610	^oR

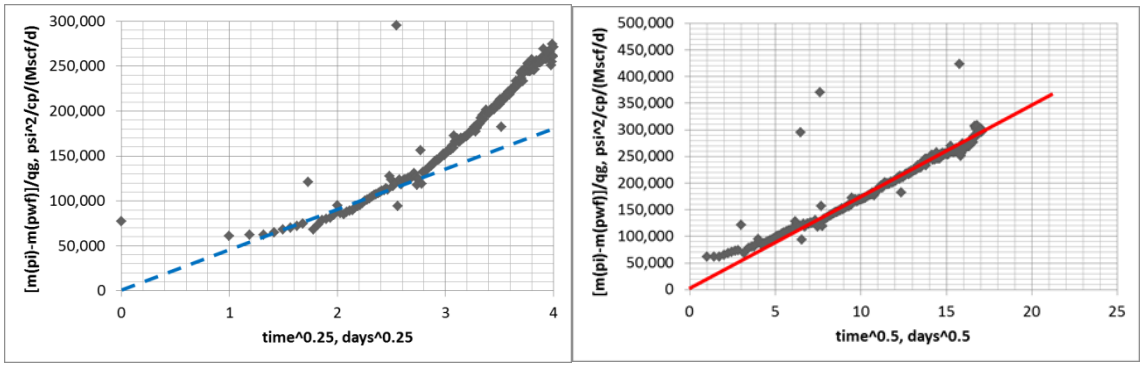

Figure 34 – Square root of time (right) and fourth root of time (left) plots of well B-86

Well B-145

Field production plot and data of the multi-transverse hydraulic fractures horizontal well, well#B-145, is showed in **Figure 35** and **Table 26**, respectively. The well has been produced with a constant bottom-hole pressure. The production plot shows a long half-slope on the log-log plot of rate versus time representing the linear flow. There is no deviation from the half-slope trend line at late time. The early period that does not follow the half-slope trend line may be from the effect of fractured treatment water which causes the skin effect in the early part. Moreover, from core data analysis, matrix permeability is estimated as 1.5×10^{-4} md.

From plotting $\Delta m(p)/q$ versus $\sqrt{t}$, slope is 24,000 as showed in **Figure 36**. To evaluate gas production data, correction factor of gas properties given by **Eq. B-1** and **Eq. B-2** is applied to the slopes. The calculated f_{CP} is 0.838. Then, corrected slope is 28,640 for square root of time plot. The end of production data, t_{end}, is around 500 days.

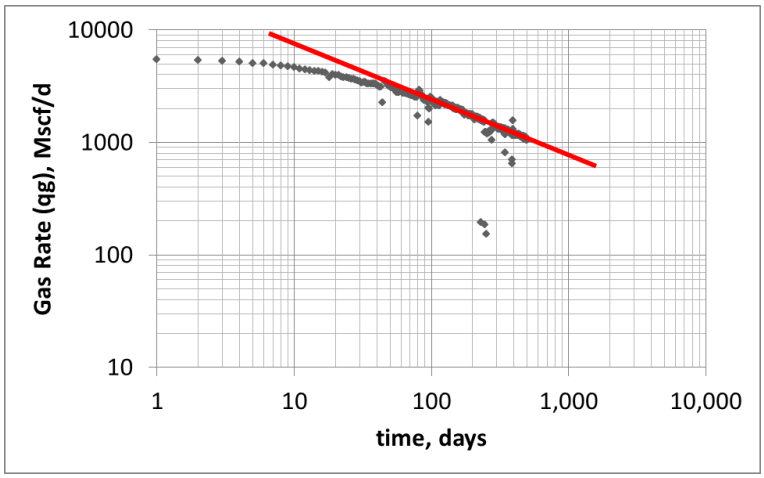

Figure 35 – Log-log plot of production gas rate versus time of well B-145

Table 26 – Well B-145 data

Thickness	h	300	ft
Perforation Interval	x_e	3360	ft
Hydraulic Fracture Spacing	L_F	80	ft
Number of Hydraulic Fracture	n_F	42	
Porosity	ϕ	0.085	
Water Saturation	S_{wi}	0.3	
Formation Volume Factor	B_{gi}	0.0051	rcf/scf
Viscosity	μ_i	0.0195	cp
Total Compressibility	c_{ti}	2.23E-04	psi^{-1}
Pseudo Initial Pressure	$m(p_i)$	5.96E+08	psi^2/cp
Pseudo Bottomhole Flowing Pressure	$m(p_{wf})$	2.01E+07	psi^2/cp
Temperature	T	610	^oR

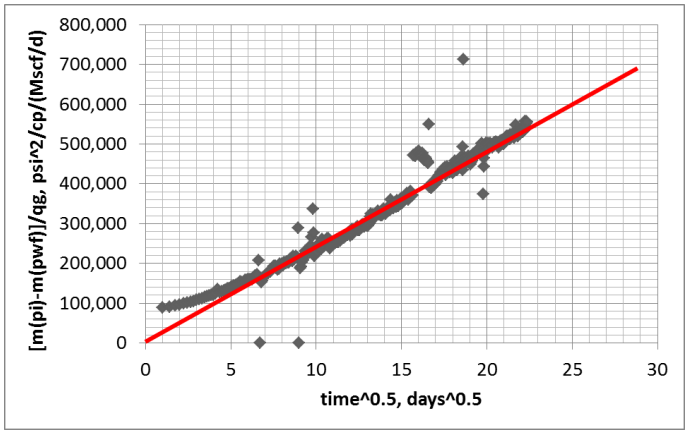

Figure 36 – Square root of time plot of well B-145

APPENDIX C

LAPLACE SOLUTION OF LINEAR TRANSIENT DUAL POROSITY MODEL

Derivations of the linear transient dual porosity model with closed boundary developed by El-Banbi (1998) are shown in this chapter. The solution is showed in Laplace domain to solve the second-order differential equation. The solution in time domain can be obtained by Stehfest algorithm. The derivation starts with constant rate solution and converts to constant pressure solution by using the technique given by Van Everdingen and Hurst (1949).

Matrix system

Diffusivity equation:

$$\frac{k_m}{\mu}\frac{\partial^2 p_m}{\partial z^2} = [\phi V' c_t]_m \frac{\partial p_m}{\partial t}$$

$$\frac{\partial^2 p_m}{\partial z^2} = \mu \left[\frac{\phi V' c_t}{k}\right]_m \frac{\partial p_m}{\partial t}$$

Inner boundary condition:

$$\left.\frac{\partial p_m}{\partial z}\right|_{z=0} = 0$$

Outer boundary condition:

$$p_m|_{z=L_F/2} = p_F$$

Hydraulic fracture system

Diffusivity equation:

$$\frac{k_F}{\mu}\frac{\partial^2 p_F}{\partial y^2} = [\phi V' c_t]_F \frac{\partial p_F}{\partial t} - q_{Fm}$$

$$q_{Fm} = -\frac{k_m}{\mu\, L_F/2}\left.\frac{\partial p_m}{\partial z}\right|_{z=L_F/2}$$

$$\frac{\partial^2 p_F}{\partial y^2} = \mu\left[\frac{\phi V' c_t}{k}\right]_F \frac{\partial p_F}{\partial t} + \frac{k_m}{k_F\, L_F/2}\left.\frac{\partial p_m}{\partial z}\right|_{z=L_F/2}$$

Inner boundary condition:

$$q = \frac{k_F A_{cw}}{B\mu}\left.\frac{\partial p_F}{\partial y}\right|_{y=0}$$

Outer boundary condition:

$$\left.\frac{\partial p_F}{\partial y}\right|_{y=y_e} = 0$$

Solution

From matrix system,

Let $z_D = \frac{z}{L_F/2}$, $p_D = \frac{1}{p_{ch}}\,(p_i - p)$ or $p = p_i - p_D p_{ch}$, and

$t_{DAcw} = \frac{k_F}{[(\phi V' c_t)_m + (\phi V' c_t)_F]\mu A_{cw}}\, t = \frac{k_F}{[\phi V' c_t]_T \mu A_{cw}}\, t$;therefore,

$$\frac{\partial^2 p_{Dm}}{\partial z_D^2} = \frac{3}{\frac{12 k_m A_{cw}}{L_F^2 k_F}}\frac{(\phi V' c_t)_m}{(\phi V' c_t)_T}\frac{\partial p_{Dm}}{\partial t_{DAcw}} \qquad \text{..... (C- 1)}$$

Let $\lambda_{Fm} = \frac{12k_mA_{cw}}{L_F^2k_F}$ and $\omega_F = 1 - \frac{(\phi V\prime c_t)_m}{(\phi V\prime c_t)_T}$,

$$\frac{\partial^2 p_{Dm}}{\partial z_D^2} = \frac{3}{\lambda_{Fm}}(1-\omega_F)\,\frac{\partial p_{Dm}}{\partial t_{DAcw}} \qquad \text{..... (C- 2)}$$

Take Laplace transform

$$\frac{d^2\overline{p_{Dm}}}{dz_D^2} = \frac{3}{\lambda_{Fm}}(1-\omega_F)\left(u\overline{p_{Dm}} - p_{Dm}(z_D,0)\right) \qquad \text{..... (C- 3)}$$

From the initial condition of matrix system, $p_{Dm}(z_D,0) = 0$

$$\frac{d^2\overline{p_{Dm}}}{dz_D^2} = \frac{3}{\lambda_{Fm}}(1-\omega_F)\,u\,\overline{p_{Dm}} \qquad \text{..... (C- 4)}$$

This can be shown by the general solution

$$\overline{p_{Dm}} = A\cosh\left(\sqrt{\frac{3(1-\omega_F)\,u}{\lambda_{Fm}}}\,z_D\right) + B\sinh\left(\sqrt{\frac{3(1-\omega_F)\,u}{\lambda_{Fm}}}\,z_D\right) \qquad \text{..... (C- 5)}$$

or

$$\frac{d\overline{p_{Dm}}}{dz_D} = A\sqrt{\frac{3(1-\omega_F)u}{\lambda_{Fm}}}\sinh\left(\sqrt{\frac{3(1-\omega_F)u}{\lambda_{Fm}}}\,z_D\right) + B\sqrt{\frac{3(1-\omega_F)u}{\lambda_{Fm}}}\cosh\left(\sqrt{\frac{3(1-\omega_F)u}{\lambda_{Fm}}}\,z_D\right) \qquad \text{..... (C- 6)}$$

From the inner boundary condition of matrix system, $\left.\frac{\partial p_m}{\partial z}\right|_{z=0} = 0$

$$\left.\frac{\partial p_{Dm}}{\partial z_D}\right|_{z_D=0} = 0 \qquad \text{..... (C- 7)}$$

Take Laplace transform

$$\left.\frac{d\overline{p_{Dm}}}{dz_D}\right|_{z_D=0} = 0 \qquad \text{..... (C- 8)}$$

Therefore, where $z_D = 0$, **Eq. C-6** becomes

$$0 = A\sqrt{\frac{3(1-\omega_F)u}{\lambda_{Fm}}}\sinh(0) + B\sqrt{\frac{3(1-\omega_F)u}{\lambda_{Fm}}}\cosh(0) \qquad \text{..... (C- 9)}$$

Since $\sinh 0 = 0$ and $\cosh 0 = 1$; therefore, $B = 0$.

From the outer boundary condition of matrix system, $p_m|_{z=L_F/2} = p_F$

$$p_{Dm}|_{z_D=1} = p_{DF} \qquad \text{..... (C- 10)}$$

Take Laplace transform

$$\overline{p_{Dm}}|_{z_D=1} = \overline{p_{DF}} \qquad \text{..... (C- 11)}$$

Therefore, where $z_D = 1$, **Eq. C-5** becomes

$$\overline{p_{DF}} = A\cosh\left(\sqrt{\frac{3(1-\omega_F)u}{\lambda_{Fm}}}\right) \qquad \text{..... (C- 12)}$$

Then,

$$A = \frac{\overline{p_{DF}}}{\cosh\left(\sqrt{\frac{3(1-\omega_F)u}{\lambda_{Fm}}}\right)} \quad \text{..... (C- 13)}$$

Therefore,

$$\overline{p_{Dm}} = \frac{\overline{p_{DF}}}{\cosh\left(\sqrt{\frac{3(1-\omega_F)u}{\lambda_{Fm}}}\right)} \cosh\left(\sqrt{\frac{3(1-\omega_F)u}{\lambda_{Fm}}}\, z_D\right) \quad \text{..... (C- 14)}$$

or

$$\frac{d\overline{p_{Dm}}}{dz_D}$$

$$= \frac{\overline{p_{DF}}}{\cosh\left(\sqrt{\frac{3(1-\omega_F)u}{\lambda_{Fm}}}\right)} \sqrt{\frac{3(1-\omega_F)u}{\lambda_{Fm}}} \sinh\left(\sqrt{\frac{3(1-\omega_F)u}{\lambda_{Fm}}}\, z_D\right) \quad \text{..... (C- 15)}$$

From hydraulic fracture system,

Let $z_D = \frac{z}{L_F/2}$, $y_D = \frac{y}{\sqrt{A_{cw}}}$, $p = p_i - p_D p_{ch}$, and $t_{DAcw} = \frac{k_F}{[\phi V' c_t]_T \mu A_{cw}} t$,

$$\frac{\partial^2 p_{DF}}{\partial y_D^2} = \frac{(\phi V' c_t)_F}{(\phi V' c_t)_T} \frac{\partial p_{DF}}{\partial t_{DAcw}} + \frac{1}{3} \frac{12 k_m A_{cw}}{L_F^2 k_F} \left.\frac{\partial p_{Dm}}{\partial z_D}\right|_{z_D=1} \quad \text{..... (C- 16)}$$

Let $\lambda_{Fm} = \frac{12 k_m A_{cw}}{L_F^2 k_F}$ and $\omega_F = 1 - \frac{(\phi V' c_t)_m}{(\phi V' c_t)_T} = \frac{(\phi V' c_t)_F}{(\phi V' c_t)_T}$,

$$\frac{\partial^2 p_{DF}}{\partial y_D^2} = \omega_F \frac{\partial p_{DF}}{\partial t_{DAcw}} + \frac{1}{3} \lambda_{Fm} \left.\frac{\partial p_{Dm}}{\partial z_D}\right|_{z_D=1} \quad \text{..... (C- 17)}$$

Take Laplace transform,

$$\frac{d^2\overline{p_{DF}}}{dy_D^2} = \omega_F \left(u\,\overline{p_{DF}} - p_{DF}(y_D, 0)\right) + \frac{\lambda_{Fm}}{3}\left.\frac{\partial\overline{p_{Dm}}}{\partial z_D}\right|_{z_D=1} \quad \text{..... (C- 18)}$$

From the initial condition of hydraulic fracture system, $p_{DF}(y_D, 0) = 0$

$$\frac{d^2\overline{p_{DF}}}{dy_D^2} = \omega_F\, u\,\overline{p_{DF}} + \frac{\lambda_{Fm}}{3}\left.\frac{\partial\overline{p_{Dm}}}{\partial z_D}\right|_{z_D=1} \quad \text{..... (C- 19)}$$

Substitute $\left.\frac{\partial\overline{p_{Dm}}}{\partial z_D}\right|_{z_D=1}$ with **Eq. C-15**,

$$\frac{d^2\overline{p_{DF}}}{dy_D^2} = \omega_F\, u\,\overline{p_{DF}} + \frac{\lambda_{Fm}}{3}\overline{p_{DF}}\sqrt{\frac{3(1-\omega_F)u}{\lambda_{Fm}}}\,\tanh\left(\sqrt{\frac{3(1-\omega_F)u}{\lambda_{Fm}}}\right) \quad \text{… (C- 20)}$$

Define

$$f(u) = \omega_F + \frac{\lambda_{Fm}}{3\,u}\sqrt{\frac{3(1-\omega_F)u}{\lambda_{Fm}}}\,\tanh\left(\sqrt{\frac{3(1-\omega_F)u}{\lambda_{Fm}}}\right) \quad \text{..... (C- 21)}$$

Therefore,

$$\frac{d^2\overline{p_{DF}}}{dy_D^2} - u\,f(u)\,\overline{p_{DF}} = 0 \quad \text{..... (C- 22)}$$

This can be shown by the general solution

$$\overline{p_{DF}} = A\cosh\left(\sqrt{u\,f(u)}\,y_D\right) + B\sinh\left(\sqrt{u\,f(u)}\,y_D\right) \quad \text{..... (C- 23)}$$

or

$$\frac{d\overline{p_{DF}}}{dy_D} = A\sqrt{u\,f(u)}\,\sinh\left(\sqrt{u\,f(u)}\,y_D\right) + B\sqrt{u\,f(u)}\,\cosh\left(\sqrt{u\,f(u)}\,y_D\right) \quad \text{..... (C- 24)}$$

From the inner boundary condition of hydraulic fracture system, $q = \frac{k_F A_{cw}}{B\mu} \frac{\partial p_F}{\partial y}\Big|_{y=0}$

Let $p = p_i - p_D p_{ch}$, and $y_D = \frac{y}{\sqrt{A_{cw}}}$,

$$\frac{\partial p_{DF}}{\partial y_D}\Big|_{y_D=0} = -\frac{1}{p_{ch}} \frac{qB\mu}{k_F\sqrt{A_{cw}}} \quad \text{..... (C- 25)}$$

Define $p_{ch} = \frac{1}{2\pi} \frac{qB\mu}{k_F\sqrt{A_{cw}}}$; therefore, $p_D = \frac{2\pi\, k_F\sqrt{A_{cw}}}{qB\mu}\ (p_i - p)$

$$\frac{\partial p_{DF}}{\partial y_D}\Big|_{y_D=0} = -2\pi \quad \text{..... (C- 26)}$$

Take Laplace transform,

$$\frac{\partial \overline{p_{DF}}}{\partial y_D}\Big|_{y_D=0} = -\frac{2\pi}{u} \quad \text{..... (C- 27)}$$

Therefore, where $y_D = 0$, **Eq. C-24** becomes,

$$-\frac{2\pi}{u} = A\sqrt{u\, f(u)}\ \sinh(0) + B\sqrt{u\, f(u)}\ \cosh(0) \quad \text{..... (C- 28)}$$

Since $\sinh 0 = 0$ and $\cosh 0 = 1$,

$$B = -\frac{2\pi}{u\sqrt{u\, f(u)}} \quad \text{..... (C- 29)}$$

From the outer boundary condition of hydraulic fracture system, $\frac{\partial p_F}{\partial y}\Big|_{y=y_e} = 0$

Define $y_{eD} = \frac{y_e}{\sqrt{A_{cw}}}$,

$$\frac{\partial p_{DF}}{\partial y_D}\Big|_{y_D=y_{eD}} = 0 \quad \text{..... (C- 30)}$$

Take Laplace transform,

$$\left.\frac{d\overline{p_{DF}}}{dy_D}\right|_{y_D=y_{eD}} = 0 \qquad \text{..... (C- 31)}$$

Therefore, where $y_e = y_{eD}$ and **Eq. C-29**, **Eq. C-24** becomes,

$$0 = A\sqrt{u\,f(u)}\,\sinh\left(\sqrt{u\,f(u)}\,y_{eD}\right) - \frac{2\pi}{u}\,\cosh\left(\sqrt{u\,f(u)}\,y_{eD}\right) \qquad \text{..... (C- 32)}$$

Then,

$$A = \frac{\frac{2\pi}{u}\,\cosh\left(\sqrt{u\,f(u)}\,y_{eD}\right)}{\sqrt{u\,f(u)}\,\sinh\left(\sqrt{u\,f(u)}\,y_{eD}\right)} \qquad \text{..... (C- 33)}$$

Therefore, **Eq. C-23** becomes,

$$\overline{p_{DF}} = \frac{\frac{2\pi}{u}\,\cosh\left(\sqrt{u\,f(u)}\,y_{eD}\right)}{\sqrt{u\,f(u)}\,\sinh\left(\sqrt{u\,f(u)}\,y_{eD}\right)}\cosh\left(\sqrt{u\,f(u)}\,y_D\right) - \frac{2\pi}{u\sqrt{u\,f(u)}}\sinh\left(\sqrt{u\,f(u)}\,y_D\right) \qquad \text{..... (C- 34)}$$

At wellbore, $y_D = 0$,

$$\overline{p_{DF@well}} = \frac{2\pi\,\cosh\left(\sqrt{u\,f(u)}\,y_{eD}\right)}{u\sqrt{u\,f(u)}\,\sinh\left(\sqrt{u\,f(u)}\,y_{eD}\right)} \qquad \text{..... (C- 35)}$$

Re-arrange in exponential term, (define $\overline{p_{wDL}} = \overline{p_{DF@well}}$)

$$\overline{p_{wDL}} = \frac{2\pi}{u\sqrt{u\,f(u)}}\left[\frac{1+e^{-2\sqrt{uf(u)}\,y_{eD}}}{1-e^{-2\sqrt{uf(u)}\,y_{eD}}}\right] \qquad \text{..... (C- 36)}$$

To change from constant rate solution to constant pressure solution, Van Everdingen and Hurst (1949) introduced the relation between constant pressure solution and constant rate in Laplace space.

$$\overline{p_{wDL}} \times \overline{q_{DL}} = \frac{1}{u^2} \quad \text{..... (C- 37)}$$

Consequently, the solution of constant pressure of transient linear slab dual porosity case (El-Banbi, 1998) is shown.

$$\frac{1}{\overline{q_{DL}}} = \frac{2\pi u}{\sqrt{uf(u)}}\left[\frac{1 + e^{-2\sqrt{uf(u)}\, y_{eD}}}{1 - e^{-2\sqrt{uf(u)}\, y_{eD}}}\right] \quad \text{..... (C- 38)}$$

Where

$$f(u) = \omega_F + \frac{\lambda_{Fm}}{3\,u}\sqrt{\frac{3(1-\omega_F)u}{\lambda_{Fm}}}\,\tanh\left(\sqrt{\frac{3(1-\omega_F)u}{\lambda_{Fm}}}\right) \quad \text{..... (C- 39)}$$

APPENDIX D

ANALYSIS EQUATIONS DERIVATIONS OF LINEAR TRANSIENT DUAL POROSITY MODEL FOR CONSTANT PRESSURE CASE

From constant pressure inner boundary and closed outer boundary of linear transient dual porosity model given by El-Banbi (1998)

$$\frac{1}{\overline{q_{DL}}} = \frac{2\pi u}{\sqrt{uf(u)}}\left[\frac{1+e^{-2\sqrt{uf(u)}\,y_{eD}}}{1-e^{-2\sqrt{uf(u)}\,y_{eD}}}\right] \quad \text{..... (D- 1)}$$

Or this can be written in term of $\coth(x)$ function.

$$\frac{1}{\overline{q_{DL}}} = \frac{2\pi u}{\sqrt{uf(u)}}\coth\left(\sqrt{uf(u)}\,y_{eD}\right) \quad \text{..... (D- 2)}$$

For transient slab model,

$$f(u) = \omega_F + \frac{\lambda_{Fm}}{3\,u}\sqrt{\frac{3(1-\omega_F)u}{\lambda_{Fm}}}\,\tanh\left(\sqrt{\frac{3(1-\omega_F)u}{\lambda_{Fm}}}\right) \quad \text{..... (D- 3)}$$

<u>Case 1</u>

With the assumption of

$$\omega_F \gg \sqrt{\frac{\lambda_{Fm}}{3u}(1-\omega_F)}\tanh\left(\sqrt{\frac{3u}{\lambda_{Fm}}(1-\omega_F)}\right)$$

$\sqrt{uf(u)}\,y_{eD}$ is large, $\therefore\ \coth\left(\sqrt{uf(u)}\,y_{eD}\right) \approx 1$

Therefore,

$$f(u) = \omega_F$$

Then,

$$\overline{q_{DL}} = \frac{\sqrt{\omega_F}}{2\pi}\frac{1}{\sqrt{u}} \quad \text{..... (D- 4)}$$

Inverting Laplace transform, the asymptotic equation of **region 1** is

$$q_{DL} = \frac{\sqrt{\omega_F}}{2\pi\sqrt{\pi}}\frac{1}{\sqrt{t_{DAcw}}} \quad \text{..... (D- 5)}$$

Case 2

With the assumption of

$$\omega_F \ll \sqrt{\frac{\lambda_{Fm}}{3u}(1-\omega_F)}\tanh\left(\sqrt{\frac{3u}{\lambda_{Fm}}(1-\omega_F)}\right)$$

And $\sqrt{\frac{3u}{\lambda_{Fm}}(1-\omega_F)}$ is large, $\therefore \tanh\left(\sqrt{\frac{3u}{\lambda_{Fm}}(1-\omega_F)}\right) \approx 1$

And $(1-\omega_F)\sim 1$

And $\sqrt{uf(u)}\,y_{eD}$ is large, $\therefore \coth\left(\sqrt{uf(u)}\,y_{eD}\right) \approx 1$

Therefore,

$$f(u) = \sqrt{\frac{\lambda_{Fm}}{3u}}$$

Then,

$$\overline{q_{DL}} = \frac{\lambda_{Fm}^{0.25}}{2\pi 3^{0.25}}\frac{1}{u^{0.75}} \quad \text{..... (D- 6)}$$

Inverting Laplace transform, the asymptotic equation of **region 2** is

$$q_{DL} = \frac{\lambda_{Fm}^{1/4}}{10.133}\frac{1}{t_{DAcw}^{1/4}} \quad \text{..... (D- 7)}$$

Case 3

With the assumption of

$\tanh\left(\sqrt{\frac{3u}{\lambda_{Fm}}(1-\omega_F)}\right) \approx \sqrt{\frac{3u}{\lambda_{Fm}}(1-\omega_F)}$ from approximation of Taylor's series expansion when $\sqrt{\frac{3u}{\lambda_{Fm}}(1-\omega_F)}$ is very low

$\sqrt{uf(u)}\, y_{eD}$ is large, $\therefore\ \coth\left(\sqrt{uf(u)}\, y_{eD}\right) \approx 1$

Therefore,

$$f(u) = \omega_F + \sqrt{\frac{\lambda_{Fm}}{3u}(1-\omega_F)}\sqrt{\frac{3u}{\lambda_{Fm}}(1-\omega_F)}$$

$$f(u) = 1$$

Then,

$$\overline{q_{DL}} = \frac{1}{2\pi}\frac{1}{\sqrt{u}} \qquad \text{..... (D- 8)}$$

Inverting Laplace transform, the asymptotic equation of **region 3** is

$$q_{DL} = \frac{1}{2\pi\sqrt{\pi}}\,\frac{1}{\sqrt{t_{DAcw}}} \qquad \text{..... (D- 9)}$$

Case 4

With the assumption of

$\omega_F \ll \sqrt{\frac{\lambda_{Fm}}{3u}(1-\omega_F)}\tanh\left(\sqrt{\frac{3u}{\lambda_{Fm}}(1-\omega_F)}\right)$

And $\sqrt{\frac{3u}{\lambda_{Fm}}(1-\omega_F)}$ is large, $\therefore \tanh\left(\sqrt{\frac{3u}{\lambda_{Fm}}(1-\omega_F)}\right) \approx 1$

And $(1-\omega_F) \sim 1$

And $\coth\left(\sqrt{uf(u)}\, y_{eD}\right) \approx \frac{1}{\sqrt{uf(u)}\, y_{eD}}$ from approximation of Taylor's series expansion when $\sqrt{uf(u)}\, y_{eD}$ is very low

Therefore,

$$f(u) = \sqrt{\frac{\lambda_{Fm}}{3u}}$$

Then,

$$\overline{q_{DL}} = \frac{y_{eD}}{2\pi}\sqrt{\frac{\lambda_{Fm}}{3}}\frac{1}{\sqrt{u}} \qquad \text{..... (D- 10)}$$

Inverting Laplace transform, the asymptotic equation of **region 4** is

$$q_{DL} = \frac{y_{eD}}{2\pi\sqrt{\pi}}\sqrt{\frac{\lambda_{Fm}}{3}}\frac{1}{\sqrt{t_{DAcw}}} \qquad \text{..... (D- 11)}$$

Case 5

With the assumption of

$$\omega_F \gg \sqrt{\frac{\lambda_{Fm}}{3u}(1-\omega_F)}\tanh\left(\sqrt{\frac{3u}{\lambda_{Fm}}(1-\omega_F)}\right)$$

And $\coth\left(\sqrt{uf(u)}\, y_{eD}\right) \approx \frac{1}{\sqrt{uf(u)}\, y_{eD}}$ from approximation of Taylor's series expansion when $\sqrt{uf(u)}\, y_{eD}$ is very low

Therefore,

$$f(u) = \omega_F$$

Then,

$$\overline{q_{DL}} = \frac{y_{eD}}{2\pi}\omega_F \quad \text{..... (D- 12)}$$

Inverting Laplace transform,

$$q_{DL} = \frac{y_{eD}}{2\pi}\omega_F \delta(t) \quad \text{..... (D- 13)}$$

which is not practical

Case 6

With the assumption of

$\tanh\left(\sqrt{\frac{3u}{\lambda_{Fm}}(1-\omega_F)}\right) \approx \sqrt{\frac{3u}{\lambda_{Fm}}(1-\omega_F)}$ from approximation of Taylor's series expansion when $\sqrt{\frac{3u}{\lambda_{Fm}}(1-\omega_F)}$ is very low

And $\coth\left(\sqrt{uf(u)}\, y_{eD}\right) \approx \frac{1}{\sqrt{uf(u)}\, y_{eD}}$ from approximation of Taylor's series expansion when $\sqrt{uf(u)}\, y_{eD}$ is very low

Therefore,

$f(u) = 1$

Then,

$$\overline{q_{DL}} = \frac{y_{eD}}{2\pi} \quad \text{..... (D- 14)}$$

Inverting Laplace transform,

$$q_{DL} = \frac{y_{eD}}{2\pi}\, \delta(t) \quad \text{..... (D- 15)}$$

which is not practical

In summary, assumptions and results of 6 cases are shown in **Table 27**.

Table 27 - Assumptions of 6 cases and the final asymptotic equations of the transient linear dual porosity model (constant pressure)

Case / Region	Estimated Terms			Asymptotic Equations
	$\overline{q_{DL}}$	$f(u)$		
	$\coth\left(\sqrt{uf(u)}\, y_{eD}\right)$	ω_F	$\tanh\left(\sqrt{\frac{3u}{\lambda_{Fm}}(1-\omega_F)}\right)$	
1	1	ω_F	-	$q_{DL} = \frac{\sqrt{\omega_F}}{2\pi\sqrt{\pi}} \frac{1}{\sqrt{t_{DAcw}}}$
2	1	-	1	$q_{DL} = \frac{\lambda_{Fm}^{1/4}}{10.133} \frac{1}{t_{DAcw}^{1/4}}$
3	1	-	$\sqrt{\frac{3u}{\lambda_{Fm}}(1-\omega_F)}$	$q_{DL} = \frac{1}{2\pi\sqrt{\pi}} \frac{1}{\sqrt{t_{DAcw}}}$
4	$\frac{1}{\sqrt{uf(u)}\, y_{eD}}$	-	1	$q_{DL} = \frac{y_{eD}}{2\pi\sqrt{\pi}} \sqrt{\frac{\lambda_{Fm}}{3}} \frac{1}{\sqrt{t_{DAcw}}}$
5	$\frac{1}{\sqrt{uf(u)}\, y_{eD}}$	ω_F	1	N/A
6	$\frac{1}{\sqrt{uf(u)}\, y_{eD}}$	-	$\sqrt{\frac{3u}{\lambda_{Fm}}(1-\omega_F)}$	N/A

Conditions and periods of dual porosity characteristic

One sensitivity set was run to see the curve characteristic of dual porosity model. The Run 1 – 5 plots are shown in **Figure 37**.

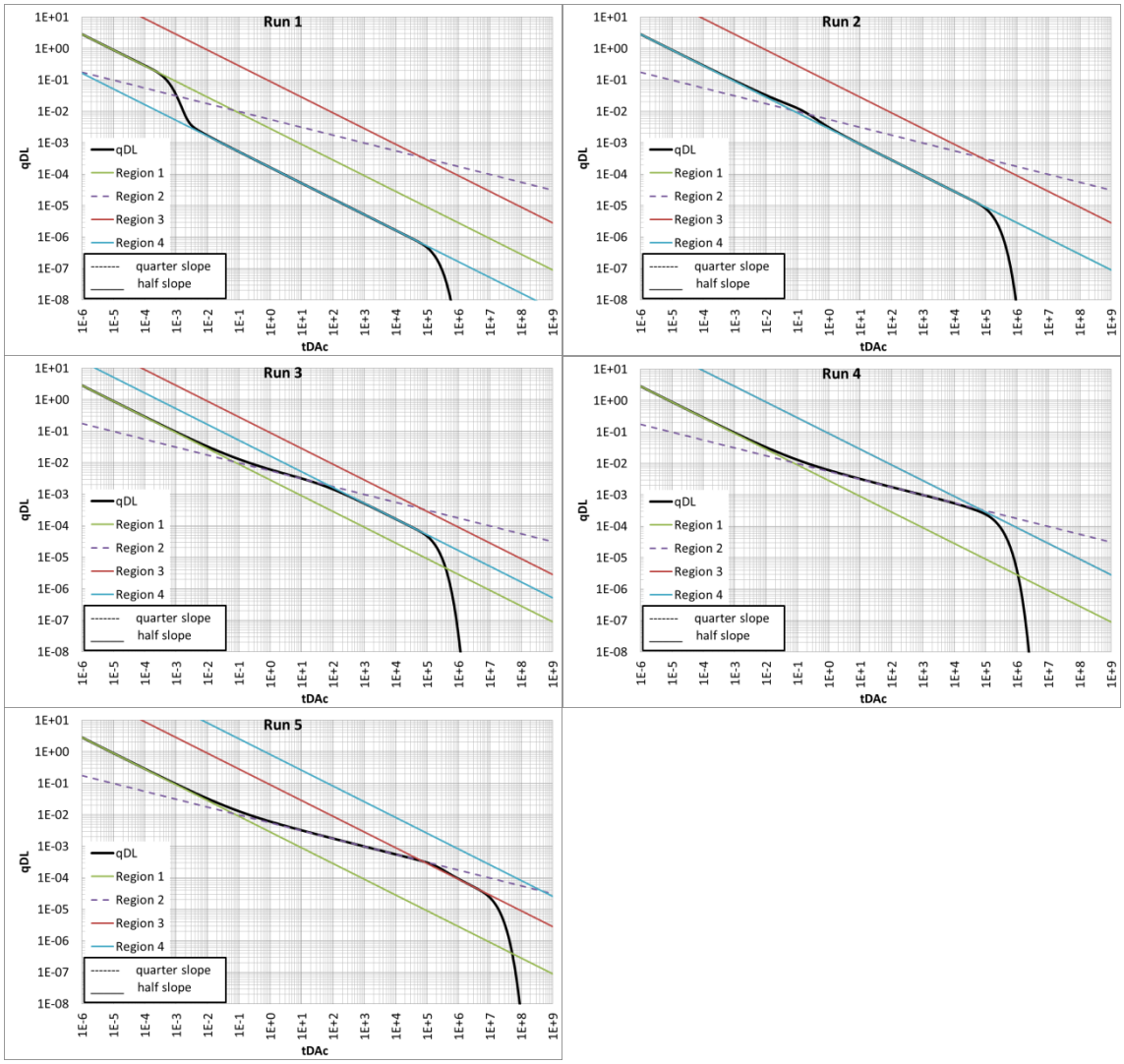

Figure 37 – Sensitivity set (Run 1 – 5) of curve characteristic of the dual porosity model

Run 1 – λ_{Fm} = 1E-5, ω_F = 1E-3, and $y_{eD} = 1$

Only two regions which are region 1 and region 4 are observed and region 4 jogs down from trend line of region 1.

Run 2 – λ_{Fm} = 1E-5, ω_F = 1E-3, and $y_{eD} = 17.32$

Only two regions which are region 1 and region 4 are observed. Moreover, region 1 and region 4 are on the same trend line.

Run 3 – λ_{Fm} = 1E-5, ω_F = 1E-3, and $y_{eD} = 100$

Three regions which are region 1, region 2 and region 4 are observed. Starting with region 1, region 2 bends up from trend line of region 1. Then, from trend line of region 2, region 4 bends down from region 2.

Run 4 – λ_{Fm} = 1E-5, ω_F = 1E-3, and $y_{eD} = 547.72$

Only two regions which are region 1 and region 2 are observed. Starting with region 1, region 2 bends up from trend line of region 1. Then, boundary dominated flow is found directly from region 2.

Run 5 – λ_{Fm} = 1E-5, ω_F = 1E-3, and $y_{eD} = 5000$

Three regions which are region 1, region 2 and region 3 are observed. Starting with region 1, region 2 bends up from trend line of region 1. Then, trend line of region 2 bends down and follows by the region 3 or homogeneous line.

All of the runs (5 runs) are shown that each region has their specific conditions to happen except region 1 which can be seen in any run. From this sensitivity set, the dual porosity model can be defined by 5 characteristic curves as shown in **Figure 38**.

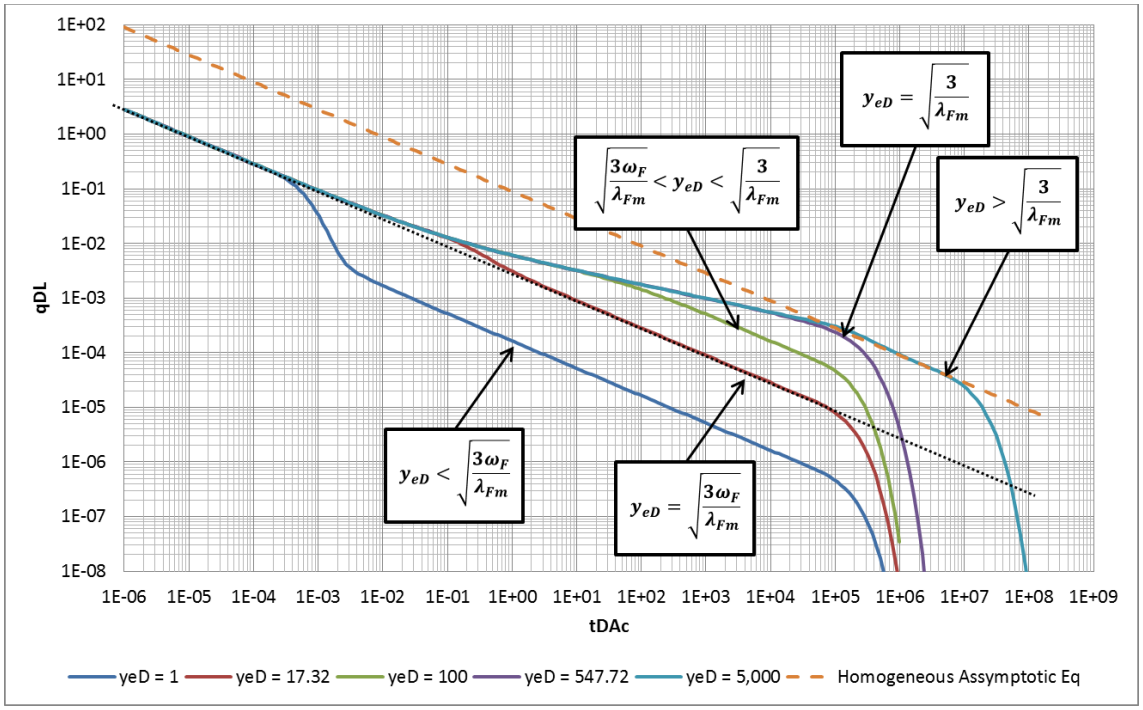

Figure 38 – Combined plots of Run 1 – 5 and the conditions

The conditions of the 5 characteristics can be derived from the asymptotic equations. The derivations are the followings.

From asymptotic equations of region 1 and region 4, the condition as run 2 (region 1 and region 4 are on the same trend line) can be derived.

Equate asymptotic equation of region 1 and region 4:

$$\frac{\sqrt{\omega_F}}{2\pi\sqrt{\pi}}\frac{1}{\sqrt{t_{DAcw}}} = \frac{y_{eD}}{2\pi\sqrt{\pi}}\sqrt{\frac{\lambda_{Fm}}{3}}\frac{1}{\sqrt{t_{DAcw}}} \quad \text{..... (D- 16)}$$

Then,

$$y_{eD} = \sqrt{\frac{3\omega_F}{\lambda_{Fm}}} \quad \text{..... (D- 17)}$$

From asymptotic equation of region 3 and region 4, the condition as run 4 (region 3 and region 4 are on the same trend line, and neither region 3 nor region 4 are found) can be derived.

Equate asymptotic equation of region 3 and region 4:

$$\frac{1}{2\pi\sqrt{\pi}}\frac{1}{\sqrt{t_{DAcw}}} = \frac{y_{eD}}{2\pi\sqrt{\pi}}\sqrt{\frac{\lambda_{Fm}}{3}}\frac{1}{\sqrt{t_{DAcw}}} \quad \text{..... (D- 18)}$$

Then,

$$y_{eD} = \sqrt{\frac{3}{\lambda_{Fm}}} \quad \text{..... (D- 19)}$$

Moreover, the conditions of run 1, run 3, and run 5 can be evaluated from these conditions and showed below.

- The condition of run 1 is $y_{eD} < \sqrt{\frac{3\omega_F}{\lambda_{Fm}}}$
- The condition of run 3 is $\sqrt{\frac{3\omega_F}{\lambda_{Fm}}} < y_{eD} < \sqrt{\frac{3}{\lambda_{Fm}}}$
- The condition of run 5 is $y_{eD} > \sqrt{\frac{3}{\lambda_{Fm}}}$

In summary, the characteristic of the linear transient dual porosity curve can be defined by 5 conditions in term of y_{eD} as follows.

1. $y_{eD} < \sqrt{\frac{3\omega_F}{\lambda_{Fm}}}$
2. $y_{eD} = \sqrt{\frac{3\omega_F}{\lambda_{Fm}}}$
3. $\sqrt{\frac{3\omega_F}{\lambda_{Fm}}} < y_{eD} < \sqrt{\frac{3}{\lambda_{Fm}}}$
4. $y_{eD} = \sqrt{\frac{3}{\lambda_{Fm}}}$
5. $y_{eD} > \sqrt{\frac{3}{\lambda_{Fm}}}$

From the assumptions of each asymptotic equation, some of starting time and end time of each region can be determined as following.

Region 1

Referring to the assumption of $\coth\left(\sqrt{uf(u)}\, y_{eD}\right) \approx 1$, $\sqrt{uf(u)}\, y_{eD}$ has to be closed to infinity number to get the most accurate value of coth function. From trial and error, $\sqrt{uf(u)}\, y_{eD} > 2$ fits with the estimation.

From $\sqrt{uf(u)}\, y_{eD} > 2$ and $f(u) = \omega_F$,

$$\sqrt{u\,\omega_F}\, y_{eD} > 2 \qquad \text{..... (D- 20)}$$

$$\frac{1}{u} > \frac{1}{u^2}\frac{2^2}{y_{eD}^2\,\omega_F} \qquad \text{..... (D- 21)}$$

Inverting Laplace transform,

$$1 > t_{DAcw}\frac{2^2}{y_{eD}^2\,\omega_F} \qquad \text{..... (D- 22)}$$

$$t_{DAcw} < \frac{y_{eD}^2\,\omega_F}{2^2} \qquad \text{..... (D- 23)}$$

From the sensitivity run case, it is found that end of region 1 is at $t_{DAcw} \cong \frac{y_{eD}^2\,\omega_F}{2^2}$ only in the first condition or when $y_{eD} < \sqrt{\frac{3\omega_F}{\lambda_{Fm}}}$.

Region 2

Referring to the assumption of $\coth\left(\sqrt{uf(u)}\, y_{eD}\right) \approx 1$, same as region 1, $\sqrt{uf(u)}\, y_{eD} > 2$ is used to estimate the time condition from trial and error.

From $\sqrt{uf(u)}\, y_{eD} > 2$ and $(u) = \sqrt{\frac{\lambda_{Fm}}{3u}}$,

$$\sqrt{u\sqrt{\lambda_{Fm}/3u}}\, y_{eD} > 2 \quad \text{..... (D- 24)}$$

$$\frac{1}{u} > \frac{1}{u^2}\frac{2^4 \times 3}{y_{eD}^4\, \lambda_{Fm}} \quad \text{..... (D- 25)}$$

Inverting Laplace transform,

$$1 > t_{DAcw}\frac{2^4 \times 3}{y_{eD}^4\, \lambda_{Fm}} \quad \text{..... (D- 26)}$$

$$t_{DAcw} < \frac{y_{eD}^4\, \lambda_{Fm}}{2^4 \times 3} \quad \text{..... (D- 27)}$$

From the sensitivity run case, it is found that the end of region 2 is at $t_{DAcw} \cong \frac{y_{eD}^4\, \lambda_{Fm}}{2^4 \times 3}$ only in the third condition or $\sqrt{\frac{3\omega_F}{\lambda_{Fm}}} < y_{eD} < \sqrt{\frac{3}{\lambda_{Fm}}}$.

Furthermore, regarding the assumption of $\tanh\left(\sqrt{\frac{3u}{\lambda_{Fm}}(1-\omega_F)}\right) \approx 1$, $\sqrt{\frac{3u}{\lambda_{Fm}}(1-\omega_F)}$ has to be closed to infinity number to get the most accurate value of tanh function. Nevertheless, from trial and error, $\sqrt{\frac{3u}{\lambda_{Fm}}(1-\omega_F)} > 2$ gives the satisfy result.

From $\sqrt{\frac{3u}{\lambda_{Fm}}(1-\omega_F)} > 2$ and $(1-\omega_F) \sim 1$,

$$u > \frac{2^2}{3}\lambda_{Fm} \quad \text{..... (D- 28)}$$

$$\frac{1}{u} > \frac{1}{u^2}\frac{2^2}{3}\lambda_{Fm} \quad \text{..... (D- 29)}$$

Inverting Laplace transform,

$$t_{DAcw} < \frac{3}{2^2 \lambda_{Fm}} \quad \text{..... (D- 30)}$$

From the sensitivity run case, it is found that the end of region 2 is at $t_{DAcw} \cong \frac{3}{2^2 \lambda_{Fm}}$ only in the fifth condition or $y_{eD} > \sqrt{3/\lambda_{Fm}}$.

Region 3

Referring to the assumption of $\coth\left(\sqrt{uf(u)}\, y_{eD}\right) \approx 1$, same as region 1, $\sqrt{uf(u)}\, y_{eD} > 2$ is used to estimate the time condition.

From $\sqrt{uf(u)}\, y_{eD} > 2$ and $f(u) = 1$,

$$\frac{1}{u} > \frac{1}{u^2} \frac{2^2}{y_{eD}^2} \quad \text{..... (D- 31)}$$

Inverting Laplace transform,

$$t_{DAcw} < \frac{y_{eD}^2}{2^2} \quad \text{..... (D- 32)}$$

Referring to the assumption of $\tanh\left(\sqrt{\frac{3u}{\lambda_{Fm}}(1-\omega_F)}\right) \approx \sqrt{\frac{3u}{\lambda_{Fm}}(1-\omega_F)}$ which is the first approximation of Taylor's series expansion, $\sqrt{\frac{3u}{\lambda_{Fm}}(1-\omega_F)}$ term is supposed to be very low (close to 0). However, it is found that $\sqrt{\frac{3u}{\lambda_{Fm}}(1-\omega_F)} < 1$ already make a satisfy result.

From $\sqrt{\frac{3u}{\lambda}(1-\omega)} < 1$ and $(1-\omega)\sim 1$,

$$\frac{1}{u} < \frac{1}{u^2}\,\frac{1}{3}\lambda_{Fm} \qquad \text{..... (D- 33)}$$

Inverting Laplace transform,

$$t_{DAcw} > \frac{3}{\lambda_{Fm}} \qquad \text{..... (D- 34)}$$

From the sensitivity run case, it is found that the start and the end of region 3 is at $t_{DAcw} \cong \frac{3}{\lambda_{Fm}}$ and $t_{DAcw} \cong \frac{y_{eD}^2}{2^2}$, respectively.

Region 4

Referring to the assumption of $\coth\left(\sqrt{uf(u)}\,y_{eD}\right) \approx \frac{1}{\sqrt{uf(u)}\,y_{eD}}$ which is the first approximation of Taylor's series expansion, $\sqrt{uf(u)}\,y_{eD}$ term is supposed to be very low (close to 0). However, it is found that $\sqrt{uf(u)}\,y_{eD} < 1$ already make a satisfy result.

From $\sqrt{uf(u)}\,y_{eD} < 1$ and $f(u) = \sqrt{\frac{\lambda_{Fm}}{3u}}$,

$$\sqrt{u\sqrt{\lambda_{Fm}/3u}}\,y_{eD} < 1 \qquad \text{..... (D- 35)}$$

$$\frac{1}{u} < \frac{1}{u^2}\,\frac{3}{y_{eD}^4\,\lambda_{Fm}} \qquad \text{..... (D- 36)}$$

Inverting Laplace transform,

$$t_{DAcw} > \frac{y_{eD}^4\,\lambda_{Fm}}{3} \qquad \text{..... (D- 37)}$$

From the sensitivity run case, it is found that the start of region 4 is at $t_{DAcw} \cong \frac{y_{eD}^4 \, \lambda_{Fm}}{3}$ only in the third condition or $\sqrt{\frac{3\omega_F}{\lambda_{Fm}}} < y_{eD} < \sqrt{\frac{3}{\lambda_{Fm}}}$.

Furthermore, regarding the assumption of $\tanh\left(\sqrt{\frac{3u}{\lambda_{Fm}}(1-\omega_F)}\right) \approx 1$, same as region 2 case, $\sqrt{\frac{3u}{\lambda_{Fm}}(1-\omega_F)} > 2$ gives the satisfy result. Also same as region 2 case, the end of region 4 is at $t \cong \frac{3}{2^2 \lambda_{Fm}}$. Moreover, from the sensitivity run case, this case will occur when $y_{eD} < \sqrt{\frac{3}{\lambda_{Fm}}}$ or from the condition 1st to 3rd.

Intersection of region 2 and region 4

Equate region 2 and region 4 asymptotic equations,

$$\frac{\lambda_{Fm}^{1/4}}{10.133} \frac{1}{t_{DAcw}^{1/4}} = \frac{y_{eD}}{2\pi\sqrt{\pi}} \sqrt{\frac{\lambda_{Fm}}{3}} \frac{1}{\sqrt{t_{DAcw}}} \quad \text{..... (D- 38)}$$

$$t_{DAcw} = 0.07615 \, \lambda_{Fm} \, y_{eD}^4 \quad \text{..... (D- 39)}$$

Intersection of region 2 and region 3

Equate region 2 and region 3 asymptotic equations,

$$\frac{\lambda_{Fm}^{1/4}}{10.133} \frac{1}{t_{DAcw}^{1/4}} = \frac{1}{2\pi\sqrt{\pi}} \frac{1}{\sqrt{t_{DAcw}}} \quad \text{..... (D- 40)}$$

$$t_{DAcw} = 0.6854 \, \frac{1}{\lambda_{Fm}} \quad \text{..... (D- 41)}$$

In summary, all the time identifications of each region are shown in **Figure 39**, **Figure 40**, and **Figure 41**.

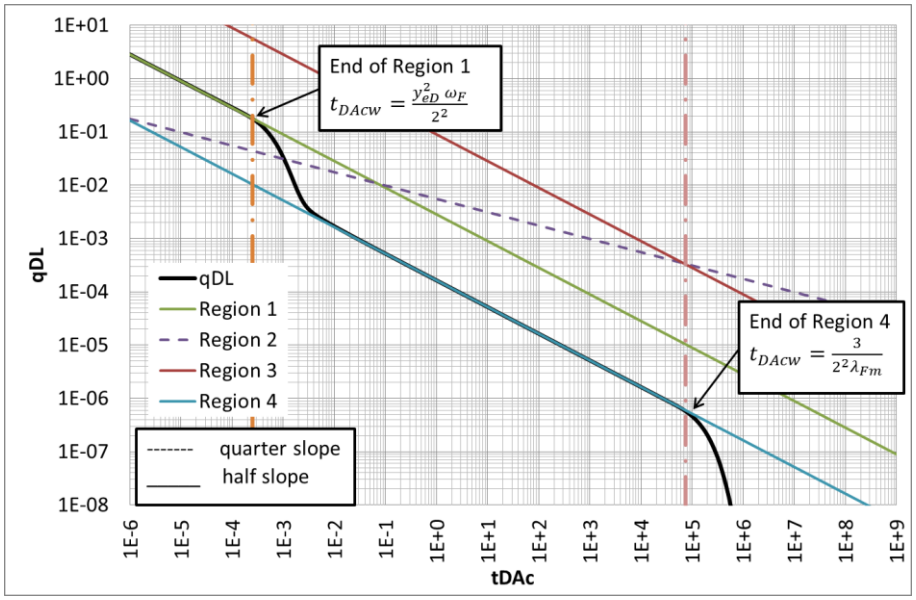

Figure 39 – The dimensionless plot of the dual porosity model of λ_{Fm} = 1E-5, ω_F = 1E-3, and $y_{eD} = 1$

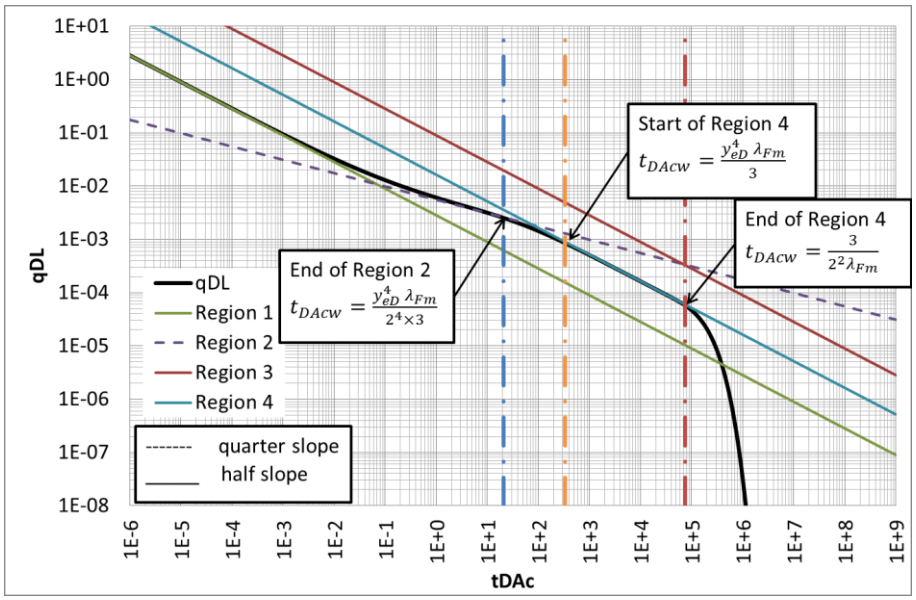

Figure 40 – The dimensionless plot of the dual porosity model of λ_{Fm} = 1E-5, ω_F = 1E-3, and $y_{eD} = 100$

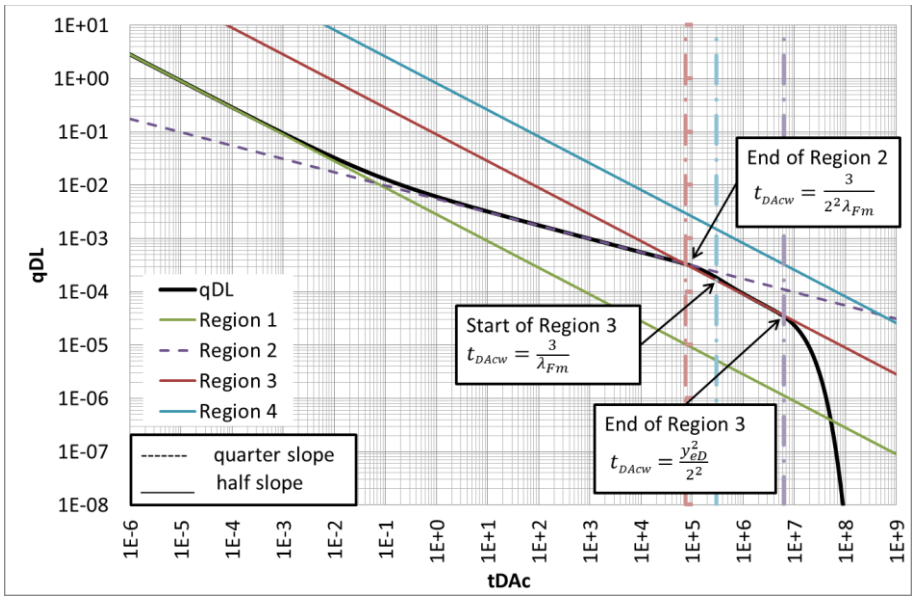

Figure 41 – The dimensionless plot of the dual porosity model of λ_{Fm} = 1E-5, ω_F = 1E-3, and $y_{eD} = 5000$

APPENDIX E

DUAL POROSITY SENSITIVITY

The dimensional parameters, $k_F, k_m, y_e, n_F,$ and $h,$ are played sensitivity analysis to see the effect of each parameters on the production curve. To represent the base case, one theoretical model was generated to represent the multi-transverse hydraulic fractures horizontal shale oil well. The information of this well is showed in **Table 28**.

Table 28 – Data of the theoretical well to represent base case of sensitivity run of dual porosity model

Thickness	h	200	ft	Hydraulic Fracture Half-Length	y_e	500	ft
Perforation Interval	x_e	5000	ft	Hydraulic Fracture Effective Permeability	k_F	0.4	md
Total Porosity	ϕ	0.05		Hydraulic Fracture Width	w_F	0.01	ft
Hydraulic Fracture Spacing	L_F	250	ft	Hydraulic Fracture Intrinsic Permeability	$k_{F,in}$	10,000	md
Number of Hydraulic Fracture	n_F	20		Hydraulic Fracture Porosity	ϕ_F	0.5	
Matrix Permeability	k_m	1.0E-05	md	Matrix Porosity	ϕ_m	0.05	
Water Saturation	S_w	0.2		Viscosity	μ	1.3	cp
Formation Volume Factor	B_o	1.3	rcf/scf	Total Compressibility	c_{ti}	2.0E-07	psi-1
Initial Pressure	p_i	3000	psia	Bottomhole Flowing Pressure	p_{wf}	500	pisa

k_F Sensitivity

The sensitivity of hydraulic fracture intrinsic permeability values, ranging from 0.1 to 10^6 md, is showed in **Figure 42**. The sensitivity result shows that while decreasing the hydraulic fracture permeability from infinite conductivity, the last linear period changes from region 4 to region 3 when $\frac{y_e}{L_F} > \frac{1}{2}\sqrt{\frac{k_F}{k_m}}$. Moreover, it is confirmed that the last linear region 4 is not affected by k_F as showed in the region 4 asymptotic equation. On the other hand, region 3 is affected by k_F as showed in the asymptotic equation.

k_m Sensitivity

The sensitivity of matrix permeability values, ranging from 10^{-8} to 10 md, is showed in **Figure 43**. The sensitivity result shows that while increasing the matrix permeability from 10^{-8} md, the last linear period changes from region 4 to region 3 when $\frac{y_e}{L_F} > \frac{1}{2}\sqrt{\frac{k_F}{k_m}}$. Moreover, it is confirmed that the last linear region 4 is affected by k_m as showed in the region 4 asymptotic equation. On the other hand, region 3 is not affected by k_m as showed in the asymptotic equation.

y_e Sensitivity

The sensitivity of hydraulic fracture half-length values, ranging from 10 ft to infinite value, is showed in **Figure 44**. The sensitivity result shows that while increasing the hydraulic fracture half-length from 10 ft, the last linear period changes from region 4 to region 3 when $\frac{y_e}{L_F} > \frac{1}{2}\sqrt{\frac{k_F}{k_m}}$. Moreover, it is confirmed that y_e affects the last linear line only the region 4. On the other hand, the end of last linear line is affected by y_e only for region 3.

n_F and L_F Sensitivity

The sensitivity of the number of hydraulic fractures related to hydraulic fracture spacing by fixing the effective well length, ranging from 1 to 40, is showed in **Figure 45**. By increasing the number of hydraulic fractures, the production rate increases while the end of linear transient period is shorter.

h Sensitivity

The sensitivity of reservoir thickness value, ranging from 10 to 5120 ft, is showed in **Figure 46**. By increasing reservoir thickness, the production rate increases while the end of linear transient period is same.

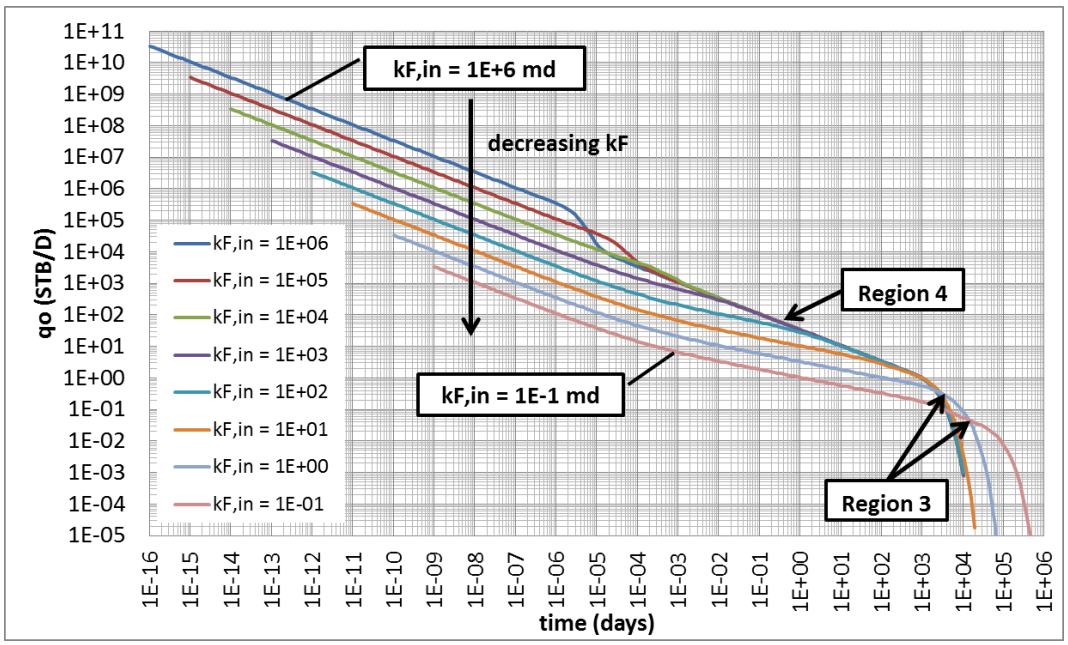

Figure 42 – The hydraulic fracture permeability sensitivity analysis of dual porosity model

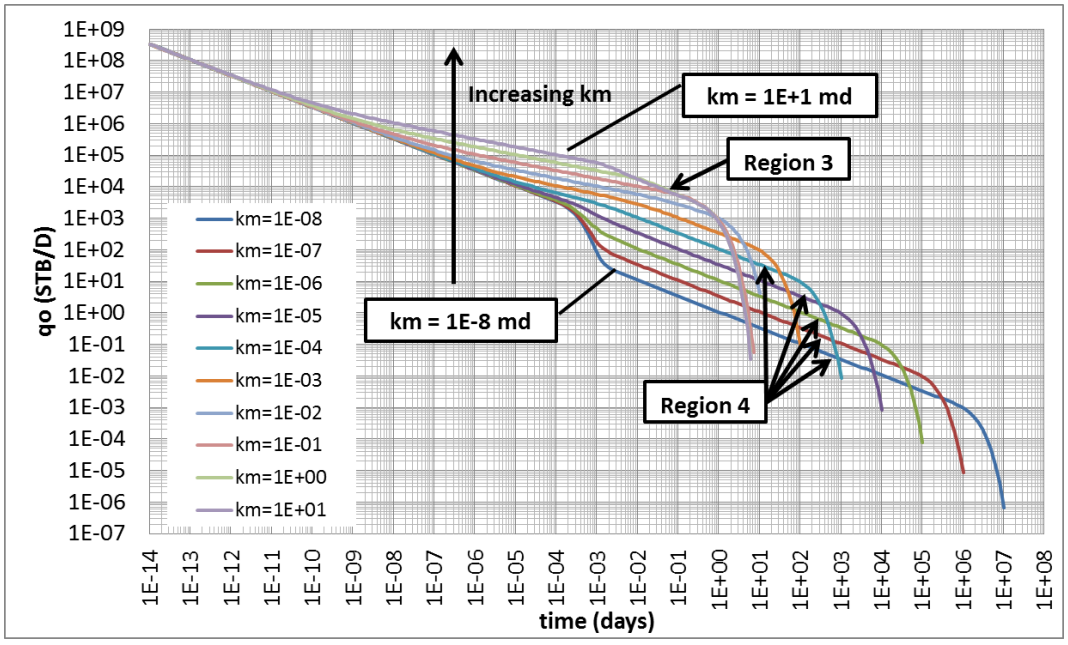

Figure 43 – The matrix permeability sensitivity analysis of dual porosity model

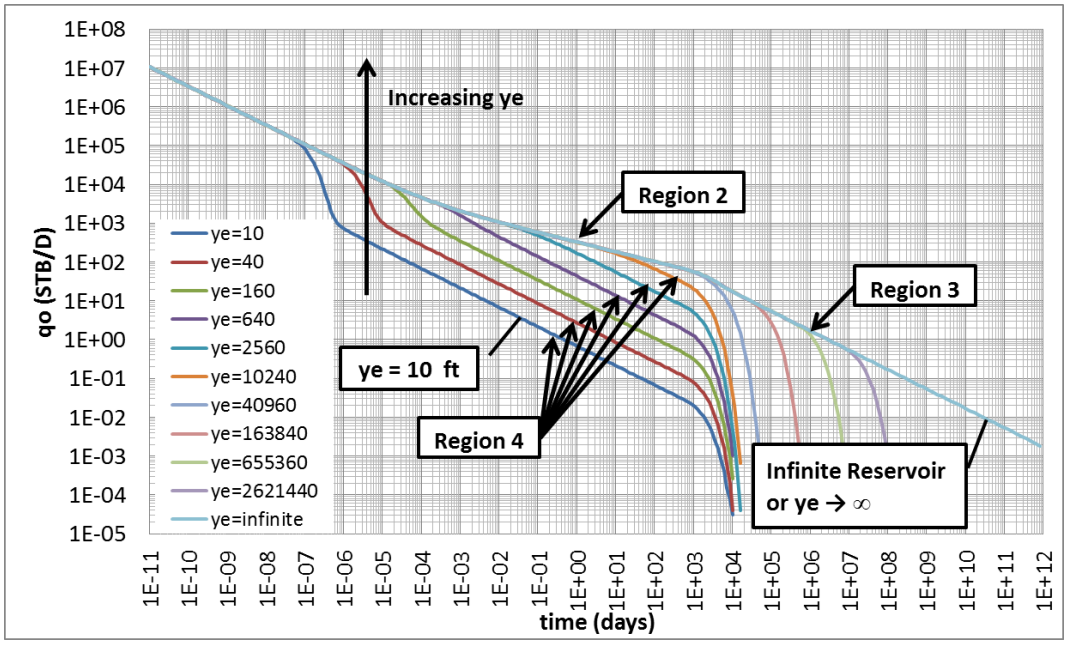

Figure 44 – The hydraulic fracture half-length sensitivity analysis of dual porosity model

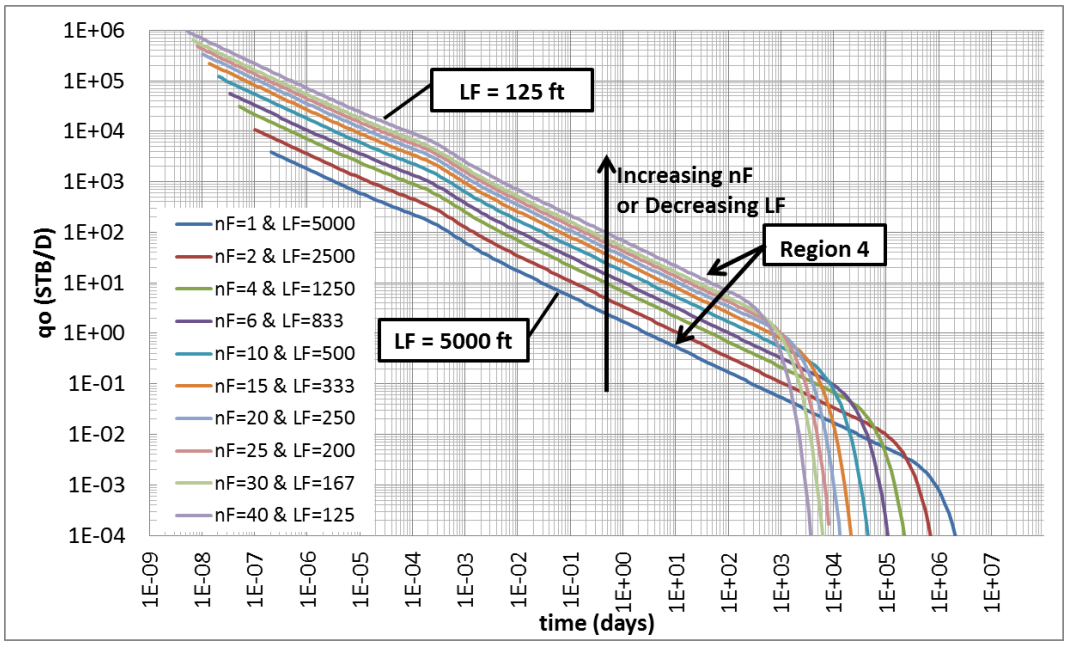

Figure 45 – The hydraulic fracture spacing sensitivity analysis of dual porosity model

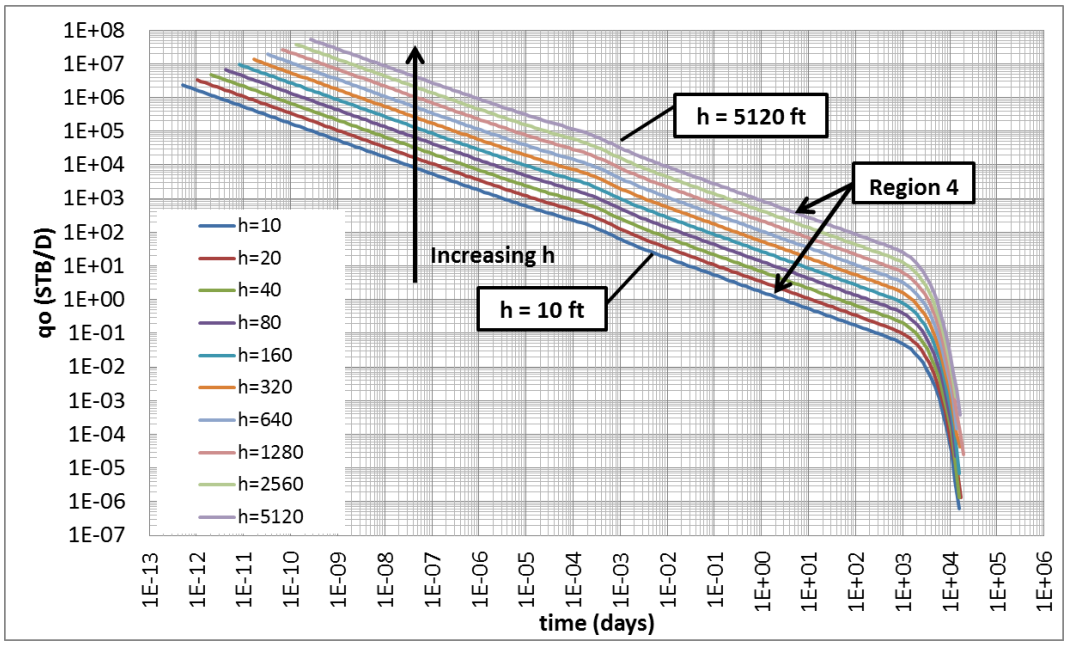

Figure 46 – The reservoir thickness sensitivity analysis of dual porosity model

APPENDIX F

LAPLACE SOLUTION OF

FULLY TRANSIENT LINEAR TRIPLE POROSITY MODEL

Derivations of the fully transient triple porosity model with closed boundary developed by Al-Ahmadi (2010) are shown in this chapter. The solution is showed in Laplace domain to solve the second-order differential equation. The solution in time domain can be obtained by Stehfest algorithm. The derivation starts with constant rate solution and converts to constant pressure solution by using the technique given by Van Everdingen and Hurst (1949).

Matrix system

Diffusivity equation:

$$\frac{k_m}{\mu}\frac{\partial^2 p_m}{\partial z^2} = [\phi V' c_t]_m \frac{\partial p_m}{\partial t}$$

$$\frac{\partial^2 p_m}{\partial z^2} = \mu \left[\frac{\phi V' c_t}{k}\right]_m \frac{\partial p_m}{\partial t}$$

Inner boundary condition:

$$\left.\frac{\partial p_m}{\partial z}\right|_{z=0} = 0$$

Outer boundary condition:

$$p_m|_{z=L_f/2} = p_f$$

Natural fracture system

Diffusivity equation:

$$\frac{k_f}{\mu}\frac{\partial^2 p_f}{\partial x^2} = [\phi V' c_t]_f \frac{\partial p_f}{\partial t} - q_{fm}$$

$$q_{fm} = -\frac{k_m}{\mu\, L_f/2}\left.\frac{\partial p_m}{\partial z}\right|_{z=L_f/2}$$

$$\frac{\partial^2 p_f}{\partial x^2} = \mu\left[\frac{\phi V' c_t}{k}\right]_f \frac{\partial p_f}{\partial t} + \frac{k_m}{k_f\, L_f/2}\left.\frac{\partial p_m}{\partial z}\right|_{z=L_f/2}$$

Inner boundary condition:

$$\left.\frac{\partial p_f}{\partial x}\right|_{x=0} = 0$$

Outer boundary condition:

$$p_f\big|_{x=L_F/2} = p_F$$

Hydraulic fracture system

Diffusivity equation:

$$\frac{k_F}{\mu}\frac{\partial^2 p_F}{\partial y^2} = [\phi V' c_t]_F \frac{\partial p_F}{\partial t} - q_{Ff}$$

$$q_{Ff} = -\frac{k_f}{\mu\, L_F/2}\left.\frac{\partial p_f}{\partial x}\right|_{x=L_F/2}$$

$$\frac{\partial^2 p_F}{\partial y^2} = \mu\left[\frac{\phi V' c_t}{k}\right]_F \frac{\partial p_F}{\partial t} + \frac{k_f}{k_F\, L_F/2}\left.\frac{\partial p_f}{\partial x}\right|_{x=L_F/2}$$

Inner boundary condition:

$$q = \frac{k_F A_{cw}}{B\mu} \frac{\partial p_F}{\partial y}\Big|_{y=0}$$

Outer boundary condition:

$$\frac{\partial p_F}{\partial y}\Big|_{y=y_e} = 0$$

Solution

From matrix system,

Let $z_D = \frac{z}{L_f/2}$ and $p_D = \frac{1}{p_{ch}}\ (p_i - p)$ or $p = p_i - p_D p_{ch}$,

Let $t_{DAcw} = \frac{k_F}{[(\phi V' c_t)_m + (\phi V' c_t)_f + (\phi V' c_t)_F]\mu A_{cw}} t = \frac{k_F}{[\phi V' c_t]_T \mu A_{cw}} t$,

$$\frac{\partial^2 p_{Dm}}{\partial z_D^2} = \frac{3}{\frac{12 k_m A_{cw}}{L_f^2 k_F}} \frac{(\phi V' c_t)_m}{(\phi V' c_t)_T} \frac{\partial p_{Dm}}{\partial t_{DAcw}} \quad \text{..... (F- 1)}$$

Let $\lambda_{fm} = \frac{12 k_m A_{cw}}{L_f^2 k_F}$ and $\omega_m = \frac{(\phi V' c_t)_m}{(\phi V' c_t)_T}$

$$\frac{\partial^2 p_{Dm}}{\partial z_D^2} = \frac{3}{\lambda_{fm}} \omega_m \frac{\partial p_{Dm}}{\partial t_{DAcw}} \quad \text{..... (F- 2)}$$

Take Laplace transform

$$\frac{d^2 \overline{p_{Dm}}}{dz_D^2} = \frac{3}{\lambda_{fm}} \omega_m \left(u \overline{p_{Dm}} - p_{Dm}(z_D, 0) \right) \quad \text{..... (F- 3)}$$

From the initial condition of matrix system, $p_{Dm}(z_D, 0) = 0$

$$\frac{d^2 \overline{p_{Dm}}}{dz_D^2} = \frac{3}{\lambda_{fm}} \omega_m \, u \, \overline{p_{Dm}} \quad \text{..... (F- 4)}$$

This can be shown by the general solution

$$\overline{p_{Dm}} = A\cosh\left(\sqrt{\frac{3\omega_m u}{\lambda_{fm}}}\ z_D\right) + B\sinh\left(\sqrt{\frac{3\omega_m u}{\lambda_{fm}}}\ z_D\right) \quad \text{..... (F- 5)}$$

or

$$\frac{d\overline{p_{Dm}}}{dz_D} = A\sqrt{\frac{3\omega_m u}{\lambda_{fm}}}\sinh\left(\sqrt{\frac{3\omega_m u}{\lambda_{fm}}}\ z_D\right) + B\sqrt{\frac{3\omega_m u}{\lambda_{fm}}}\cosh\left(\sqrt{\frac{3\omega_m u}{\lambda_{fm}}}\ z_D\right) \quad \text{(F- 6)}$$

From the inner boundary condition of matrix system, $\frac{\partial p_m}{\partial z}\Big|_{z=0} = 0$

$$\frac{\partial p_{Dm}}{\partial z_D}\Big|_{z_D=0} = 0 \quad \text{..... (F- 7)}$$

Take Laplace transform,

$$\frac{d\overline{p_{Dm}}}{dz_D}\Big|_{z_D=0} = 0 \quad \text{..... (F- 8)}$$

Therefore, where $z_D = 0$,

Since $\sinh 0 = 0$ and $\cosh 0 = 1$, $B = 0$ from **Eq. F-6**

From the outer boundary condition of matrix system, $p_m|_{z=L_f/2} = p_f$

$$p_{Dm}|_{z_D=1} = p_{Df} \quad \text{..... (F- 9)}$$

Take Laplace transform,

$$\overline{p_{Dm}}|_{z_D=1} = \overline{p_{Df}} \quad \text{..... (F- 10)}$$

Therefore, where $z_D = 1$, $A = \frac{\overline{p_{Df}}}{\cosh\left(\sqrt{\frac{3\omega_m u}{\lambda_{fm}}}\right)}$ from **Eq. F-5**

Therefore, **Eq. F-5** becomes

$$\overline{p_{Dm}} = \frac{\overline{p_{Df}}}{\cosh\left(\sqrt{\frac{3\omega_m u}{\lambda_{fm}}}\right)} \cosh\left(\sqrt{\frac{3\omega_m u}{\lambda_{fm}}}\, z_D\right) \quad \text{..... (F- 11)}$$

or

$$\frac{d\overline{p_{Dm}}}{dz_D} = \frac{\overline{p_{Df}}}{\cosh\left(\sqrt{\frac{3\omega_m u}{\lambda_{fm}}}\right)} \sqrt{\frac{3\omega_m u}{\lambda_{fm}}} \sinh\left(\sqrt{\frac{3\omega_m u}{\lambda_{fm}}}\, z_D\right) \quad \text{..... (F- 12)}$$

From natural fracture system,

Let $x_D = \frac{x}{L_F/2}$, $z_D = \frac{z}{L_f/2}$, $p = p_i - p_D p_{ch}$, and $t_{DAcw} = \frac{k_F}{[\phi V' c_t]_T \mu A_{cw}} t$,

$$\frac{\partial^2 p_{Df}}{\partial x_D^2} = \frac{3}{\frac{12 k_f A_{cw}}{L_F^2 k_F}} \frac{(\phi V' c_t)_f}{(\phi V' c_t)_T} \frac{\partial p_{Df}}{\partial t_{DAcw}} + \frac{\frac{12 k_m A_{cw}}{L_f^2 k_F}}{\frac{12 k_f A_{cw}}{L_F^2 k_F}} \frac{\partial p_{Dm}}{\partial z_D}\bigg|_{z_D=1} \quad \text{..... (F- 13)}$$

Let $\lambda_{fm} = \frac{12 k_m A_{cw}}{L_f^2 k_F}$, $\lambda_{Ff} = \frac{12 k_f A_{cw}}{L_F^2 k_F}$ and $\omega_f = \frac{(\phi V' c_t)_f}{(\phi V' c_t)_T}$,

$$\frac{\partial^2 p_{Df}}{\partial x_D^2} = \frac{3}{\lambda_{Ff}} \omega_f \frac{\partial p_{Df}}{\partial t_{DAcw}} + \frac{\lambda_{fm}}{\lambda_{Ff}} \frac{\partial p_{Dm}}{\partial z_D}\bigg|_{z_D=1} \quad \text{..... (F- 14)}$$

Take Laplace transform

$$\frac{d^2\overline{p_{Df}}}{dx_D^2} = \frac{3}{\lambda_{Ff}} \omega_f \left(u\overline{p_{Df}} - p_{Df}(x_D, 0)\right) + \frac{\lambda_{fm}}{\lambda_{Ff}} \frac{\partial \overline{p_{Dm}}}{\partial z_D}\bigg|_{z_D=1} \quad \text{..... (F- 15)}$$

From the initial condition of natural fracture system, $p_{Df}(x_D, 0) = 0$

$$\frac{d^2\overline{p_{Df}}}{dx_D^2} = \frac{3}{\lambda_{Ff}} \omega_f\, u\, \overline{p_{Df}} + \frac{\lambda_{fm}}{\lambda_{Ff}} \frac{\partial \overline{p_{Dm}}}{\partial z_D}\bigg|_{z_D=1} \quad \text{..... (F- 16)}$$

Substitute $\left.\frac{\partial \overline{p_{Dm}}}{\partial z_D}\right|_{z_D=1}$ with **Eq. F-12**,

$$\frac{d^2\overline{p_{Df}}}{dx_D^2} = u\,\overline{p_{Df}}\left[\frac{3}{\lambda_{Ff}}\omega_f + \frac{\lambda_{fm}}{\lambda_{Ff}}\frac{1}{u}\sqrt{\frac{3\omega_m u}{\lambda_{fm}}}\tanh\left(\sqrt{\frac{3\omega_m u}{\lambda_{fm}}}\right)\right] \quad \text{..... (F- 17)}$$

Define

$$f_f(u) = \frac{3}{\lambda_{Ff}}\omega_f + \frac{\lambda_{fm}}{\lambda_{Ff}}\frac{1}{u}\sqrt{\frac{3\omega_m u}{\lambda_{fm}}}\tanh\left(\sqrt{\frac{3\omega_m u}{\lambda_{fm}}}\right) \quad \text{..... (F- 18)}$$

Therefore,

$$\frac{d^2\overline{p_{Df}}}{dx_D^2} - u\,f_f(u)\,\overline{p_{Df}} = 0 \quad \text{..... (F- 19)}$$

This can be shown by the general solution

$$\overline{p_{Df}} = A\cosh\left(\sqrt{u\,f_f(u)}\,x_D\right) + B\sinh\left(\sqrt{u\,f_f(u)}\,x_D\right) \quad \text{..... (F- 20)}$$

or

$$\frac{d\overline{p_{Df}}}{dx_D} = A\sqrt{u\,f_f(u)}\,\sinh\left(\sqrt{u\,f_f(u)}\,x_D\right) + B\sqrt{u\,f_f(u)}\,\cosh\left(\sqrt{u\,f_f(u)}\,x_D\right) \quad \text{..... (F- 21)}$$

From the inner boundary condition of natural fracture system, $\left.\frac{\partial p_f}{\partial x}\right|_{x=0} = 0$,

$$\left.\frac{\partial p_{Df}}{\partial x_D}\right|_{x_D=0} = 0 \quad \text{..... (F- 22)}$$

Take Laplace transform,

$$\left.\frac{d\overline{p_{Df}}}{dx_D}\right|_{x_D=0} = 0 \quad \text{..... (F- 23)}$$

Therefore, where $x_D = 0$,

Since $\sinh 0 = 0$ and $\cosh 0 = 1$, $B = 0$ from **Eq. F-20**.

From the outer boundary condition of natural fracture system, $p_f\big|_{x=L_F/2} = p_F$,

$$p_{Df}\big|_{x_D=1} = p_{DF} \qquad \text{..... (F- 24)}$$

Take Laplace transform,

$$\overline{p_{Df}}\big|_{x_D=1} = \overline{p_{DF}} \qquad \text{..... (F- 25)}$$

Therefore, where $x_D = 1,\ A = \frac{\overline{p_{DF}}}{\cosh\left(\sqrt{u\, f_f(u)}\right)}$ from Eq. **F-21**.

Therefore, **Eq. F-20** becomes,

$$\overline{p_{Df}} = \frac{\overline{p_{DF}}}{\cosh\left(\sqrt{u\, f_f(u)}\right)} \cosh\left(\sqrt{u\, f_f(u)}\, x_D\right) \qquad \text{..... (F- 26)}$$

or

$$\frac{d\overline{p_{Df}}}{dx_D} = \frac{\overline{p_{DF}}}{\cosh\left(\sqrt{u\, f_f(u)}\right)} \sqrt{u\, f_f(u)}\ \sinh\left(\sqrt{u\, f_f(u)}\, x_D\right) \qquad \text{..... (F- 27)}$$

From hydraulic fracture system,

Let $x_D = \frac{x}{L_F/2}$, $y_D = \frac{y}{\sqrt{A_{cw}}}$, $p = p_i - p_D p_{ch}$, and $t_{DAcw} = \frac{k_F}{[\phi V' c_t]_T \mu A_{cw}} t$,

$$\frac{\partial^2 p_{DF}}{\partial y_D^2} = \frac{(\phi V' c_t)_F}{(\phi V' c_t)_T} \frac{\partial p_{DF}}{\partial t_{DAcw}} + \frac{1}{3} \frac{12 k_f A_{cw}}{L_F^2 k_F} \frac{\partial p_{Df}}{\partial x_D}\bigg|_{x_D=1} \qquad \text{..... (F- 28)}$$

Let $\lambda_{Ff} = \frac{12 k_f A_{cw}}{L_F^2 k_F}$ and $\omega_F = \frac{(\phi V' c_t)_F}{(\phi V' c_t)_T}$,

$$\frac{\partial^2 p_{DF}}{\partial y_D^2} = \omega_F \frac{\partial p_{DF}}{\partial t_{DAcw}} + \frac{1}{3}\, \lambda_{Ff}\, \frac{\partial p_{Df}}{\partial x_D}\bigg|_{x_D=1} \qquad \text{..... (F- 29)}$$

Take Laplace transform,

$$\frac{d^2\overline{p_{DF}}}{dy_D^2} = \omega_F \left(u\overline{p_{DF}} - p_{DF}(y_D, 0)\right) + \frac{\lambda_{Ff}}{3} \left.\frac{\partial\overline{p_{Df}}}{\partial x_D}\right|_{x_D=1} \quad \text{..... (F- 30)}$$

From the initial condition of hydraulic fracture system, $p_{DF}(y_D, 0) = 0$

$$\frac{d^2\overline{p_{DF}}}{dy_D^2} = \omega_F\, u\, \overline{p_{DF}} + \frac{\lambda_{Ff}}{3} \left.\frac{\partial\overline{p_{Df}}}{\partial x_D}\right|_{x_D=1} \quad \text{..... (F- 31)}$$

Substitute $\left.\frac{\partial\overline{p_{Df}}}{\partial x_D}\right|_{x_D=1}$ with **Eq. F-27**,

$$\frac{d^2\overline{p_{DF}}}{dy_D^2} = u\, \overline{p_{DF}} \left[\omega_F + \frac{\lambda_{Ff}}{3\,u} \sqrt{u\, f_f(u)}\, \tanh\left(\sqrt{u\, f_f(u)}\right)\right] \quad \text{..... (F- 32)}$$

Define

$$f(u) = \omega_F + \frac{\lambda_{Ff}}{3\,u} \sqrt{u\, f_f(u)}\, \tanh\left(\sqrt{u\, f_f(u)}\right) \quad \text{..... (F- 33)}$$

Therefore,

$$\frac{d^2\overline{p_{DF}}}{dy_D^2} - u\, f(u)\, \overline{p_{DF}} = 0 \quad \text{..... (F- 34)}$$

This can be shown by the general solution

$$\overline{p_{DF}} = A \cosh\left(\sqrt{u\, f(u)}\, y_D\right) + B \sinh\left(\sqrt{u\, f(u)}\, y_D\right) \quad \text{..... (F- 35)}$$

or

$$\frac{d\overline{p_{DF}}}{dy_D} = A\sqrt{u\, f(u)}\, \sinh\left(\sqrt{u\, f(u)}\, y_D\right) + B\sqrt{u\, f(u)}\, \cosh\left(\sqrt{u\, f(u)}\, y_D\right) \quad \text{..... (F- 36)}$$

From the inner boundary condition of hydraulic fracture system,

$$\left.\frac{\partial p_F}{\partial y}\right|_{y=0} = \frac{qB\mu}{k_F A_{cw}} \quad \text{..... (F- 37)}$$

Let $p = p_i - p_D p_{ch}$, $y_D = \frac{y}{\sqrt{A_{cw}}}$

$$\left.\frac{\partial p_{DF}}{\partial y_D}\right|_{y_D=0} = -\frac{1}{p_{ch}} \frac{qB\mu}{k_F\sqrt{A_{cw}}} \quad \text{..... (F- 38)}$$

Define $p_{ch} = \frac{1}{2\pi}\frac{qB\mu}{k_F\sqrt{A_{cw}}}$; therefore, $p_D = \frac{2\pi\, k_F\sqrt{A_{cw}}}{qB\mu}\ (p_i - p)$

$$\left.\frac{\partial p_{DF}}{\partial y_D}\right|_{y_D=0} = -2\pi \quad \text{..... (F- 39)}$$

Take Laplace transform,

$$\left.\frac{\partial \overline{p_{DF}}}{\partial y_D}\right|_{y_D=0} = -\frac{2\pi}{u} \quad \text{..... (F- 40)}$$

Therefore, where $y_D = 0$,

Since $\sinh 0 = 0$ and $\cosh 0 = 1$, $B = -\frac{2\pi}{u\sqrt{u\, f(u)}}$ from **Eq. F-36**,

$$\frac{d\overline{p_{DF}}}{dy_D} = A\sqrt{u\, f(u)}\ \sinh\left(\sqrt{u\, f(u)}\, y_D\right) - \frac{2\pi}{u}\ \cosh\left(\sqrt{u\, f(u)}\, y_D\right) \quad \text{..... (F- 41)}$$

From the outer boundary condition of hydraulic fracture system, $\left.\frac{\partial p_F}{\partial y}\right|_{y=y_e} = 0$

Define $y_{eD} = \frac{y_e}{\sqrt{A_{cw}}}$,

$$\left.\frac{\partial p_{DF}}{\partial y_D}\right|_{y_D=y_{eD}} = 0 \quad \text{..... (F- 42)}$$

Take Laplace transform,

$$\left.\frac{d\overline{p_{DF}}}{dy_D}\right|_{y_D=y_{eD}} = 0 \qquad \text{..... (F- 43)}$$

Therefore, where $y_e = y_{eD}$, $A = \frac{\frac{2\pi}{u}\cosh\left(\sqrt{u\,f(u)}\,y_{eD}\right)}{\sqrt{u\,f(u)}\,\sinh\left(\sqrt{u\,f(u)}\,y_{eD}\right)}$ from **Eq. F-41**.

Therefore, **Eq. F-35** becomes,

$$\overline{p_{DF}} = \frac{\frac{2\pi}{u}\cosh\left(\sqrt{u\,f(u)}\,y_{eD}\right)}{\sqrt{u\,f(u)}\,\sinh\left(\sqrt{u\,f(u)}\,y_{eD}\right)}\cosh\left(\sqrt{u\,f(u)}\,y_D\right) - \frac{2\pi}{u\sqrt{u\,f(u)}}\sinh\left(\sqrt{u\,f(u)}\,y_D\right) \qquad \text{..... (F- 44)}$$

At wellbore, $y_D = 0$,

$$\overline{p_{DF@well}} = \frac{2\pi\cosh\left(\sqrt{u\,f(u)}\,y_{eD}\right)}{u\sqrt{u\,f(u)}\,\sinh\left(\sqrt{u\,f(u)}\,y_{eD}\right)} \qquad \text{..... (F- 45)}$$

Re-arrange in exponential term, (define $\overline{p_{wDL}} = \overline{p_{DF@well}}$)

$$\overline{p_{wDL}} = \frac{2\pi}{u\sqrt{u\,f(u)}}\left[\frac{1+e^{-2\sqrt{uf(u)}\,y_{eD}}}{1-e^{-2\sqrt{uf(u)}\,y_{eD}}}\right] \qquad \text{..... (F- 46)}$$

To change from constant rate solution to constant pressure solution, Van Everdingen and Hurst (1949) introduced the relation between constant pressure solution and constant rate in Laplace space.

$$\overline{p_{wDL}} \times \overline{q_{DL}} = \frac{1}{u^2} \qquad \text{..... (F- 47)}$$

Consequently, the solution of constant pressure of fully transient triple porosity case (model 1 in Al Ahmadi, 2010) is shown.

$$\frac{1}{q_{DL}} = \frac{2\pi u}{\sqrt{uf(u)}}\left[\frac{1+e^{-2\sqrt{uf(u)}\,y_{eD}}}{1-e^{-2\sqrt{uf(u)}\,y_{eD}}}\right] \quad \text{..... (F- 48)}$$

Where

$$f(u) = \omega_F + \frac{\lambda_{Ff}}{3\,u}\ \sqrt{u\,f_f(u)}\ \tanh\left(\sqrt{u\,f_f(u)}\right) \quad \text{..... (F- 49)}$$

$$f_f(u) = \frac{3}{\lambda_{Ff}}\omega_f + \frac{\lambda_{fm}}{\lambda_{Ff}}\frac{1}{u}\sqrt{\frac{3\omega_m u}{\lambda_{fm}}}\tanh\left(\sqrt{\frac{3\omega_m u}{\lambda_{fm}}}\right) \quad \text{..... (F- 50)}$$

APPENDIX G

VALIDATION OF THE TRIPLE POROSITY MODEL

To validate the triple porosity model (Al-Ahmadi, 2010), the numerical model was used to compare the results. Although, Al-Ahmadi already compared the model with the numerical simulation in different situation and gave a satisfy result, time period that he compared is starting at the last linear flow (starting at 1E-3 days for oil case and 1 day for gas case). Therefore, the early time (the first linear flow) will be compared in this study.

The numerical model was built by the CMG reservoir simulator software. One section (one-quarter) of hydraulic fractures with natural fractures and matrix blocks was simulated in this study. Then, the simulated well production rate, which is output production rate times four times number of hydraulic fractures, was compared to the triple porosity model result. Also, both gas and liquid cases were run for comparison. The synthetic data used in this comparison are shown in **Table 29**.

The model was built in 2-D model (1 cell in z-direction) with 20 grids in x-direction and 200 grids in y-direction. To represent 10 natural fractures, 200 grids in y-direction with logarithmic spacing from the middle of natural fracture to half of natural fracture spacing were built to capture transient period flow from matrix cells to natural fracture cells (20 grids per one natural fracture). And to represent transient flow from natural fractures to hydraulic fractures, logarithmic length of 20 grids in x-direction were

constructed. The first column of grids is represented a half of hydraulic fracture. The top view of the model is shown in **Figure 47**.

Table 29 – Synthetic data of triple porosity model for validation

Macro-Frac (Hydraulic)	Porosity	$\Phi_{F,in}$	0.2	
	Permeability	$k_{F,in}$	5000	md
	Width	w_F	0.1	ft
	Spacing	L_F	100	ft
Micro-Frac (Natural)	Porosity	$\Phi_{f,in}$	0.1	
	Permeability	$k_{f,in}$	50	md
	Width	w_f	0.01	ft
	Spacing	L_f	20	ft
Matrix	Porosity	Φ_m	0.06	
	Permeability	k_m	0.00015	md
General	Thickness	h	300	ft
	Perforated Length	x_e	2000	ft
	Fracture Half-Length	y_e	200	ft
	# of Macro-fractures	n_F	20	
	# of Micro-fractures	n_f	10	
	Rock Compressibility	c_f	1.00E-06	1/psi
	Initial Pressure	p_i	3000	psi
	Bottom-hole Pressure	p_{wf}	500	psi

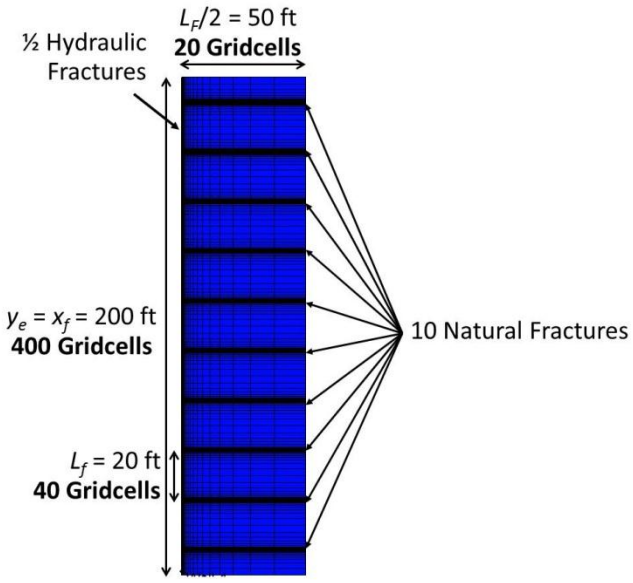

Figure 47 – Numerical model of one-fourth of hydraulic fracture

The analytical solution of water with the same model as numerical model was run and compared the results with the reservoir simulation first to eliminate the effect of non-linearity of gas properties as shown in **Figure 48**. The comparison shows that the analytical solution can fit well almost completely with the numerical solution.

Then, the analytical solution of gas with the same model as water case was run and compared the results with the reservoir simulation. The normalized time to correct non linearity of gas properties was applied. However, gas adsorption was neglected in this evaluation to reduce the confusion from gas adsorption calculation in simulator. The plot comparison is shown in **Figure 48**. There is a narrow discrepancy between the analytical solution and the numerical solution plot. It is believed that this small inconsistent comes from the non-linearity of gas properties and the correlation in gas properties calculation.

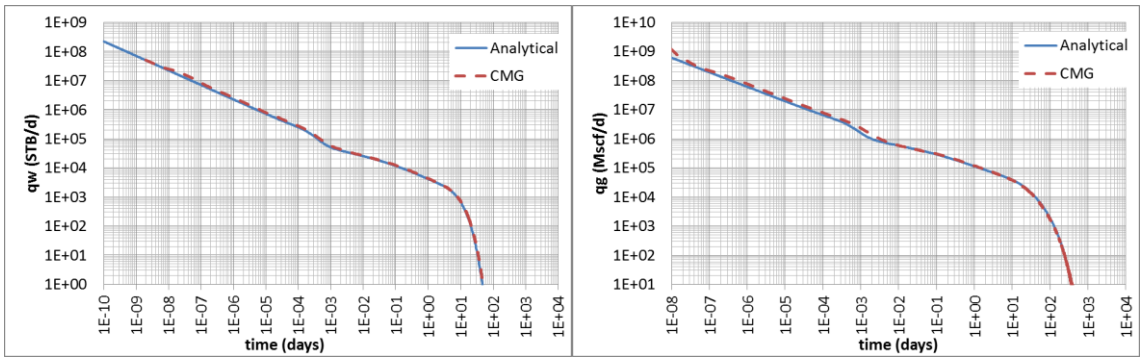

Figure 48 – Comparison plots of analytical solution and numerical solution with the synthetic water and gas data.

Furthermore, more sensitivity cases were run to examine the analytical solution and showed the satisfied results. For example, the **Figure 49** shows the results of changing the matrix permeability to 0.000015 md of water and gas cases. The **Figure 50** shows the results of water and gas cases that the matrix and natural fractures permeability are changed to 0.000015 md and 1 md, respectively. The **Figure 51** shows the results of changing the natural fractures permeability to 0.5 md for water case.

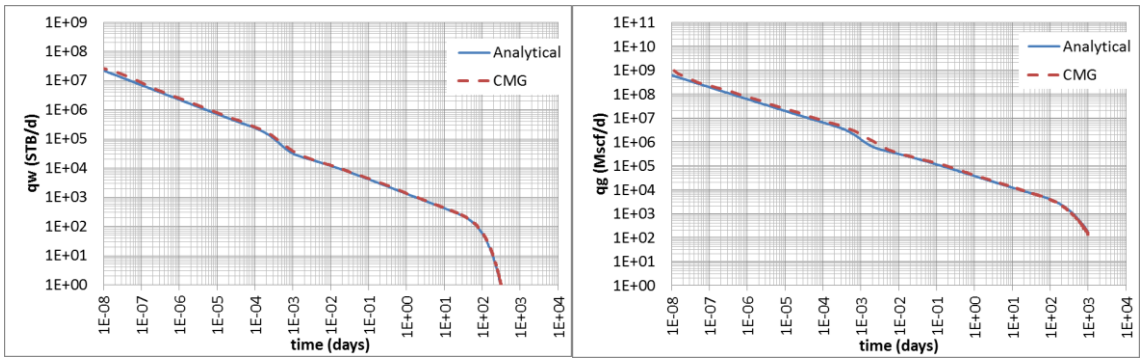

Figure 49 – Comparison plots of analytical solution and numerical solution with the synthetic water and gas data with modification of matrix permeability as 0.000015 md.

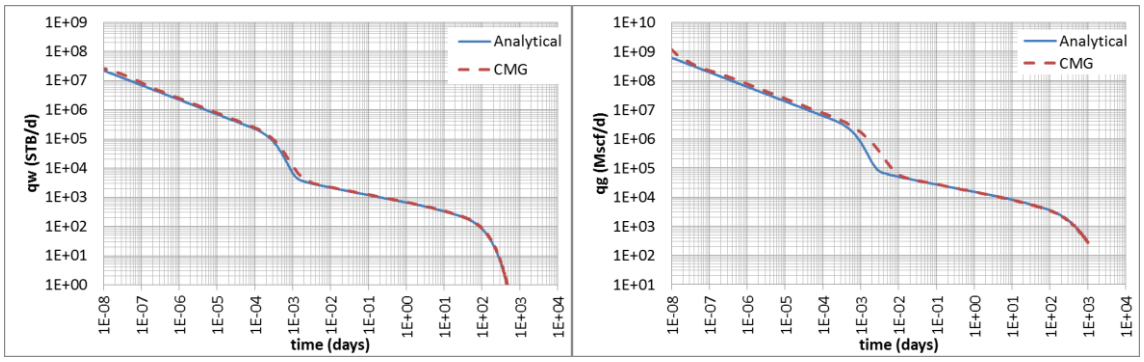

Figure 50 – Comparison plots of analytical solution and numerical solution with the synthetic water and gas data with modification of matrix permeability as 0.000015 md and natural fracture permeability as 1 md.

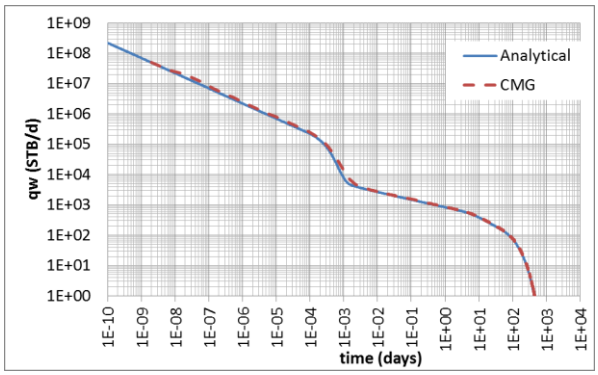

Figure 51 – Comparison plots of analytical solution and numerical solution with the synthetic water and gas data with modification of natural fracture permeability as 0.5 md.

APPENDIX H

ANALYSIS EQUATIONS DERIVATIONS OF FULLY TRANSIENT TRIPLE POROSITY MODEL FOR CONSTANT PRESSURE CASE

This derivation is based on the fully transient triple porosity model (Model 1) proposed by Al-Ahmadi (2010).

From constant pressure inner boundary and closed outer boundary

$$\frac{1}{\overline{q_{DL}}} = \frac{2\pi u}{\sqrt{uf(u)}}\left[\frac{1+e^{-2\sqrt{uf(u)}\,y_{eD}}}{1-e^{-2\sqrt{uf(u)}\,y_{eD}}}\right] \quad \text{..... (H- 1)}$$

Or this can be written in term of $\coth(x)$ function.

$$\frac{1}{\overline{q_{DL}}} = \frac{2\pi u}{\sqrt{uf(u)}}\coth\left(\sqrt{uf(u)}\,y_{eD}\right) \quad \text{..... (H- 2)}$$

For fully transient slab model (Model 1),

$$f(u) = \omega_F + \frac{\lambda_{Ff}}{3u}\sqrt{uf_f(u)}\tanh\left(\sqrt{uf_f(u)}\right) \quad \text{..... (H- 3)}$$

$$f_f(u) = \frac{3\omega_f}{\lambda_{Ff}} + \frac{\lambda_{fm}}{\lambda_{Ff}}\frac{1}{u}\sqrt{\frac{3\omega_m u}{\lambda_{fm}}}\tanh\sqrt{\frac{3\omega_m u}{\lambda_{fm}}} \quad \text{..... (H- 4)}$$

Case 1

With the assumption of $\omega_F \gg \frac{\lambda_{Ff}}{3u}\sqrt{uf_f(u)}\tanh\left(\sqrt{uf_f(u)}\right)$ and $\sqrt{uf(u)}\,y_{eD}$ is large,

$\therefore\ \coth\left(\sqrt{uf(u)}\,y_{eD}\right) \approx 1$

Therefore,

$$f(u) = \omega_F \quad \text{..... (H- 5)}$$

Then,

$$\overline{q_{DL}} = \frac{\sqrt{\omega_F}}{2\pi\sqrt{u}} \quad \text{..... (H- 6)}$$

Inverting Laplace transform,

$$q_{DL} = \frac{\sqrt{\omega_F}}{2\pi\sqrt{\pi}} \frac{1}{\sqrt{t_{DAcw}}} \quad \text{..... (H- 7)}$$

Case 2

With the assumption of

$\omega_F \ll \frac{\lambda_{Ff}}{3u}\sqrt{uf_f(u)}\tanh\left(\sqrt{uf_f(u)}\right)$

And $\sqrt{uf_f(u)}$ is large, $\therefore \tanh\left(\sqrt{uf_f(u)}\right) \approx 1$

And $\frac{3\omega_f}{\lambda_{Ff}} \gg \frac{\lambda_{fm}}{\lambda_{Ff}} \frac{1}{u} \sqrt{\frac{3\omega_m u}{\lambda_{fm}}} \tanh \sqrt{\frac{3\omega_m u}{\lambda_{fm}}}$

And $\sqrt{uf(u)}\, y_{eD}$ is large, $\therefore \coth\left(\sqrt{uf(u)}\, y_{eD}\right) \approx 1$

Therefore,

$$f_f(u) = \frac{3\omega_f}{\lambda_{Ff}} \quad \text{..... (H- 8)}$$

$$f(u) = \frac{\lambda_{Ff}}{3u}\sqrt{uf_f(u)} \quad \text{..... (H- 9)}$$

$$\overline{q_{DL}} = \frac{\sqrt{f(u)}}{2\pi\sqrt{u}} \quad \text{..... (H- 10)}$$

Then,

$$\overline{q_{DL}} = \frac{\lambda_{Ff}^{0.25}\omega_f^{0.25}}{2\pi\ 3^{0.25}}\frac{1}{u^{0.75}} \quad \text{..... (H- 11)}$$

Inverting Laplace transform,

$$q_{DL} = \frac{\lambda_{Ff}^{0.25}\omega_f^{0.25}}{2\pi\ 3^{0.25}}\frac{0.816049}{t_{DAcw}^{1/4}} \quad \text{..... (H- 12)}$$

$$q_{DL} = \frac{\lambda_{Ff}^{1/4}\ \omega_f^{1/4}}{10.133}\frac{1}{t_{DAcw}^{1/4}} \quad \text{..... (H- 13)}$$

Case 3

With the assumption of

$\omega_F \ll \frac{\lambda_{Ff}}{3u}\sqrt{uf_f(u)}\tanh\left(\sqrt{uf_f(u)}\right)$

And $\sqrt{uf_f(u)}$ is large, $\therefore \tanh\left(\sqrt{uf_f(u)}\right) \approx 1$

And $\frac{3\omega_f}{\lambda_{Ff}} \ll \frac{\lambda_{fm}}{\lambda_{Ff}}\ \frac{1}{u}\ \sqrt{\frac{3\omega_m u}{\lambda_{fm}}}\ \tanh\sqrt{\frac{3\omega_m u}{\lambda_{fm}}}$

And $\sqrt{\frac{3\omega_m u}{\lambda_{fm}}}$ is large, $\therefore \tanh\left(\sqrt{\frac{3\omega_m u}{\lambda_{fm}}}\right) \approx 1$

And $\omega_m \sim 1$

And $\sqrt{uf(u)}\ y_{eD}$ is large, $\therefore\ \coth\left(\sqrt{uf(u)}\ y_{eD}\right) \approx 1$

Therefore,

$$f_f(u) = \frac{\lambda_{fm}}{\lambda_{Ff}} \frac{1}{u} \sqrt{\frac{3u}{\lambda_{fm}}} \quad \text{..... (H- 14)}$$

$$f(u) = \frac{\lambda_{Ff}}{3u} \sqrt{u f_f(u)} \quad \text{..... (H- 15)}$$

$$\overline{q_{DL}} = \frac{\sqrt{f(u)}}{2\pi\sqrt{u}} \quad \text{..... (H- 16)}$$

Then,

$$\overline{q_{DL}} = \frac{\lambda_{fm}^{0.125}\, \lambda_{Ff}^{0.25}}{2\pi\, 3^{3/8}} \frac{1}{u^{0.875}} \quad \text{..... (H- 17)}$$

Inverting Laplace transform,

$$q_{DL} = \frac{\lambda_{fm}^{0.125}\, \lambda_{Ff}^{0.25}}{2\pi\, 3^{3/8}} \frac{0.917724}{t_{DAcw}^{1/8}} \quad \text{..... (H- 18)}$$

$$q_{DL} = \frac{\lambda_{fm}^{1/8}\, \lambda_{Ff}^{1/4}}{10.337} \frac{1}{t_{DAcw}^{1/8}} \quad \text{..... (H- 19)}$$

Case 4

With the assumption of

$\omega_F \ll \frac{\lambda_{Ff}}{3u} \sqrt{u f_f(u)} \tanh\left(\sqrt{u f_f(u)}\right)$

And $\sqrt{u f_f(u)}$ is large, $\therefore \tanh\left(\sqrt{u f_f(u)}\right) \approx 1$

And $\frac{3\omega_f}{\lambda_{Ff}} \ll \frac{\lambda_{fm}}{\lambda_{Ff}} \frac{1}{u} \sqrt{\frac{3\omega_m u}{\lambda_{fm}}} \tanh \sqrt{\frac{3\omega_m u}{\lambda_{fm}}}$

And $\tanh\left(\sqrt{\frac{3\omega_m u}{\lambda_{fm}}}\right) \approx \sqrt{\frac{3\omega_m u}{\lambda_{fm}}}$ from approximation of Taylor's series expansion when $\sqrt{\frac{3\omega_m u}{\lambda_{fm}}}$ is very low

And $\omega_m \sim 1$

And $\sqrt{uf(u)}\, y_{eD}$ is large, $\therefore \coth\left(\sqrt{uf(u)}\, y_{eD}\right) \approx 1$

Therefore,

$$f_f(u) = \frac{\lambda_{fm}}{\lambda_{Ff}} \frac{1}{u} \frac{3u}{\lambda_{fm}} \quad \text{..... (H- 20)}$$

$$f(u) = \frac{\lambda_{Ff}}{3u} \sqrt{u f_f(u)} \quad \text{..... (H- 21)}$$

$$\overline{q_{DL}} = \frac{\sqrt{f(u)}}{2\pi\sqrt{u}} \quad \text{..... (H- 22)}$$

Then,

$$\overline{q_{DL}} = \frac{\lambda_{Ff}^{1/4}}{2\pi\, 3^{1/4}} \frac{1}{u^{3/4}} \quad \text{..... (H- 23)}$$

Inverting Laplace transform,

$$q_{DL} = \frac{\lambda_{Ff}^{1/4}}{2\pi\, 3^{1/4}} \frac{0.816049}{t_{DAcw}^{1/4}} \quad \text{..... (H- 24)}$$

$$q_{DL} = \frac{\lambda_{Ff}^{1/4}}{10.133} \frac{1}{t_{DAcw}^{1/4}} \quad \text{..... (H- 25)}$$

Case 5

With the assumption of

$\omega_F \ll \frac{\lambda_{Ff}}{3u}\sqrt{uf_f(u)}\tanh\left(\sqrt{uf_f(u)}\right)$

And $\tanh\left(\sqrt{uf_f(u)}\right) \approx \sqrt{uf_f(u)}$ from approximation of Taylor's series expansion when $\sqrt{uf_f(u)}$ is very low

And $\frac{3\omega_f}{\lambda_{Ff}} \gg \frac{\lambda_{fm}}{\lambda_{Ff}}\frac{1}{u}\sqrt{\frac{3\omega_m u}{\lambda_{fm}}}\tanh\sqrt{\frac{3\omega_m u}{\lambda_{fm}}}$

And $\sqrt{uf(u)}\, y_{eD}$ is large, $\therefore \coth\left(\sqrt{uf(u)}\, y_{eD}\right) \approx 1$

Therefore,

$$f_f(u) = \frac{3\omega_f}{\lambda_{Ff}} \quad \text{..... (H- 26)}$$

$$f(u) = \frac{\lambda_{Ff}}{3u} uf_f(u) \quad \text{..... (H- 27)}$$

$$\overline{q_{DL}} = \frac{\sqrt{f(u)}}{2\pi\sqrt{u}} \quad \text{..... (H- 28)}$$

Then,

$$\overline{q_{DL}} = \frac{\sqrt{\omega_f}}{2\pi}\frac{1}{\sqrt{u}} \quad \text{..... (H- 29)}$$

Inverting Laplace transform,

$$q_{DL} = \frac{\sqrt{\omega_f}}{2\pi\sqrt{\pi}}\frac{1}{\sqrt{t_{DAcw}}} \quad \text{..... (H- 30)}$$

Case 6

With the assumption of

$\omega_F \ll \frac{\lambda_{Ff}}{3u}\sqrt{uf_f(u)}\tanh\left(\sqrt{uf_f(u)}\right)$

And $\tanh\left(\sqrt{uf_f(u)}\right) \approx \sqrt{uf_f(u)}$ from approximation of Taylor's series expansion when $\sqrt{uf_f(u)}$ is very low

And $\frac{3\omega_f}{\lambda_{Ff}} \ll \frac{\lambda_{fm}}{\lambda_{Ff}}\ \frac{1}{u}\ \sqrt{\frac{3\omega_m u}{\lambda_{fm}}}\ \tanh\sqrt{\frac{3\omega_m u}{\lambda_{fm}}}$

And $\sqrt{\frac{3\omega_m u}{\lambda_{fm}}}$ is large, $\therefore \tanh\left(\sqrt{\frac{3\omega_m u}{\lambda_{fm}}}\right) \approx 1$

And $\omega_m \sim 1$

And $\sqrt{uf(u)}\ y_{eD}$ is large, $\therefore\ \coth\left(\sqrt{uf(u)}\ y_{eD}\right) \approx 1$

Therefore,

$$f_f(u) = \frac{\lambda_{fm}}{\lambda_{Ff}}\ \frac{1}{u}\ \sqrt{\frac{3u}{\lambda_{fm}}} \qquad \text{..... (H- 31)}$$

$$f(u) = \frac{\lambda_{Ff}}{3u} u f_f(u) \qquad \text{..... (H- 32)}$$

$$\overline{q_{DL}} = \frac{\sqrt{f(u)}}{2\pi\sqrt{u}} \qquad \text{..... (H- 33)}$$

Then,

$$\overline{q_{DL}} = \frac{\lambda_{fm}^{0.25}}{2\pi\ 3^{0.25}} \frac{1}{u^{0.75}} \qquad \text{..... (H- 34)}$$

Inverting Laplace transform,

$$q_{DL} = \frac{\lambda_{fm}^{0.25}}{2\pi\ 3^{0.25}} \frac{0.816049}{t_{DAcw}^{1/4}} \quad \text{..... (H- 35)}$$

$$q_{DL} = \frac{\lambda_{fm}^{1/4}}{10.133} \frac{1}{t_{DAcw}^{1/4}} \quad \text{..... (H- 36)}$$

Case 7

With the assumption of

$\omega_F \ll \frac{\lambda_{Ff}}{3u} \sqrt{uf_f(u)} \tanh\left(\sqrt{uf_f(u)}\right)$

And $\tanh\left(\sqrt{uf_f(u)}\right) \approx \sqrt{uf_f(u)}$ from approximation of Taylor's series expansion when $\sqrt{uf_f(u)}$ is very low

And $\frac{3\omega_f}{\lambda_{Ff}} \ll \frac{\lambda_{fm}}{\lambda_{Ff}} \frac{1}{u} \sqrt{\frac{3\omega_m u}{\lambda_{fm}}} \tanh \sqrt{\frac{3\omega_m u}{\lambda_{fm}}}$

And $\tanh\left(\sqrt{\frac{3\omega_m u}{\lambda_{fm}}}\right) \approx \sqrt{\frac{3\omega_m u}{\lambda_{fm}}}$ from approximation of Taylor's series expansion when $\sqrt{\frac{3\omega_m u}{\lambda_{fm}}}$ is very low

And $\omega_m \sim 1$

And $\sqrt{uf(u)}\ y_{eD}$ is large, $\therefore\ \coth\left(\sqrt{uf(u)}\ y_{eD}\right) \approx 1$

Therefore,

$$f_f(u) = \frac{\lambda_{fm}}{\lambda_{Ff}} \frac{1}{u} \frac{3u}{\lambda_{fm}} \quad \text{..... (H- 37)}$$

$$f(u) = \frac{\lambda_{Ff}}{3u} u f_f(u) \quad \text{..... (H- 38)}$$

$$\overline{q_{DL}} = \frac{\sqrt{f(u)}}{2\pi\sqrt{u}} \quad \text{..... (H- 39)}$$

Then,

$$\overline{q_{DL}} = \frac{1}{2\pi\sqrt{u}} \quad \text{..... (H- 40)}$$

Inverting Laplace transform,

$$q_{DL} = \frac{1}{2\pi\sqrt{\pi}} \frac{1}{\sqrt{t_{DAcw}}} \quad \text{..... (H- 41)}$$

which is homogeneous reservoir

Case 8

With the assumption of

$\omega_F \gg \frac{\lambda_{Ff}}{3u} \sqrt{u f_f(u)} \tanh\left(\sqrt{u f_f(u)}\right)$

And $\coth\left(\sqrt{uf(u)}\, y_{eD}\right) \approx \frac{1}{\sqrt{uf(u)}\, y_{eD}}$ from approximation of Taylor's series expansion when $\sqrt{uf(u)}\, y_{eD}$ is very low

Therefore,

$$f(u) = \omega_F \quad \text{..... (H- 42)}$$

$$\overline{q_{DL}} = \frac{f(u)}{2\pi} y_{eD} \quad \text{..... (H- 43)}$$

Then,

$$\overline{q_{DL}} = \frac{\omega_F}{2\pi} y_{eD} \quad \text{..... (H- 44)}$$

Inverting Laplace transform,

$$q_{DL} = \frac{\omega_F}{2\pi} y_{eD} \delta(t) \quad \text{..... (H- 45)}$$

which is not practical

Case 9

With the assumption of

$\omega_F \ll \frac{\lambda_{Ff}}{3u} \sqrt{u f_f(u)} \tanh\left(\sqrt{u f_f(u)}\right)$

And $\sqrt{u f_f(u)}$ is large, $\therefore \tanh\left(\sqrt{u f_f(u)}\right) \approx 1$

And $\frac{3\omega_f}{\lambda_{Ff}} \gg \frac{\lambda_{fm}}{\lambda_{Ff}} \frac{1}{u} \sqrt{\frac{3\omega_m u}{\lambda_{fm}}} \tanh \sqrt{\frac{3\omega_m u}{\lambda_{fm}}}$

And $\coth\left(\sqrt{uf(u)}\, y_{eD}\right) \approx \frac{1}{\sqrt{uf(u)}\, y_{eD}}$ from approximation of Taylor's series expansion when $\sqrt{uf(u)}\, y_{eD}$ is very low

Therefore,

$$f_f(u) = \frac{3\omega_f}{\lambda_{Ff}} \quad \text{..... (H- 46)}$$

$$f(u) = \frac{\lambda_{Ff}}{3u} \sqrt{u f_f(u)} \quad \text{..... (H- 47)}$$

$$\overline{q_{DL}} = \frac{f(u)}{2\pi} y_{eD} \quad \text{..... (H- 48)}$$

Then,

$$\overline{q_{DL}} = \frac{\lambda_{Ff}^{0.5}\ \omega_f^{0.5}}{2\pi\ 3^{0.5}}\ y_{eD}\frac{1}{\sqrt{u}} \quad \text{..... (H- 49)}$$

Inverting Laplace transform,

$$q_{DL} = \frac{\lambda_{Ff}^{1/2}\ \omega_f^{1/2}}{2\pi\sqrt{\pi}\ 3^{1/2}}\ y_{eD}\frac{1}{\sqrt{t_{DAcw}}} \quad \text{..... (H- 50)}$$

Case 10

With the assumption of

$\omega_F \ll \frac{\lambda_{Ff}}{3u}\sqrt{uf_f(u)}\tanh\left(\sqrt{uf_f(u)}\right)$

And $\sqrt{uf_f(u)}$ is large, $\therefore \tanh\left(\sqrt{uf_f(u)}\right) \approx 1$

And $\frac{3\omega_f}{\lambda_{Ff}} \ll \frac{\lambda_{fm}}{\lambda_{Ff}}\ \frac{1}{u}\ \sqrt{\frac{3\omega_m u}{\lambda_{fm}}}\ \tanh\sqrt{\frac{3\omega_m u}{\lambda_{fm}}}$

And $\sqrt{\frac{3\omega_m u}{\lambda_{fm}}}$ is large, $\therefore \tanh\left(\sqrt{\frac{3\omega_m u}{\lambda_{fm}}}\right) \approx 1$

And $\omega_m \sim 1$

And $\coth\left(\sqrt{uf(u)}\ y_{eD}\right) \approx \frac{1}{\sqrt{uf(u)}\ y_{eD}}$ from approximation of Taylor's series expansion when $\sqrt{uf(u)}\ y_{eD}$ is very low

Therefore,

$$f_f(u) = \frac{\lambda_{fm}}{\lambda_{Ff}}\ \frac{1}{u}\ \sqrt{\frac{3u}{\lambda_{fm}}} \quad \text{..... (H- 51)}$$

$$f(u) = \frac{\lambda_{Ff}}{3u}\sqrt{uf_f(u)} \quad \text{..... (H- 52)}$$

$$\overline{q_{DL}} = \frac{f(u)}{2\pi} y_{eD} \quad \text{..... (H- 53)}$$

Then,

$$\overline{q_{DL}} = \frac{\lambda_{Ff}^{0.5}\,\lambda_{fm}^{0.25}}{2\pi\ 3^{0.75}}\ y_{eD}\,\frac{1}{u^{0.75}} \quad \text{..... (H- 54)}$$

Inverting Laplace transform,

$$q_{DL} = \frac{\lambda_{Ff}^{0.5}\,\lambda_{fm}^{0.25}}{2\pi\ 3^{0.75}}\ y_{eD}\,\frac{0.816049}{t_{DAcw}^{1/4}} \quad \text{..... (H- 55)}$$

$$q_{DL} = \frac{\lambda_{Ff}^{1/2}\,\lambda_{fm}^{1/4}}{17.551}\ y_{eD}\,\frac{1}{t_{DAcw}^{1/4}} \quad \text{..... (H- 56)}$$

Case 11

With the assumption of

$\omega_F \ll \frac{\lambda_{Ff}}{3u}\sqrt{uf_f(u)}\tanh\left(\sqrt{uf_f(u)}\right)$

And $\sqrt{uf_f(u)}$ is large, $\therefore \tanh\left(\sqrt{uf_f(u)}\right) \approx 1$

And $\frac{3\omega_f}{\lambda_{Ff}} \ll \frac{\lambda_{fm}}{\lambda_{Ff}}\ \frac{1}{u}\ \sqrt{\frac{3\omega_m u}{\lambda_{fm}}}\ \tanh\sqrt{\frac{3\omega_m u}{\lambda_{fm}}}$

And $\tanh\left(\sqrt{\frac{3\omega_m u}{\lambda_{fm}}}\right) \approx \sqrt{\frac{3\omega_m u}{\lambda_{fm}}}$ from approximation of Taylor's series expansion when $\sqrt{\frac{3\omega_m u}{\lambda_{fm}}}$ is very low

And $\omega_m \sim 1$

And $\coth\left(\sqrt{uf(u)}\, y_{eD}\right) \approx \frac{1}{\sqrt{uf(u)}\, y_{eD}}$ from approximation of Taylor's series expansion when $\sqrt{uf(u)}\, y_{eD}$ is very low

Therefore,

$$f_f(u) = \frac{\lambda_{fm}}{\lambda_{Ff}} \frac{1}{u} \frac{3u}{\lambda_{fm}} \quad \text{..... (H- 57)}$$

$$f(u) = \frac{\lambda_{Ff}}{3u} \sqrt{uf_f(u)} \quad \text{..... (H- 58)}$$

$$\overline{q_{DL}} = \frac{f(u)}{2\pi} y_{eD} \quad \text{..... (H- 59)}$$

Then,

$$\overline{q_{DL}} = \frac{\lambda_{Ff}^{0.5}}{2\pi\, 3^{0.5}} y_{eD} \frac{1}{u^{0.5}} \quad \text{..... (H- 60)}$$

Inverting Laplace transform,

$$q_{DL} = \frac{\lambda_{Ff}^{1/2}}{2\pi\sqrt{\pi}\, 3^{1/2}}\, y_{eD} \frac{1}{\sqrt{t_{DAcw}}} \quad \text{..... (H- 61)}$$

Case 12

With the assumption of

$\omega_F \ll \frac{\lambda_{Ff}}{3u} \sqrt{uf_f(u)} \tanh\left(\sqrt{uf_f(u)}\right)$

And $\tanh\left(\sqrt{uf_f(u)}\right) \approx \sqrt{uf_f(u)}$ from approximation of Taylor's series expansion when $\sqrt{uf_f(u)}$ is very low

And $\frac{3\omega_f}{\lambda_{Ff}} \gg \frac{\lambda_{fm}}{\lambda_{Ff}} \frac{1}{u} \sqrt{\frac{3\omega_m u}{\lambda_{fm}}} \tanh \sqrt{\frac{3\omega_m u}{\lambda_{fm}}}$

And $\coth\left(\sqrt{uf(u)}\, y_{eD}\right) \approx \frac{1}{\sqrt{uf(u)}\, y_{eD}}$ from approximation of Taylor's series expansion when $\sqrt{uf(u)}\, y_{eD}$ is very low

Therefore,

$$f_f(u) = \frac{3\omega_f}{\lambda_{Ff}} \quad \text{..... (H- 62)}$$

$$f(u) = \frac{\lambda_{Ff}}{3u} u f_f(u) \quad \text{..... (H- 63)}$$

$$\overline{q_{DL}} = \frac{f(u)}{2\pi} y_{eD} \quad \text{..... (H- 64)}$$

Then,

$$\overline{q_{DL}} = \frac{\omega_f}{2\pi} y_{eD} \quad \text{..... (H- 65)}$$

Inverting Laplace transform,

$$q_{DL} = \frac{\omega_f}{2\pi} y_{eD} \delta(t) \quad \text{..... (H- 66)}$$

which is not practical

Case 13

With the assumption of

$\omega_F \ll \frac{\lambda_{Ff}}{3u}\sqrt{uf_f(u)}\tanh\left(\sqrt{uf_f(u)}\right)$

And $\tanh\left(\sqrt{uf_f(u)}\right) \approx \sqrt{uf_f(u)}$ from approximation of Taylor's series expansion when $\sqrt{uf_f(u)}$ is very low

And $\frac{3\omega_f}{\lambda_{Ff}} \ll \frac{\lambda_{fm}}{\lambda_{Ff}}\ \frac{1}{u}\ \sqrt{\frac{3\omega_m u}{\lambda_{fm}}}\ \tanh\sqrt{\frac{3\omega_m u}{\lambda_{fm}}}$

And $\sqrt{\frac{3\omega_m u}{\lambda_{fm}}}$ is large, $\therefore \tanh\left(\sqrt{\frac{3\omega_m u}{\lambda_{fm}}}\right) \approx 1$

And $\omega_m \sim 1$

And $\coth\left(\sqrt{uf(u)}\ y_{eD}\right) \approx \frac{1}{\sqrt{uf(u)}\ y_{eD}}$ from approximation of Taylor's series expansion when $\sqrt{uf(u)}\ y_{eD}$ is very low

Therefore,

$$f_f(u) = \frac{\lambda_{fm}}{\lambda_{Ff}}\ \frac{1}{u}\ \sqrt{\frac{3u}{\lambda_{fm}}} \quad \text{..... (H- 67)}$$

$$f(u) = \frac{\lambda_{Ff}}{3u} u f_f(u) \quad \text{..... (H- 68)}$$

$$\overline{q_{DL}} = \frac{f(u)}{2\pi} y_{eD} \quad \text{..... (H- 69)}$$

Then,

$$\overline{q_{DL}} = \frac{\lambda_{fm}^{1/2}}{2\pi\ 3^{1/2}} y_{eD} \frac{1}{\sqrt{u}} \quad \text{..... (H- 70)}$$

Inverting Laplace transform,

$$q_{DL} = \frac{\lambda_{fm}^{1/2}}{2\pi\sqrt{\pi}\ 3^{1/2}}\ y_{eD} \frac{1}{\sqrt{t_{DAcw}}} \quad \text{..... (H- 71)}$$

Case 14

With the assumption of

$\omega_F \ll \frac{\lambda_{Ff}}{3u}\sqrt{uf_f(u)}\tanh\left(\sqrt{uf_f(u)}\right)$

And $\tanh\left(\sqrt{uf_f(u)}\right) \approx \sqrt{uf_f(u)}$ from approximation of Taylor's series expansion when $\sqrt{uf_f(u)}$ is very low

And $\frac{3\omega_f}{\lambda_{Ff}} \ll \frac{\lambda_{fm}}{\lambda_{Ff}}\ \frac{1}{u}\ \sqrt{\frac{3\omega_m u}{\lambda_{fm}}}\ \tanh\sqrt{\frac{3\omega_m u}{\lambda_{fm}}}$

And $\tanh\left(\sqrt{\frac{3\omega_m u}{\lambda_{fm}}}\right) \approx \sqrt{\frac{3\omega_m u}{\lambda_{fm}}}$ from approximation of Taylor's series expansion when $\sqrt{\frac{3\omega_m u}{\lambda_{fm}}}$ is very low

And $\omega_m \sim 1$

And $\coth\left(\sqrt{uf(u)}\ y_{eD}\right) \approx \frac{1}{\sqrt{uf(u)}\ y_{eD}}$ from approximation of Taylor's series expansion when $\sqrt{uf(u)}\ y_{eD}$ is very low

Therefore,

$$f_f(u) = \frac{\lambda_{fm}}{\lambda_{Ff}} \frac{1}{u} \frac{3u}{\lambda_{fm}} \quad \text{..... (H- 72)}$$

$$f(u) = \frac{\lambda_{Ff}}{3u} u f_f(u) \quad \text{..... (H- 73)}$$

$$\overline{q_{DL}} = \frac{f(u)}{2\pi} y_{eD} \quad \text{..... (H- 74)}$$

Then,

$$\overline{q_{DL}} = \frac{1}{2\pi} y_{eD} \quad \text{..... (H- 75)}$$

Inverting Laplace transform,

$$q_{DL} = \frac{1}{2\pi} y_{eD} \delta(t) \quad \text{..... (H- 76)}$$

which is not practical

In summary, the assumptions and results of 14 cases are shown in **Table 30**. Only 11 cases can be identified as the asymptotic equation. From total 11 regions, it is composed of 6 linear flow regions, 4 bilinear flow regions, and 1 trilinear flow region. The region name is defined as **Table 31**. The capital letter “L” is represented “Linear”, “B” is represented “Bilinear”, and “T” is represented “Trilinear”.

Table 30 – Assumptions of deriving asymptotic equations of triple porosity model for constant pressure case

Case	Estimated Terms					Asymptotic Equations
	$\overline{q_{DL}}$	$f(u)$		$f_f(u)$		
	$\coth\left(\sqrt{uf(u)}\,y_{eD}\right)$	ω_F	$\tanh\left(\sqrt{uf_f(u)}\right)$	$\frac{3\omega_f}{\lambda_{Ff}}$	$\tanh\sqrt{\frac{3\omega_m u}{\lambda_{fm}}}$	
1	1	ω_F	-			$q_{DL}=\frac{\sqrt{\omega_F}}{2\pi\sqrt{\pi}}\frac{1}{\sqrt{t_{DAcw}}}$
2	1	-	1	$\frac{3\omega_f}{\lambda_{Ff}}$	-	$q_{DL}=\frac{\lambda_{Ff}^{1/4}\,\omega_f^{1/4}}{10.133}\frac{1}{t_{DAcw}^{1/4}}$
3	1	-	1	-	1	$q_{DL}=\frac{\lambda_{fm}^{1/8}\,\lambda_{Ff}^{1/4}}{10.337}\frac{1}{t_{DAcw}^{1/8}}$
4	1	-	1	-	$\sqrt{\frac{3\omega_m u}{\lambda_{fm}}}$	$q_{DL}=\frac{\lambda_{Ff}^{1/4}}{10.133}\frac{1}{t_{DAcw}^{1/4}}$
5	1	-	$\sqrt{uf_f(u)}$	$\frac{3\omega_f}{\lambda_{Ff}}$	-	$q_{DL}=\frac{\sqrt{\omega_f}}{2\pi\sqrt{\pi}}\frac{1}{\sqrt{t_{DAcw}}}$
6	1	-	$\sqrt{uf_f(u)}$	-	1	$q_{DL}=\frac{\lambda_{fm}^{1/4}}{10.133}\frac{1}{t_{DAcw}^{1/4}}$
7	1	-	$\sqrt{uf_f(u)}$	-	$\sqrt{\frac{3\omega_m u}{\lambda_{fm}}}$	$q_{DL}=\frac{1}{2\pi\sqrt{\pi}}\frac{1}{\sqrt{t_{DAcw}}}$
8	$\frac{1}{\sqrt{uf(u)}\,y_{eD}}$	ω_F	-			N/A
9	$\frac{1}{\sqrt{uf(u)}\,y_{eD}}$	-	1	$\frac{3\omega_f}{\lambda_{Ff}}$	-	$q_{DL}=\frac{\lambda_{Ff}^{1/2}\,\omega_f^{1/2}}{2\pi\sqrt{\pi}\,3^{1/2}}\,y_{eD}\frac{1}{\sqrt{t_{DAcw}}}$
10	$\frac{1}{\sqrt{uf(u)}\,y_{eD}}$	-	1	-	1	$q_{DL}=\frac{\lambda_{Ff}^{1/2}\,\lambda_{fm}^{1/4}}{17.551}\,y_{eD}\frac{1}{t_{DAcw}^{1/4}}$
11	$\frac{1}{\sqrt{uf(u)}\,y_{eD}}$	-	1	-	$\sqrt{\frac{3\omega_m u}{\lambda_{fm}}}$	$q_{DL}=\frac{\lambda_{Ff}^{1/2}}{2\pi\sqrt{\pi}\,3^{1/2}}\,y_{eD}\frac{1}{\sqrt{t_{DAcw}}}$
12	$\frac{1}{\sqrt{uf(u)}\,y_{eD}}$	-	$\sqrt{uf_f(u)}$	$\frac{3\omega_f}{\lambda_{Ff}}$	-	N/A
13	$\frac{1}{\sqrt{uf(u)}\,y_{eD}}$	-	$\sqrt{uf_f(u)}$	-	1	$q_{DL}=\frac{\lambda_{fm}^{1/2}}{2\pi\sqrt{\pi}\,3^{1/2}}\,y_{eD}\frac{1}{\sqrt{t_{DAcw}}}$
14	$\frac{1}{\sqrt{uf(u)}\,y_{eD}}$	-	$\sqrt{uf_f(u)}$	-	$\sqrt{\frac{3\omega_m u}{\lambda_{fm}}}$	N/A

Table 31 – Region name definition with asymptotic equations

Region	Case	Asymptotic Equations
L1	**1**	$q_{DL} = \frac{\sqrt{\omega_F}}{2\pi\sqrt{\pi}} \frac{1}{\sqrt{t_{DAcw}}}$
B1	**2**	$q_{DL} = \frac{\lambda_{Ff}^{1/4}\ \omega_f^{1/4}}{10.133} \frac{1}{t_{DAcw}^{1/4}}$
T1	**3**	$q_{DL} = \frac{\lambda_{fm}^{1/8}\ \lambda_{Ff}^{1/4}}{10.337} \frac{1}{t_{DAcw}^{1/8}}$
B2	**4**	$q_{DL} = \frac{\lambda_{Ff}^{1/4}}{10.133} \frac{1}{t_{DAcw}^{1/4}}$
L2	**5**	$q_{DL} = \frac{\sqrt{\omega_f}}{2\pi\sqrt{\pi}} \frac{1}{\sqrt{t_{DAcw}}}$
B3	**6**	$q_{DL} = \frac{\lambda_{fm}^{1/4}}{10.133} \frac{1}{t_{DAcw}^{1/4}}$
L3	**7**	$q_{DL} = \frac{1}{2\pi\sqrt{\pi}} \frac{1}{\sqrt{t_{DAcw}}}$
	8	N/A
L4	**9**	$q_{DL} = \frac{\lambda_{Ff}^{1/2}\ \omega_f^{1/2}}{2\pi\sqrt{\pi}\ 3^{1/2}}\ y_{eD} \frac{1}{\sqrt{t_{DAcw}}}$
B4	**10**	$q_{DL} = \frac{\lambda_{Ff}^{1/2}\ \lambda_{fm}^{1/4}}{17.551}\ y_{eD} \frac{1}{t_{DAcw}^{1/4}}$
L5	**11**	$q_{DL} = \frac{\lambda_{Ff}^{1/2}}{2\pi\sqrt{\pi}\ 3^{1/2}}\ y_{eD} \frac{1}{\sqrt{t_{DAcw}}}$
	12	N/A
L6	**13**	$q_{DL} = \frac{\lambda_{fm}^{1/2}}{2\pi\sqrt{\pi}\ 3^{1/2}}\ y_{eD} \frac{1}{\sqrt{t_{DAcw}}}$
	14	N/A

Conditions and periods of triple porosity characteristic

The conditions of the triple porosity model characteristic are derived as follow. From the last linear line, possible region is composed of 3 regions – region L3, L5, and L6. The conditions of presenting each region are given by

- When $\lambda_{Ff} > \lambda_{fm}$,
  - If $y_{eD} < \sqrt{3/\lambda_{fm}}$, region L6 is found.
  - If $y_{eD} > \sqrt{3/\lambda_{fm}}$, region L3 is found.
- When $\lambda_{Ff} < \lambda_{fm}$,
  - If $y_{eD} < \sqrt{3/\lambda_{Ff}}$, region L5 is found.
  - If $y_{eD} > \sqrt{3/\lambda_{Ff}}$, region L3 is found.

The first criteria can be derived from equating asymptotic equation of region L5 and L6,

$$\frac{\lambda_{Ff}^{1/2}}{2\pi\sqrt{\pi}\,3^{1/2}}\,y_{eD}\frac{1}{\sqrt{t_{DAcw}}} = \frac{\lambda_{fm}^{1/2}}{2\pi\sqrt{\pi}\,3^{1/2}}\,y_{eD}\frac{1}{\sqrt{t_{DAcw}}} \quad \text{..... (H- 77)}$$

$$\lambda_{Ff} = \lambda_{fm} \quad \text{..... (H- 78)}$$

The sub-criteria of the first condition can be derived from equating asymptotic equation of region L3 and L6,

$$\frac{1}{2\pi\sqrt{\pi}}\frac{1}{\sqrt{t_{DAcw}}} = \frac{\lambda_{fm}^{1/2}}{2\pi\sqrt{\pi}\,3^{1/2}}\,y_{eD}\frac{1}{\sqrt{t_{DAcw}}} \quad \text{..... (H- 79)}$$

$$y_{eD} = \sqrt{\frac{3}{\lambda_{fm}}} \quad \text{..... (H- 80)}$$

The sub-criteria of the second condition can be derived from equating asymptotic equation of region L3 and L5,

$$\frac{1}{2\pi\sqrt{\pi}}\frac{1}{\sqrt{t_{DAcw}}} = \frac{\lambda_{Ff}^{1/2}}{2\pi\sqrt{\pi}\,3^{1/2}}\,y_{eD}\frac{1}{\sqrt{t_{DAcw}}} \quad \text{..... (H- 81)}$$

$$y_{eD} = \sqrt{\frac{3}{\lambda_{Ff}}} \quad \text{..... (H- 82)}$$

For the bilinear line, possible bilinear region is composed of 3 regions – region B2, B3, and B4. The conditions of presenting each region are given by

- Among region B3, B4, and BDF can be appeared before region L6.
    - Two set of conditions are used to identify the possible region prior to region L6.
    - The first set is either region B4 or BDF is presented prior to region L6. The selective condition is $\sqrt{\frac{\lambda_{Ff}\omega_f}{\lambda_{fm}}} = 1$ by equating asymptotic equation of region L4 and L6,

$$\frac{\lambda_{Ff}^{1/2}\,\omega_f^{1/2}}{2\pi\sqrt{\pi}\,3^{1/2}}\,y_{eD}\frac{1}{\sqrt{t_{DAcw}}} = \frac{\lambda_{fm}^{1/2}}{2\pi\sqrt{\pi}\,3^{1/2}}\,y_{eD}\frac{1}{\sqrt{t_{DAcw}}} \quad \text{..... (H- 83)}$$

$$\sqrt{\frac{\lambda_{Ff}\omega_f}{\lambda_{fm}}} = 1 \quad \text{..... (H- 84)}$$

- The second set is either region B3 or BDF is presented prior to region L6. The selective condition is $y_{eD} = \sqrt{\frac{3\omega_f}{\lambda_{fm}}}$ by equating asymptotic equation of region L2 and L6,

$$\frac{\sqrt{\omega_f}}{2\pi\sqrt{\pi}}\frac{1}{\sqrt{t_{DAcw}}} = \frac{\lambda_{fm}^{1/2}}{2\pi\sqrt{\pi}\ 3^{1/2}}\ y_{eD}\frac{1}{\sqrt{t_{DAcw}}} \quad \text{..... (H- 85)}$$

$$y_{eD} = \sqrt{\frac{3\omega_f}{\lambda_{fm}}} \quad \text{..... (H- 86)}$$

- Among region B2, B4, and BDF can be appeared before region L5.
  - Two set of conditions are used to identify the possible region prior to region L5.
  - The first set is either region B2 or B4 is presented prior to region L5. The selective condition is $y_{eD} = \frac{\sqrt{3}}{\lambda_{Ff}^{1/4}\ \lambda_{fm}^{1/4}}$ by equating asymptotic equation of region B2 and B4,

$$\frac{\lambda_{Ff}^{1/4}}{10.133}\frac{1}{t_{DAcw}^{1/4}} = \frac{\lambda_{Ff}^{1/2}\ \lambda_{fm}^{1/4}}{17.551}\ y_{eD}\frac{1}{t_{DAcw}^{1/4}} \quad \text{..... (H- 87)}$$

$$y_{eD} = \frac{\sqrt{3}}{\lambda_{Ff}^{1/4}\ \lambda_{fm}^{1/4}} \quad \text{..... (H- 88)}$$

  - The second set is either region B2 or BDF is presented prior to region L5. The selective condition is $y_{eD} = \sqrt{\frac{3\omega_F}{\lambda_{Ff}}}$ by equating asymptotic equation of region L1 and L5,

$$\frac{\sqrt{\omega_F}}{2\pi\sqrt{\pi}}\frac{1}{\sqrt{t_{DAcw}}} = \frac{\lambda_{Ff}^{1/2}}{2\pi\sqrt{\pi}\ 3^{1/2}}\ y_{eD}\frac{1}{\sqrt{t_{DAcw}}} \quad \text{..... (H- 89)}$$

$$y_{eD} = \sqrt{\frac{3\omega_F}{\lambda_{Ff}}} \quad \text{..... (H- 90)}$$

- Either region B2 or B3 can be appeared before region L3.
    - The selective condition is $\lambda_{Ff} = \lambda_{fm}$ and can be derived by equating asymptotic equation of region B2 and B3,

$$\frac{\lambda_{Ff}^{1/4}}{10.133}\frac{1}{t_{DAcw}^{1/4}} = \frac{\lambda_{fm}^{1/4}}{10.133}\frac{1}{t_{DAcw}^{1/4}} \quad \text{..... (H- 91)}$$

$$\lambda_{Ff} = \lambda_{fm} \quad \text{..... (H- 92)}$$

From the assumptions of the asymptotic equation and check with the sensitivity run case, end time of region L3, L5, and L6 can be derived in Laplace space and convert to time domain as following.

End Region L3

Referring to the assumption of $\coth\left(\sqrt{uf(u)}\ y_{eD}\right) \approx 1$, $\sqrt{uf(u)}\ y_{eD}$ has to be closed to infinity number to get the most accurate value of coth function. From trial and error, $\sqrt{uf(u)}\ y_{eD} > 2$ fits with the estimation.

From $\sqrt{uf(u)}\ y_{eD} > 2$, $f(u) = \frac{\lambda_{Ff}}{3u} u f_f(u)$ and $f_f(u) = \frac{\lambda_{fm}}{\lambda_{Ff}}\ \frac{1}{u}\ \frac{3u}{\lambda_{fm}}$,

$$\sqrt{u\frac{\lambda_{Ff}}{3u}u\frac{\lambda_{fm}}{\lambda_{Ff}}\frac{1}{u}\frac{3u}{\lambda_{fm}}}\ y_{eD} > 2 \quad \text{..... (H- 93)}$$

$$u > \frac{2^2}{y_{eD}^2} \quad \text{..... (H- 94)}$$

Inverting Laplace transform,

$$t_{DAcw} < \frac{y_{eD}^2}{2^2} \quad \text{..... (H- 95)}$$

Therefore, the end of region L3 is at $t_{DAcw,end\ L3} \cong \frac{y_{eD}^2}{2^2}$.

End Region L5

Referring to the assumption of $\tanh\left(\sqrt{uf_f(u)}\right) \approx 1$, $\sqrt{uf_f(u)}$ has to be closed to infinity number to get the most accurate value of tanh function. From trial and error, $\sqrt{uf_f(u)} > 2$ fits with the estimation.

From $\sqrt{uf_f(u)} > 2$ and $f_f(u) = \frac{\lambda_{fm}}{\lambda_{Ff}}\frac{1}{u}\frac{3u}{\lambda_{fm}}$,

$$\sqrt{u\frac{\lambda_{fm}}{\lambda_{Ff}}\frac{1}{u}\frac{3u}{\lambda_{fm}}} > 2 \quad \text{..... (H- 96)}$$

$$u > \frac{2^2}{3}\lambda_{Ff} \quad \text{..... (H- 97)}$$

Inverting Laplace transform,

$$t_{DAcw} < \frac{3}{2^2}\frac{1}{\lambda_{Ff}} \quad \text{..... (H- 98)}$$

Therefore, the end of region L5 is at $t_{DAcw,end\ L5} \cong \frac{3}{2^2}\frac{1}{\lambda_{Ff}}$.

End Region L6

Referring to the assumption of $\tanh\left(\sqrt{\frac{3\omega_m u}{\lambda_{fm}}}\right) \approx 1$, $\sqrt{\frac{3\omega_m u}{\lambda_{fm}}}$ has to be closed to infinity number to get the most accurate value of tanh function. From trial and error, $\sqrt{\frac{3\omega_m u}{\lambda_{fm}}} > 2$ fits with the estimation.

From $\sqrt{\frac{3\omega_m u}{\lambda_{fm}}} > 2$ and $\omega_m \sim 1$,

$$\frac{1}{u} > \frac{1}{u^2}\frac{2^2}{3}\lambda_{fm} \quad \text{..... (H- 99)}$$

Inverting Laplace transform,

$$t_{DAcw} < \frac{3}{2^2}\frac{1}{\lambda_{fm}} \quad \text{..... (H- 100)}$$

Therefore, the end of region L6 is $t_{DAcw,end\ L6} \cong \frac{3}{2^2}\frac{1}{\lambda_{fm}}$.

APPENDIX I

ANALYSIS OF LINEAR TRANSIENT DUAL POROSITY CYLINDER MODEL FOR CONSTANT PRESSURE CASE

From constant pressure inner boundary and closed outer boundary of linear transient dual porosity model given by El-Banbi (1998)

$$\frac{1}{\overline{q_{DL}}} = \frac{2\pi u}{\sqrt{uf(u)}} \coth\left(\sqrt{uf(u)}\, y_{eD}\right) \quad \text{..... (I- 1)}$$

For transient slab model,

$$f(u) = \omega_F + \frac{\lambda_{Fm}}{4\,u}\sqrt{\frac{8(1-\omega_F)u}{\lambda_{Fm}}}\,\frac{\mathrm{I}_1\left(\sqrt{\frac{8(1-\omega_F)u}{\lambda_{Fm}}}\right)}{\mathrm{I}_0\left(\sqrt{\frac{8(1-\omega_F)u}{\lambda_{Fm}}}\right)} \quad \text{..... (I- 2)}$$

Case 1

With the assumption of

$$\omega_F \gg \frac{\lambda_{Fm}}{4\,u}\sqrt{\frac{8(1-\omega_F)u}{\lambda_{Fm}}}\,\frac{\mathrm{I}_1\left(\sqrt{\frac{8(1-\omega_F)u}{\lambda_{Fm}}}\right)}{\mathrm{I}_0\left(\sqrt{\frac{8(1-\omega_F)u}{\lambda_{Fm}}}\right)}$$

$\sqrt{uf(u)}\, y_{eD}$ is large, $\therefore\ \coth\left(\sqrt{uf(u)}\, y_{eD}\right) \approx 1$

Therefore,

$f(u) = \omega_F$

Then,

$$\overline{q_{DL}} = \frac{\sqrt{\omega_F}}{2\pi}\frac{1}{\sqrt{u}} \quad \text{..... (I- 3)}$$

Inverting Laplace transform, the asymptotic equation of **region 1** is

$$q_{DL} = \frac{\sqrt{\omega_F}}{2\pi\sqrt{\pi}}\frac{1}{\sqrt{t_{DAcw}}} \quad \text{..... (I- 4)}$$

Case 2

With the assumption of

$$\omega_F \ll \frac{\lambda_{Fm}}{4\,u}\sqrt{\frac{8(1-\omega_F)u}{\lambda_{Fm}}}\,\frac{\mathrm{I}_1\left(\sqrt{\frac{8(1-\omega_F)u}{\lambda_{Fm}}}\right)}{\mathrm{I}_0\left(\sqrt{\frac{8(1-\omega_F)u}{\lambda_{Fm}}}\right)}$$

And $\sqrt{\frac{8(1-\omega_F)u}{\lambda_{Fm}}}$ is large, $\therefore \frac{\mathrm{I}_1\left(\sqrt{\frac{8(1-\omega_F)u}{\lambda_{Fm}}}\right)}{\mathrm{I}_0\left(\sqrt{\frac{8(1-\omega_F)u}{\lambda_{Fm}}}\right)} \approx 1$

And $(1-\omega_F)\sim 1$

And $\sqrt{uf(u)}\,y_{eD}$ is large, $\therefore\ \coth\left(\sqrt{uf(u)}\,y_{eD}\right) \approx 1$

Therefore,

$$f(u) = \sqrt{\frac{\lambda_{Fm}}{2u}}$$

Then,

$$\overline{q_{DL}} = \frac{\lambda_{Fm}^{0.25}}{2\pi 2^{0.25}}\frac{1}{u^{0.75}} \quad \text{..... (I- 5)}$$

Inverting Laplace transform, the asymptotic equation of **region 2** is

$$q_{DL} = \frac{\lambda_{Fm}^{1/4}}{9.156} \frac{1}{t_{DAcw}^{1/4}} \quad \text{..... (I- 6)}$$

Case 3

With the assumption of

$\frac{I_1(x)}{I_0(x)} \approx x/2$ when x is very low $\left(x = \sqrt{\frac{8(1-\omega_F)u}{\lambda_{Fm}}}\right)$

$\sqrt{uf(u)}\, y_{eD}$ is large, $\therefore \coth\left(\sqrt{uf(u)}\, y_{eD}\right) \approx 1$

Therefore,

$$f(u) = \omega_F + \frac{\lambda_{Fm}}{4\,u} \sqrt{\frac{8(1-\omega_F)u}{\lambda_{Fm}}} \sqrt{\frac{8(1-\omega_F)u}{\lambda_{Fm}}} \frac{1}{2}$$

$$f(u) = 1$$

Then,

$$\overline{q_{DL}} = \frac{1}{2\pi} \frac{1}{\sqrt{u}} \quad \text{..... (I- 7)}$$

Inverting Laplace transform, the asymptotic equation of **region 3** is

$$q_{DL} = \frac{1}{2\pi\sqrt{\pi}} \frac{1}{\sqrt{t_{DAcw}}} \quad \text{..... (I- 8)}$$

Case 4

With the assumption of

$$\omega_F \ll \frac{\lambda_{Fm}}{4\,u}\sqrt{\frac{8(1-\omega_F)u}{\lambda_{Fm}}}\,\frac{\mathrm{I}_1\left(\sqrt{\frac{8(1-\omega_F)u}{\lambda_{Fm}}}\right)}{\mathrm{I}_0\left(\sqrt{\frac{8(1-\omega_F)u}{\lambda_{Fm}}}\right)}$$

And $\sqrt{\frac{8(1-\omega_F)u}{\lambda_{Fm}}}$ is large, $\therefore \frac{\mathrm{I}_1\left(\sqrt{\frac{8(1-\omega_F)u}{\lambda_{Fm}}}\right)}{\mathrm{I}_0\left(\sqrt{\frac{8(1-\omega_F)u}{\lambda_{Fm}}}\right)} \approx 1$

And $(1-\omega_F)\sim 1$

And $\coth\left(\sqrt{uf(u)}\,y_{eD}\right) \approx \frac{1}{\sqrt{uf(u)}\,y_{eD}}$ from approximation of Taylor's series expansion when $\sqrt{uf(u)}\,y_{eD}$ is very low

Therefore,

$$f(u) = \sqrt{\frac{\lambda_{Fm}}{2u}}$$

Then,

$$\overline{q_{DL}} = \frac{y_{eD}}{2\pi}\sqrt{\frac{\lambda_{Fm}}{2}}\frac{1}{\sqrt{u}} \qquad \text{..... (I- 9)}$$

Inverting Laplace transform, the asymptotic equation of **region 4** is

$$q_{DL} = \frac{y_{eD}}{2\pi\sqrt{\pi}}\sqrt{\frac{\lambda_{Fm}}{2}}\frac{1}{\sqrt{t_{DAcw}}} \qquad \text{..... (I- 10)}$$

In summary, assumptions and results of 4 cases are shown in **Table 32**. The dimensional estimated asymptotic equations of gas and oil are shown in **Table 33** and **Table 34**, respectively.

Table 32 – Assumptions of 6 cases and the final asymptotic equations of the transient linear dual porosity model (constant pressure)

Case / Region	**Estimated Terms**			**Asymptotic Equations**
	$\overline{q_{DL}}$	$f(u)$		
	$\coth\left(\sqrt{uf(u)}\, y_{eD}\right)$	ω_F	$\dfrac{I_1\left(\sqrt{\frac{8(1-\omega_F)u}{\lambda_{Fm}}}\right)}{I_0\left(\sqrt{\frac{8(1-\omega_F)u}{\lambda_{Fm}}}\right)}$	
1	1	ω_F	-	$q_{DL} = \dfrac{\sqrt{\omega_F}}{2\pi\sqrt{\pi}} \dfrac{1}{\sqrt{t_{DAcw}}}$
2	1	-	1	$q_{DL} = \dfrac{\lambda_{Fm}^{1/4}}{9.156} \dfrac{1}{t_{DAcw}^{1/4}}$
3	1	-	$\sqrt{\dfrac{8(1-\omega_F)u}{\lambda_{Fm}}}/2$	$q_{DL} = \dfrac{1}{2\pi\sqrt{\pi}} \dfrac{1}{\sqrt{t_{DAcw}}}$
4	$\dfrac{1}{\sqrt{uf(u)}\, y_{eD}}$	-	1	$q_{DL} = \dfrac{y_{eD}}{2\pi\sqrt{\pi}} \sqrt{\dfrac{\lambda_{Fm}}{2}} \dfrac{1}{\sqrt{t_{DAcw}}}$

Table 33 – Asymptotic equations of cylinder case of dual porosity model for gas analysis in dimensional (constant pressure)

Region	Asymptotic Equation for Gas Analysis
1 – 1st Linear	$q_g = \frac{\Delta m(p)}{1260T} A_{cw} \sqrt{k_F} \sqrt{\mu(\phi V' c_t)_F} \frac{1}{\sqrt{t}}$
2 – 1st Bilinear	$q_g = \frac{\Delta m(p)}{1544.1\,T} A_{cw} k_F^{1/2} k_m^{1/4} \frac{1}{\sqrt{L}} [\mu(\phi V' c_t)_{F+m}]^{1/4} \frac{1}{t^{1/4}}$
3 – Infinite-acting	$q_g = \frac{\Delta m(p)}{1260T} A_{cw} \sqrt{k_F} \sqrt{\mu(\phi V' c_t)_{F+m}} \frac{1}{\sqrt{t}}$
4 – 2nd Linear	$q_g = \frac{\Delta m(p)}{315T} A_{cw} \sqrt{k_m} \frac{y_e}{L} \sqrt{\mu(\phi V' c_t)_{F+m}} \frac{1}{\sqrt{t}}$
5 – Exponential decline	

Table 34 – Asymptotic equations of cylinder case of dual porosity model for oil analysis in dimensional (constant pressure)

Region	Asymptotic Equation for Oil Analysis
1 – 1st Linear	$q_o = \frac{\Delta p}{125.1B\sqrt{\mu}} A_{cw} \sqrt{k_F} \sqrt{(\phi V' c_t)_F} \frac{1}{\sqrt{t}}$
2 – 1st Bilinear	$q_o = \frac{\Delta p}{153.3B} \frac{1}{\mu^{3/4}} A_{cw} k_F^{1/2} k_m^{1/4} \frac{1}{\sqrt{L}} [(\phi V' c_t)_{F+m}]^{1/4} \frac{1}{t^{1/4}}$
3 – Infinite-acting	$q_o = \frac{\Delta p}{125.1B\sqrt{\mu}} A_{cw} \sqrt{k_F} \sqrt{(\phi V' c_t)_{F+m}} \frac{1}{\sqrt{t}}$
4 – 2nd Linear	$q_o = \frac{\Delta p}{31.28B\sqrt{\mu}} A_{cw} \sqrt{k_m} \frac{y_e}{L} \sqrt{(\phi V' c_t)_{F+m}} \frac{1}{\sqrt{t}}$
5 – Exponential decline	

VITA

Name: Vartit Tivayanonda

Address: Harold Vance Dept. of Petroleum Engineering,
Texas A&M University, College Station, TX 77843-3116.

Email Address: vartitt@gmail.com

Education: B.Eng., Petroleum Engineering, Chulalongkorn University,
Bangkok, THAILAND, 2006

M.S., Petroleum Engineering, Texas A&M University,
College Station, TX, USA, 2012